Universitat Politècnica de Catalunya

Final Degree Project

Study of Earth-Moon trajectories with solar sail propulsion

Author: David Canales García

Supervisor: Dr. Elena Fantino

Collaborator: Dr. Yuan Ren

A thesis submitted in fulfilment of the requirements for the degree of Aeronautical Engineering in the

Department of Aerospace Engineering

September 2014

“The secret of seeing is to sail on solar wind. Hone and spread your spirit, till you yourself are a sail, whetted, translucent, broadside to the merest puff."

Annie Dillard

Universitat Politècnica de Catalunya

Abstract

Escola Tècnica Superior d'Enginyeries Industrial i Aeronàutica de Terrassa
Department of Aerospace Engineering

Aeronautical Engineering

Study of Earth-Moon trajectories with solar sail propulsion

by David Canales García

The computation of Earth-to-Moon trajectories constitutes an important and interesting chapter of spacecraft trajectory design. The traditional techniques based on Hohmann maneuvers and patched conics allowed the fast transfer of the Apollo's to our natural satellite in less than four days, and proved to be the only option for manned missions. However, we are now in an epoch in which robotic missions dominate the exploration of our planetary system and in particular in a historical and economical moment in which in many situations "cost-efficient" is preferred to "time-efficient". Many alternative solutions to the Earth-to-Moon transfer problem have been proposed based on dynamical models and assumptions that imply long flight times: it is the case, for example, of the low-energy transfers in the circular restricted three-body problem, where the gravitational influence of the Sun is taken into account by letting the s/c travel as far as the equilibrium points of the Sun-Earth system before flying back to the Earth-Moon system and getting captured by the gravity field of the Moon.

In this work we investigate the design of Earth-to-Moon trajectories propelled by the action of solar radiation pressure on a sail. Solar sails have been demonstrated in orbit and are undergoing such a rapid technological development that they are being applied also to the class of nanosatellites with off-the-shelf hardware components. We formulate the trajectory design problem as an optimal control problem. Optimal control is based on the theory of calculus of variations and on the Pontryagin minimum principle. It is an indirect optimization method whose formulation is especially suitable to problems where a control is present (in this case the acceleration produced by the momentum exchange between the solar radiation and the sail), and a cost function (such as the transfer time) is to be minimized in the presence of end-point constraints (such as the conditions for capture at the Moon). Therefore, this work shows how to solve an Earth-to-Moon trajectory with solar sail propulsion applying the optimal control theory.

Keywords: Moon, Trajectory, Optimal Control, Non-linear Programming

Acknowledgements

The delivery of this project represents a milestone in my life for obtaining the degree of Aeronautical Engineer. A project of such difficulty throughout a difficult year provided me with the desire of self-improvement and enhanced my human and intellectual maturity. Therefore, I would like to give a few words to all those who have supported me not only this last year, but also thoughout all my degree.

Firstly, I would like to express my sincere gratitude to my supervisor, Elena Fantino, for his encouragement and support of my research work. She did not only help me to understand the space field with her classes and tutoring. Her knowledge, patience and open-mindedness have provided me with lifetime benefits. This is why I can assure that she is more than the best teacher one can have. I would also like to express my gratitude to her colleague, Yuan Ren, who has been helping me to understand the optimal control and nonlinear programming issues, and all without making any profit out of it. He is a part of our team and the three of us will definitely continue working with this project.

Secondly, I would like to thank my family, but specially my parents, Miguel and Isabel, my sister, Ainhoa, and my grandparents, Luis and Virginia. I would also like to thank Toni Piera, who gave me emotional strength throughout these months, and Xavier Albabart, who also helped me to understand some issues of nonlinear programming.

Finally, I would like to thank my friends, Manel, Matias and Cristian, who have always been next to me and I know they will always be, likewise I would like to thank a woman who has been next to me all my degree. But since everything in life must come to an end: “Don’t cry because it’s over, smile because it happened.” Dr. Seuss.

I hope that you enjoy the reading of this document.

Sincerely,

David Canales Garcia

Contents

List of Figures

List of Tables

Introduction

This study deals with the optimization of an Earth-to-Moon trajectory propelled by a solar sail. The optimization method here considered is optimal control.

The result of an optimal control problem gives which is the optimum way of solving it. By applying optimal control to an Earth-to-Moon trajectory with solar sail propulsion, one obtains the most efficient way to orient the sail with respect to the Sun in order to reach the Moon in the shortest time. In order to do this, a dynamical model is set up and used together with the boundary conditions of the mission to define the optimal control problem. Non-linear programming plays an important role when solving optimal control problems, since the final solution of these problems is not directly proportional to the inputs.

Since the 1960's, a large part of the space research has been devoted to trajectory optimization of orbit transfers including Earth-to-Moon and interplanetary trajectories. Trip time is crucial to the design of spacecrafts and to ensure a longer operational life. Another important factor to optimize is the fuel consumption, since the less mass of fuel is used, the more payload the spacecraft can carry. Nevertheless, we are in a historical and economical moment in which cost efficiency is much more important than time efficiency. One of the main differences between low-thrust and high-thrust is that the specific impulse, I_{sp}, is generally higher for low-thrust, which means that the efficiency of the engine is also higher. High-thrust propulsion can boost the spacecraft with a powerful acceleration, yet the energy is limited because the fuel onboard is limited as well. On the other hand, low-thrust propulsion gives a continuous long-lasting acceleration so the overall energy can be larger.

The study of low-energy transfers to the Moon by means of the restricted three-body problem has been of significance throughout the last years ([1]). This method consists in performing a low-energy transfer to one of the Lagrangian points of the Sun-Earth system and then going from this point to the Moon.

Nevertheless, these trajectories are not optimum and maybe, by using optimal control, the fuel consumption or the time spent to reach the Moon could be reduced. Some Earth-to-Moon low-energy transfers have been carried out using the optimal control theory, i.e., the SMART-1 mission ([2]). Moreover, different studies deal with the issue of optimal control for Earth-to-Moon trajectories using, for example, nuclear electric propulsion ([3]), evolutionary neurocontrol ([4]), the restricted three-body problem of the Earth-to-Moon system ([5],[6]), ballistic capture ([7]), etc. Nevertheless, not a single Earth-to-Moon transfer study with optimal control has been carried out with solar sails.

Solar sails are considered to be a promising option for nean-term future space missions. The spacecraft that have solar sails as propulsion system are pushed by light particles from the Sun, which reflect off giant mirror-like sails. Given that they carry no fuel and keeps accelerating over unlimited distances, it is one of the possible technologies that can one day carry payload to the stars. Eventually, the continuous force of the sunlight on a solar sail may thrust spacecrafts several times faster than traditional engines. Optimization of trajectories with solar sail propulsion has been carried out, but mainly for Earth orbiting satellites ([8],[9]).

Since 1999, thanks to the Cubesat concept developed by Jordi Puig-Suari (Cal Poly) and Bob Twiggs (Stanford University), nanosatellites are filling a niche in space that larger spacecrafts, due to their high cost and long design-to-space cycles, are not filling. Bearing in mind that, when a spacecraft is launched, most of the weight consists in the launch fuel, space-exploration is devoting to enhance the technology of nanosatellites. Given that cubesats are very small, it has been demonstrated that solar sails of huge dimensions ([10]) can be folded into them and they are considered a good propulsion system for nanosatellites.

This disseration presents how to solve the optimal Earth-to-Moon trajectory with a solar sail as the propulsion system of the spacecraft. The outline of the dissertation is as follows: Chapter 1 provides an overview of the optimal control theory and how to solve an optimal control problem depending on the boundary conditions; Chapter 2 deals with the dynamical model, including reference frames, the solar sail model, the acceleration due to the terrestrial, lunar and solar gravity field, the solar eclipses due to the Earth and the Moon and the equations of motion of the spacecraft; Chapter 3 explains how to solve nonlinear problems and gives a mathematical background of the package used to solve them (MINPACK-1); Chapter 4 states the problem of the dissertation,

shows the conjugate equations that come from the optimal control theory, gives an explanation on how the orbit integrator works and explains how to solve the problem by means of MINPACK-1; finally, Chapter 5 gives an overview of this project and provides its conclusions.

Scope

The scope of this project can be divided into the following:

- Understand the optimal control problem as a two-point boundary value problem and how to solve nonlinear problems.
- Research of missions where optimal control theory has been implemented.
- Research of solar sail missions.
- Development of a dynamical model with four bodies: the Earth, the spacecraft, the Moon and the Sun. The equations of motion of the spacecraft are also found out.
- Statement of the two-point boundary value problem of the Earth-to-Moon trajectory with solar sail propulsion.
- Implementation of the formulation into Fortran 95.
- Use of numerical methods to propagate the resulting orbit.
- Learning how to use MINPACK-1's Fortran package to solve the problem.

Due to the difficulties encountered whilst carrying out the study, the final optimum Earth-to-Moon trajectory is out of scope of this project.

Chapter 1

Trajectory optimization with optimal control theory

Trajectory optimization is the process of designing a trajectory that minimizes or maximizes some measure of performance within prescribed constraint boundaries. In this chapter we will present the theory of optimal control which is the framework for the solution of the trajectory optimization problem. Optimal control is an important subject in mathematics. It develops through calculus of variations. However, we do not intend to provide an exhaustive and fully-comprehensive discussion on this wide subject. For this, the reader is referred to the specialized literature:[11],[12],[13],[14],[15],[16],[17],[18]. Here we focus our attention on the fundamental definitions and principles, and we work out some examples in order to guide the reader through the possible types of boundary conditions and lay the grounds to our specific application, i.e., the optimization of a trajectory from the Earth to the Moon with solar sail propulsion. Section 1.1 reviews the history of optimal control theory with the formulation of the two-point boundary value problem. Sec. 4.2 explains the optimal control problem in terms of the two-point boundary value problem. Finally, sec. 1.3 presents the four main problems that can be solved by optimal control depending on the boundary conditions, and an example of each is included.

1.1 Introduction

Trajectory optimization began in earnest in the 1950s as digital computers became available for the computation of trajectories. The first efforts were based

on optimal control approaches which grew out of the calculus of variations developed at the University of Chicago in the first half of the 20^{th} century most notably by Gilbert Ames Bliss. Pontryagin in Russia and Bryson and Bellmann in America were prominent researchers in the development of optimal control. Early application of trajectory optimization had to do with the optimization of rocket thrust profiles in a vacuum and in an atmosphere.

Optimal control theory is a mathematical optimization method for deriving control policies. It deals with the problem of finding a control law for a given system such that a certain optimality criterion is achieved. A control problem includes a cost functional, that is a function of state and control variables, and a set of differential equations describing the paths of the control variables that minimize the cost functional.

We begin with a simple example. Consider a car traveling on a straight line through a hilly road. The question is, how should the driver press the accelerator pedal in order to minimize the total traveling time? Clearly in this example, the term control law refers specifically to the way in which the driver presses the accelerator and shifts the gears. The "system" consists of both the car and the road, and the optimality criterion is the minimization of the total traveling time. Control problems usually include ancillary constraints. For example, the amount of available fuel might be limited, the accelerator pedal cannot be pushed through the floor of the car, speed limits, etc. A proper cost functional is a mathematical expression giving the traveling time as a function of the speed, geometrical considerations, and initial conditions of the system. Another optimal control problem is to find the way to drive the car so as to minimize its fuel consumption, given that it must complete a given course in a time not exceeding some amount. Yet another control problem is to minimize the total monetary cost of completing the trip, given assumed monetary prices for time and fuel.

In more abstract and general terms, the problem consists in minimizing the continuous-time cost functional

$$J = \Phi[\mathbf{x}(t_0), t_0, \mathbf{x}(t_f), t_f] + \int_{t_0}^{t_f} L[\mathbf{x}(t), \mathbf{u}(t), t]dt \tag{1.1}$$

subject to the first-order nonlinear dynamic constraints

$$\dot{\mathbf{x}}(t) = f[\mathbf{x}(t), \mathbf{u}(t), t]. \tag{1.2}$$

In the above equations, $\mathbf{x}(t)$ is the state, $\mathbf{u}(t)$ is the control and t is the independent variable (generally speaking, time). The terms Φ and L are called the endpoint cost and Lagrangian, respectively. Problems involving a cost only on the final and initial state, which is the beginning and the end of the problem, i.e., $\Phi[\mathbf{x}(t_0), t_0, \mathbf{x}(t_f), t_f]$, are referred to as Mayer problems, those involving only the integral or running cost, i.e., $\int_{t_0}^{t_f} L[\mathbf{x}(t), \mathbf{u}(t), t]dt$, are called Lagrange problems and costs of the form of Eq. 1.1 are referred to as Bolza problems. We admit also a constraint on the final state

$$\psi[\mathbf{x}(t), t] = 0. \tag{1.3}$$

It should be noted that the optimal control problem as stated above may have multiple solutions. Thus, it is more often the case that any solution is *locally* minimizing. In the following, we shall assume that the initial condition $\mathbf{x}(t_0) = \mathbf{x}_0$ and the initial time, t_0, are specified and we shall write Eq. 1.1 as

$$J = \Phi[\mathbf{x}(t_f), t_f] + \int_{t_0}^{t_f} L[\mathbf{x}(t), \mathbf{u}(t), t]dt. \tag{1.4}$$

1.2 The optimal control problem as a two-point boundary-value problem

Optimal control problems are generally nonlinear and therefore they do not have analytic solutions. As a result, it is necessary to employ numerical methods to solve them. In the early years of optimal control (1950s to 1980s) the favored approach for solving optimal control problems was that of indirect methods. In an indirect method, the calculus of variations is employed to obtain the first-order optimality conditions. These conditions result in a two-point (or, in the case of a complex problem, a multi-point) boundary-value problem (TPBVP), i.e., a system of differential equations together with a set of additional constraints, called the boundary conditions. In other words, a solution to a boundary-value problem is a solution to the differential equations which also satisfies the boundary conditions.

1.2.1 Lagrange multipliers

In mathematical optimization, the method of Lagrange multipliers (named after Joseph Louis Lagrange) is a strategy for finding the local maxima and minima of a function subject to equality constraints. For instance, consider the optimization problem
maximize $g(x, y)$
subject to $q(x, y) = c$.
We need both g and q to have continuous first partial derivatives. Then, we introduce a new variable λ, called a Lagrange multiplier, and study the Lagrange function (or Lagrangian) Λ defined by

$$\Lambda(x, y, \lambda) = g(x, y) + \lambda \cdot [q(x, y) - c], \tag{1.5}$$

where the λ term may be either added or subtracted. If $g(x_0, y_0)$ is a maximum of $g(x, y)$ for the original constrained problem, then there exists λ_0 such that (x_0,y_0,λ_0) is a stationary point for the Lagrange function (stationary points are those points where the partial derivatives of Λ are zero). However, not all stationary points yield a solution of the original problem. Thus, the method of Lagrange multipliers represents a necessary condition for optimality in constrained problems. Sufficient conditions for a minimum or maximum also exist.

1.2.2 The augmented functions

To include the differential equation constraints, we form the augmented cost functional J_a

$$J_a = \phi[\mathbf{x}(t_f), t_f] + \nu^T \psi[\mathbf{x}(t), t] + \int_{t_0}^{t_f} \left\{ L[\mathbf{x}(t), \mathbf{u}(t), t] + \lambda^T [f(\mathbf{x}(t), \mathbf{u}(t), t) - \dot{\mathbf{x}}(t)] \right\} dt, \tag{1.6}$$

where two time-varying Lagrange multiplier vectors ν and λ have been introduced. The elements of λ are called the *costates* of the system. Eq. 1.6 can be expressed in a more compact form as

$$J_a = \phi + \nu^T \psi + \int_{t_0}^{t_f} [L + \lambda^T (f - \dot{\mathbf{x}})] dt, \tag{1.7}$$

which, after introducing the Hamiltonian H,

$$H = L + \lambda^T f, \tag{1.8}$$

becomes

$$J_a = \phi + \nu^T \psi + \int_{t_0}^{t_f} (H - \lambda^T \dot{\mathbf{x}}) dt. \tag{1.9}$$

1.2.3 Necessary conditions for optimality: Pontryagin's minimum principle

In order to determine the minimum of J_a, we set to zero its variation

$$\begin{aligned} \delta J_a \equiv 0 &= (D_x\phi + D_x\psi^T\nu)\delta\mathbf{x}(t_f) + (D_t\phi + D_t\psi^T\nu)\delta t_f + \psi^T\delta\nu + H\delta t_f \\ &+ \int_{t_0}^{t_f} \left[D_x H\delta\mathbf{x} + D_u H\delta\mathbf{u} - \lambda^T\delta\dot{\mathbf{x}} + (D_\lambda H^T - \dot{\mathbf{x}}^T\delta\lambda) \right] dt, \end{aligned} \tag{1.10}$$

where $D_x = \partial/\partial\mathbf{x}$, $D_t = \partial/\partial t_f$, $D_\lambda = \partial/\partial\lambda$ and $D_u = \partial/\partial\mathbf{u}$. Integrating by parts $\int \lambda^T\delta\dot{\mathbf{x}}dt$ yields

$$\begin{aligned} \delta J_a \equiv 0 &= (D_x\phi + D_x\psi^T\nu - \lambda^T)\delta\mathbf{x}(t_f) + (D_t\phi + D_t\psi^T\nu + H)\delta t_f + \psi^T\delta\nu \\ &+ \int_{t_0}^{t_f} \left[(D_x H + \dot{\lambda}^T)\delta\mathbf{x} + D_u H\delta\mathbf{u} + (D_\lambda H^T - \dot{\mathbf{x}}^T)\delta\lambda \right] dt. \end{aligned} \tag{1.11}$$

Setting to zero the three terms between parentheses in the integral in Eq. 1.11 yields the Euler-Lagrange equations:

$$-\frac{\partial H}{\partial \mathbf{x}} = \dot{\lambda} \qquad [\delta\mathbf{x}], \tag{1.12}$$

$$\frac{\partial H}{\partial \mathbf{u}} = 0 \qquad [\delta\mathbf{u}], \tag{1.13}$$

$$\frac{\partial H}{\partial \lambda} = f[\mathbf{x}^*(t), \mathbf{u}^*(t), t] = \dot{\mathbf{x}} \qquad [\delta\lambda], \tag{1.14}$$

where $[\mathbf{x}^*(t), \mathbf{u}^*(t)]$ is the given extremal for J_a. Eq. 1.14 (*state equation*) and Eq. 1.12 (*costate equation*) are called *optimality conditions*. Eq. 1.13 is the *stationarity* condition. Also the terms outside the integral in Eq. 1.11 must vanish, providing the *boundary conditions* or *transversality conditions*:

$$D_x\phi + D_x\psi^T\nu - \lambda^T = 0 \qquad [\delta\mathbf{x}(t_f)], \tag{1.15}$$

$$D_t\phi + D_t\psi^T\nu + H = 0 \qquad [\delta t_f], \tag{1.16}$$

and the *end point constraint equation*

$$\psi = 0 \qquad [\delta\nu]. \tag{1.17}$$

Pontryagin's minimum principle[1] states that the optimal state trajectory $\mathbf{x}^*$, optimal control $\mathbf{u}^*$, and corresponding Lagrange multiplier vector λ^* must minimize the Hamiltonian H so that

$$H[\mathbf{x}^*(t), \mathbf{u}^*(t), \lambda^*(t), t] \leq H[\mathbf{x}^*(t), \mathbf{u}(t), \lambda^*(t), t] \tag{1.18}$$

for all time t in the given domain and for all permissible control inputs $\mathbf{u}$.

The beauty of using an indirect method is that the state and adjoint (i.e., λ) are solved for and the resulting solution is readily verified to be an extremal trajectory. The disadvantage of indirect methods is that the boundary-value problem is often extremely difficult to solve (particularly for problems that span large time intervals or problems with interior point constraints).

1.3 Types of boundary conditions

Fig. 1.1 illustrates the possible boundary conditions of the system. We shall analyse each of them separately: Fig. 1.1-a represents a problem to be solved in a fixed terminal time, but where the ending point is free; Fig. 1.1-b shows a problem that has the time and the end point constrained; Fig. 1.1-c describes problems where either the ending point and the final time are free; finally, Fig. 1.1-d represents problems where the ending point is fixed, yet the final time to reach this point is free.

1.3.1 Fixed terminal time, free end point

In this case $\delta t_f = 0$ and $\delta \mathbf{x}_f = \delta \mathbf{x}(t_f)$. Concerning the boundary conditions, Eq. 1.16 vanishes. The initial condition $x(t_0)$ is given. Furthermore, if there are no terminal state constraint, Eq. 1.15 becomes

$$\lambda(t_f) = \frac{\partial \phi}{\partial \mathbf{x}}(\mathbf{x}(t_f)). \tag{1.19}$$

For example, we shall study the minimum-drag nose shape in a hypersonic flow (Fig. 1.2). The problem consists of finding the $r(x)$ that minimizes the drag D for

[1] The principle was first known as Pontryagin's *maximum* principle and its proof is historically based on maximizing the Hamiltonian. The initial application of this principle was to the maximization of the terminal speed of a rocket. However, as it was subsequently mostly used for minimization of a performance index, it is normally referred to as the minimum principle.

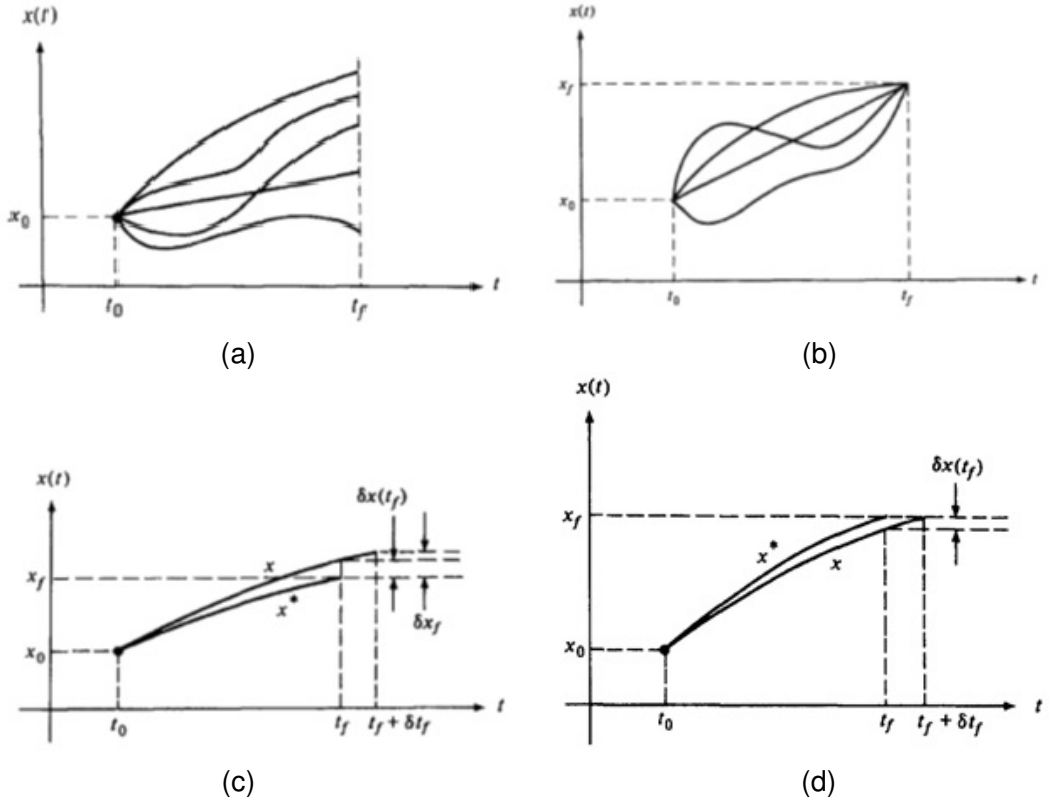

Figure 1.1: The possible types of boundary conditions: a) fixed time, free end point; b) fixed time, fixed end point; c) free time, free end point; d) free time, fixed end point.

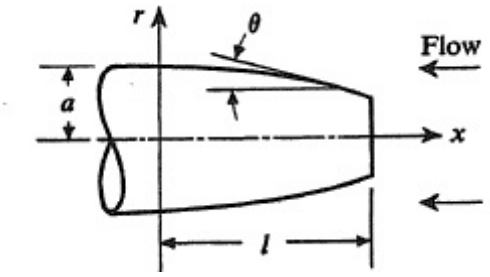

Figure 1.2: Minimum-drag nose shape (courtesy of[13]).

given values of the dynamic pressure (q), length of the body (l) and maximum radius of the body (a). First of all, one should take into account that the variation of the shape as a function of the radius r and the position x is given by

$$\tan\theta = -\frac{dr}{dx}, \tag{1.20}$$

where $\tan\theta$ is considered the control variable u. The variation of the pressure drag at zero angle of attack in a hypersonic flow is given by the following expression:

$$\frac{D}{4\pi q} = \frac{1}{2}[r(l)]^2 + \int_0^l \frac{ru^3}{1+u^2}dx. \tag{1.21}$$

Then, let us define the Hamiltonian as

$$H = \frac{ru^3}{1+u^2} + \lambda(-u). \tag{1.22}$$

The Euler-Lagrange equations are:

$$\dot{\lambda} = -\frac{\delta H}{\delta r} = -\frac{u^3}{1+u^2}, \tag{1.23}$$

$$\frac{\delta H}{\delta u} = \frac{ru^2(3+u^2)}{(1+u^2)^2} - \lambda = 0\ . \tag{1.24}$$

Replacing the previous λ into the Hamiltonian yields

$$H = \frac{ru^3}{1+u^2} - \frac{ru^2(3+u^2)}{(1+u^2)^2}u = \frac{ru^3(1+u^2) - ru^3(3+u^2)}{(1+u^2)^2} = -\frac{2ru^3}{(1+u^2)^2} = constant. \tag{1.25}$$

Looking into Fig. 1.2, one obtains that the initial boundary condition is given by $r(0) = a$. According to Eq. 1.53 and being $\phi[r(l), l] = \frac{1}{2}[r(l)]^2$, the optimal value of $r(l)$ is

$$\lambda(l) = r(l). \tag{1.26}$$

Thus, these two boundary conditions must be satisfied by the differential equation 1.20 and the conjugate equation 1.23. So, by replacing Eq. 1.26 into Eq. 1.24, we obtain the last boundary condition:

$$r(l)\left[1 - \frac{u^2(3+u^2)}{(1+u^2)^2}\right]_{x=l} = 0, \tag{1.27}$$

which yields $u(l) = 1$. Then, upon replacing $u(l)$ in Eq. 1.25, the Hamiltonian in the final boundary condition becomes $-H = \frac{r(l)}{2}$, which can be related to Eq. 1.25 again, resulting in the radius of the body, r, being a function of the slope, u:

$$\frac{r}{r(l)} = \frac{(1+u^2)^2}{4u^3}. \tag{1.28}$$

By replacing Eq. 1.20 in Eq. 1.28 one obtains:

$$\frac{dx}{dr} = -\frac{1}{u}, \tag{1.29}$$

$$\frac{l-x}{r(l)} = \int_l^u \frac{1}{u}\frac{d}{du}\frac{(1+u^2)^2}{4u^3}du, \tag{1.30}$$

$$\frac{l}{r(l)} = \frac{1}{4}(\frac{3}{4u_0^4} + \frac{1}{u_0^2} - \frac{7}{4} - log\frac{1}{u_0}). \tag{1.31}$$

1.3.2 Fixed terminal time, fixed end point

In this case, $\delta t_f = 0$ again. Consequently, Eq. 1.16 vanishes. Given that a fixed end point implies a constrained function, one should bear in mind the following constraint:

$$\psi[x(t_f), t_f] = 0. \tag{1.32}$$

The endpoint cost becomes:

$$\Phi = \phi + \nu^T \psi. \tag{1.33}$$

Therefore, Eq. 1.15 is used to solve the problem:

$$\lambda^T(t_f) = \left(\frac{\delta\phi}{\delta x} + \nu^T\frac{\delta\psi}{\delta x}\right)_{t=t_f}. \tag{1.34}$$

Finally, the initial condition $x(t_0)$ is given.

For example, the thrust-direction history, $\phi(t)$, is desired to be obtained when transfering a rocket vehicle (with constant thrust, T) from a given initial circular orbit to the largest possible circular orbit operating for a given length of time, t_f. The problem at hand is illustrated in Fig. 1.3.

The equations that govern the motion are:

$$\dot{r} = u, \tag{1.35}$$

$$\dot{u} = \frac{v^2}{r} - \frac{\mu}{r^2} + \frac{T\sin\phi}{m_0 - |\dot{m}|t}, \tag{1.36}$$

$$\dot{v} = -\frac{uv}{r} + \frac{T\cos\phi}{m_0 - |\dot{m}|t}, \tag{1.37}$$

where $\dot{r}$, $\dot{u}$ and $\dot{v}$ are the radial velocity of the spacecraft, the radial acceleration of the spacecraft and the tangential acceleration of the spacecraft, respectively.

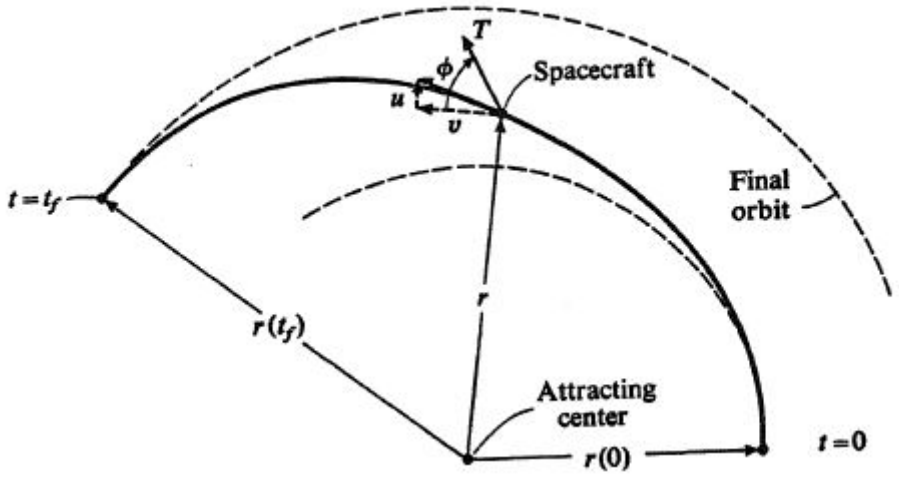

Figure 1.3: Maximum radius orbit transfer in a given time (courtesy of[13]).u is the radial component of the velocity, v is the tangential component of the veolocity, m is the mass of the spacecraft, $\dot{m}$ is the fuel consumption rate, r is the radial distance and μ is the gravitational parameter.

The boundary conditions are:

$$r(0) = r_0, \tag{1.38}$$

$$u(0) = 0, \tag{1.39}$$

$$v(0) = \sqrt{\frac{\mu}{r_0}}, \tag{1.40}$$

$$\psi_1 = u(t_f) = 0, \tag{1.41}$$

$$\psi_2 = v(t_f) - \sqrt{\frac{\mu}{r(t_f)}} = 0. \tag{1.42}$$

Once the equations of motions are defined, the Hamiltonian, H, can be obtained:

$$H = \lambda_r u + \lambda_u \left(\frac{v^2}{r} - \frac{\mu}{r^2} + \frac{T \sin\phi}{m_0 - |\dot{m}|t} \right) + \lambda_v \left(-\frac{uv}{r} + \frac{T\cos\phi}{m_0 - |\dot{m}|t} \right). \tag{1.43}$$

Equation 1.73 turns into:

$$\Phi = r(t_f) + \nu_1 u(t_f) + \nu_2 \left[v(t_f) - \sqrt{\frac{\mu}{r(t_f)}} \right]. \tag{1.44}$$

Once the system is presented, each value of $\dot{\lambda}$ is obtained by means of Eq. 1.12:

$$\dot{\lambda}_r = -\lambda_u[-\frac{v^2}{r^2} + \frac{2\mu}{r^3}] - \lambda_v \frac{uv}{r^2}, \tag{1.45}$$

$$\dot{\lambda}_u = -\lambda_r + \lambda_v \frac{v}{r}, \tag{1.46}$$

$$\dot{\lambda}_v = -\lambda_u \frac{2v}{r} + \lambda_v \frac{u}{r}. \tag{1.47}$$

Moreover, Eq. 1.13 must be also satisfied:

$$\frac{\delta H}{\delta \phi} = [\lambda_u \cos\phi - \lambda_v \sin\phi] \frac{T}{m_0 - |\dot{m}|t} = 0, \tag{1.48}$$

$$\tan\phi = \frac{\lambda_u}{\lambda_v}. \tag{1.49}$$

Eventually, the final boundary conditions are obtained by applying Equation 1.34:

$$\lambda_r(t_f) = 1 + \frac{\nu_2\sqrt{\mu}}{2[r(t_f)]^{3/2}}, \tag{1.50}$$

$$\lambda_u(t_f) = \nu_1, \tag{1.51}$$

$$\lambda_v(t_f) = \nu_2. \tag{1.52}$$

To conclude, all the differential equations are to be solved subject to the initial and final boundary conditions.

1.3.3 Free terminal time, free end point

In this case, $\delta\mathbf{x}_f = \delta\mathbf{x}(t_f)$. If there are no terminal state constraint, Eq. 1.15 becomes:

$$\lambda(t_f) = \frac{\partial \phi}{\partial \mathbf{x}}(\mathbf{x}(t_f)). \tag{1.53}$$

On the other hand, taking into account that a δt_f exists in this problem, one must recall Eq. 1.16 as a boundary condition in order to solve the problem:

$$\left[\frac{\delta\phi}{\delta t} + \frac{\delta\phi}{\delta x}\dot{x} + L\right]_{t=t_f} = 0. \tag{1.54}$$

Finally, the initial condition $x(t_0)$ is given.

1.3.3.1 Minimum-time solutions

One should take into account Eq. 1.55 when the performance index of interest is the minimum time to transfer the system from its initial to its final state:

$$\phi = 0 \qquad L = 1, \tag{1.55}$$

which implies that

$$J = t_f - t_0 \tag{1.56}$$

Hence, the TPBVP is set as:

$$\begin{aligned} \dot{x} &= f(x, u, t), && (1.57)\\ \dot{\lambda}_x &= -(f_x)^T \lambda, && (1.58)\\ \lambda(t_f) &= 0, && (1.59)\\ f_u^T \lambda &= 0, && (1.60)\\ (\lambda^T \dot{x})_{t=t_f} &= -1. && (1.61) \end{aligned}$$

Finally, another way to express Eq.1.61 is saying that the Hamiltonian at t_f must be 0 for minimum-time problems: $H(t_f) = 0$.

For example, a ship is travelling through a region of strong currents. The magnitude and direction of the current are known as functions of position: $u(x, y)$ and $v(x, y)$. Knowing that the velocity of the ship relative to the water is V, the equations of motion are known:

$$\begin{aligned} \dot{x} &= V\cos\theta + u(x, y), && (1.62)\\ \dot{y} &= V\sin\theta + v(x, y), && (1.63) \end{aligned}$$

being θ the heading angle of the ship's axis relative to the coordinate axes and (x, y) the position of the ship. The aim is to minimize the time of the ship travelling from A to B. The Hamiltonian, H, of the system is

$$H = \lambda_x(V\cos\theta + u) + \lambda_y(V\sin\theta + v) + 1. \tag{1.64}$$

The Euler-Lagrange equations are obtained using Eq. 1.58 and Eq. 1.60:

$$\dot{\lambda}_x = -\lambda_x \frac{\delta u}{\delta x} - \lambda_y \frac{\delta v}{\delta x}, \tag{1.65}$$

$$\dot{\lambda}_y = -\lambda_x \frac{\delta u}{\delta y} - \lambda_y \frac{\delta v}{\delta y}, \tag{1.66}$$

$$\frac{\delta H}{\delta \theta} = \lambda_x V \sin\theta - \lambda_y V \cos\theta = 0, \tag{1.67}$$

$$\tan\theta = \frac{\lambda_y}{\lambda_x}. \tag{1.68}$$

Adjoining Eq. 1.68 inside H, and knowing that this one must be 0 as the time is being minimized, the following is obtained:

$$\lambda_x = \frac{-\cos\theta}{V + u\cos\theta + v\sin\theta}, \tag{1.69}$$

$$\lambda_y = \frac{-\sin\theta}{V + u\cos\theta + v\sin\theta}. \tag{1.70}$$

Including both into one of the Euler-Lagrange equations, the following is obtained:

$$\dot{\theta} = sin^2\theta \frac{\delta v}{\delta x} + sin\theta cos\theta \left(\frac{\delta u}{\delta x} - \frac{\delta v}{\delta y} \right) - cos^2\theta \frac{\delta u}{\delta y}. \tag{1.71}$$

Finally, with the latter equation and both equations of motion, with the correct guess of θ_A , the desired minimum time paths will be given solving the problem with numerical methods.

1.3.4 Free terminal time, fixed end point

Given that a fixed end point implies a constrained function, one should bear in mind the following constraint:

$$\psi[x(t_f), t_f] = 0. \tag{1.72}$$

The endpoint cost becomes:

$$\Phi = \phi + \nu^T \psi. \tag{1.73}$$

Therefore, Eq. 1.15 is used to solve the problem:

$$\lambda^T(t_f) = \left(\frac{\delta \phi}{\delta x} + \nu^T \frac{\delta \psi}{\delta x} \right)_{t=t_f}. \tag{1.74}$$

On the other hand, taking into account that a δt_f exists in this problem, one must recall Eq. 1.16 as a boundary condition in order to solve the problem:

$$\Omega = \left[\frac{\delta\phi}{\delta t} + \nu^T \frac{\delta\psi}{\delta t} + \left(\frac{\delta\phi}{\delta x} + \nu^T \frac{\delta\psi}{\delta x}\right)\dot{x} + L\right]_{t=t_f} = 0. \tag{1.75}$$

Finally, the initial condition $x(t_0)$ is given.

1.3.4.1 Minimum-time solutions

The difference between a minimum-time solution when the end point is fixed and when it is not is that Eq. 1.75 becomes:

$$\Omega = \left[\nu^T \left(\frac{\delta\psi}{\delta t} + \frac{\delta\psi}{\delta x}\dot{x}\right) + 1\right]_{t=t_f} = 0. \tag{1.76}$$

Nevertheless, the previous equation still means that $H(t_f) = 0$ must be satisfied for any feasible solution.

1.4 Application of the optimal control theory to our problem

This dissertation wants to deal with the optimal control problem of an Earth-to-Moon trajectory with solar sail propulsion. The optimal solution obtained is based on time, that is to say, the spacecraft should take the least possible time to reach the Moon. In order to do this, given that the problem has a control variable, which is the normal vector of the solar sail, a state, which are the dynamical equations of the spacecraft, and initial and final boundary conditions, the problem can be treated with the TPBVP. The initial boundary conditions of the problem are the position and velocity of the spacecraft in a Geostationary Earth Orbit (GEO), and the final boundary conditions are the position and velocity of the spacecraft in a Low-Lunar Orbit (LLO). Therefore, given that the end point is constrained and the time of flight is free (and must be minimized), one can realize that we are dealing with a problem with free terminal time and fixed end point (Section 1.3.4). In order to apply the optimal control theory to this problem, firstly the differential equations must be defined, which are the dynamical equations from the Earth-to-Moon-Sun-spacecraft system.

Chapter 2

Dynamical model

The dynamical model adopted for this study is a Restricted Four-Body Problem (RFBP) perturbed by the solar radiation pressure. The four bodies involved are the spacecraft (s/c), the Earth, the Moon and the Sun. The *restriction* consists in the fact that the s/c does not affect the motion of the other three bodies. Furthermore, such motion is assumed to be *a priori* known. The pressure exerted by the solar radiation on the s/c constitutes a non-conservative perturbation and plays the role of the propulsion system since it is exploited to drive the sail from an initial geocentric orbit towards the Moon. The motion of the s/c is studied in an Earth-centered inertial frame. In this chapter we define the RFBP. Section 2.1 is dedicated to the definition of reference frames and related transformations. Section 2.2 illustrates the solar sail model and the acceleration produced by the solar radiation pressure. Sections 2.3-2.5 describe the gravitational accelerations acting on the s/c, whereas Section 2.6 deals with the double cone model employed to take care of the solar eclipses. Finally, Section 2.7 presents the system of equations that govern the motion of the s/c and a study of the variation of each acceleration as a function of the height.

2.1 Reference frames

2.1.1 The geocentric equatorial reference frame (GEQ)

The origin of GEQ (Fig. 2.1) is the center of mass of the Earth. GEQ is based on the Earth's Mean Equator and Equinox at 12:00 Terrestrial Time on 1 January 2000. The x-axis is aligned with the mean equinox, the z-axis is aligned with the Earth's spin axis or celestial North Pole. The y-axis is rotated by 90° East about the celestial equator.

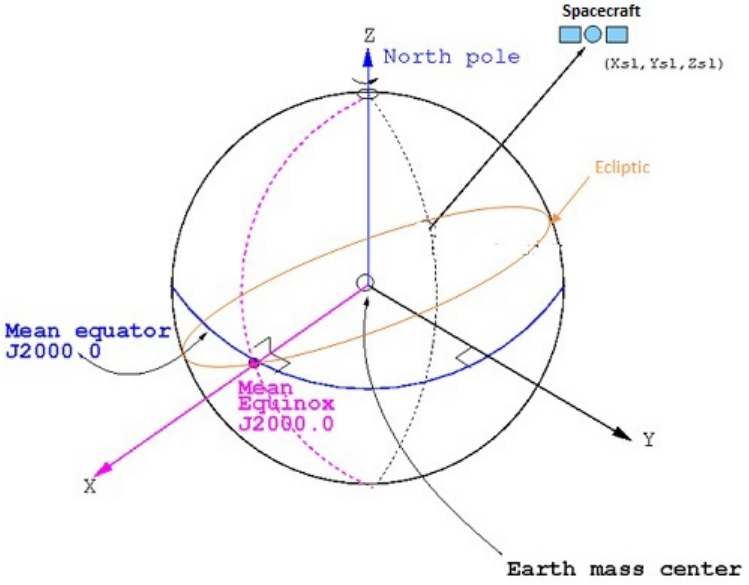

Figure 2.1: Representation of the GEQ reference frame[19].

2.1.2 The body-fixed reference frame

We shall indicate this reference frame (see Fig. 2.2 and[20]) by the names of its axes, i.e., $\mathbf{x}_b$, $\mathbf{y}_b$ and $\mathbf{z}_b$. The origin is set at the center of mass of the s/c and the orientation is determined by the direction of thrust: $\mathbf{y}_b$ is defined parallel to the vector normal to the solar sail (see later) and, consequently, to the thrust; $\mathbf{x}_b$ is orthogonal to $\mathbf{y}_b$ in the plane of the thrust direction; eventually, $\mathbf{z}_b = \mathbf{x}_b \times \mathbf{y}_b$.

2.1.3 Transformation from the body-fixed reference frame to GEQ

The equations of motion of the s/c shall be expressed in GEQ, but the thrust on the sail is oriented according to the normal to the sail (see Sect. 2.2) and hence

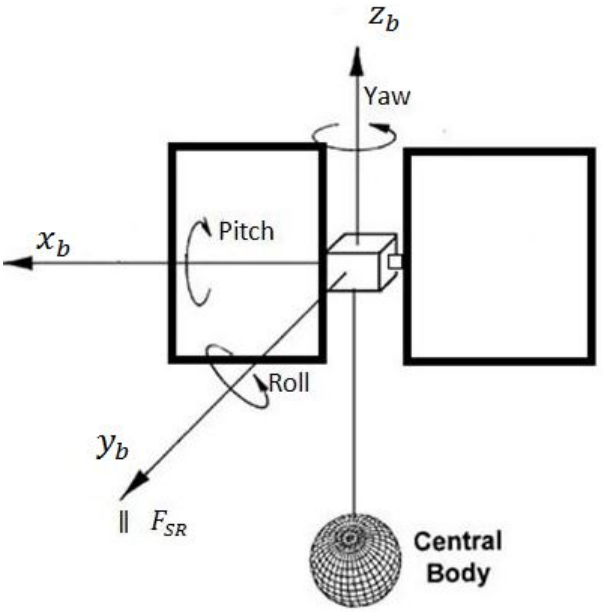

Figure 2.2: The body-fixed reference frame.

it is expressed in the body-fixed reference frame. The transformation required to change from body-fixed to GEQ consists in two rotations. In particular (see Fig. 2.3),

- a rotation around the x_b-axis by the angle $-\mu$ (pitch) between the orbital plane and the thrust direction;
- a rotation around the new z-axis (called z_1) by the angle $-\psi$ (yaw) between the velocity of the spacecraft and the thrust direction (this angle belongs to the orbital plane).

As a whole,

$$R_{body2NTW} = \begin{bmatrix} \cos\psi & -\sin\psi & 0 \\ \sin\psi & \cos\psi & 0 \\ 0 & 0 & 1 \end{bmatrix} \cdot \begin{bmatrix} 1 & 0 & 0 \\ 0 & \cos\mu & -\sin\mu \\ 0 & \sin\mu & \cos\mu \end{bmatrix}. \tag{2.1}$$

Eventually, the overall transformation from body-fixed to GEQ is represented by $R_{body2NTW}$. It shall be employed, for example, to express the thrust $\mathbf{F}_{SR}$ of the

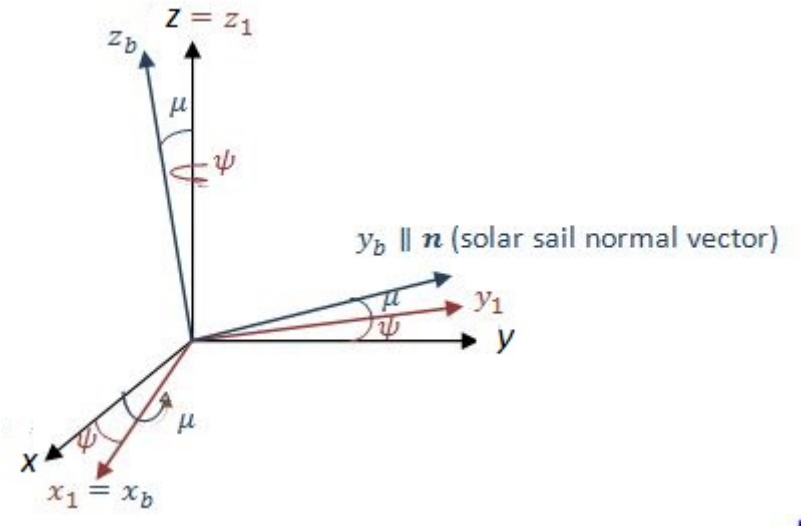

Figure 2.3: Rotation from the body-frame to NTW.

solar radiation pressure in GEQ:

$$\begin{pmatrix} F_{SRx} \\ F_{SRy} \\ F_{SRz} \end{pmatrix} = \begin{bmatrix} \cos\psi & -\sin\psi & 0 \\ \sin\psi & \cos\psi & 0 \\ 0 & 0 & 1 \end{bmatrix} \cdot \begin{bmatrix} 1 & 0 & 0 \\ 0 & \cos\mu & -\sin\mu \\ 0 & \sin\mu & \cos\mu \end{bmatrix} \mathbf{F}_{SRP}, \tag{2.2}$$

where

$$\mathbf{F}_{SRP} = F_{SRP}\mathbf{n}, \tag{2.3}$$

$\mathbf{n}$ being the normal to the sail, parallel to the y_b-axis (see Sect. 2.2).

2.2 The solar sail model

The photons of the solar radiation transfer momentum to a surface, thus exerting a pressure on it. The solar radiation pressure P_{SR} at a distance r from the Sun is

$$P_{SR} = \frac{S_\odot}{c}\left(\frac{r_0}{r}\right)^2 = 4.563\left(\frac{r_0}{r}\right)^2 \frac{\mu N}{m^2}, \tag{2.4}$$

$S_\odot$ being the solar constant (here 1368 W/m^2), c the speed of light in vacuum and r_0 the astronomical unit (1 AU). When impinging upon a large surface, the resulting force can be used to cause displacements, i.e., to propell a s/c. This is the principle of solar sails. Following[21], different levels of simplification for the optical characteristics of a solar sail result in different models for the magnitude and direction of the force acting on the sail:

- Ideal Reflection Model (IRM): the surface is ideally reflective.
- Non-Perfect Reflection Model (NPRM): sophisticated model that takes into account six optical coefficients of the solar sail film, each of which will be further explained later.
- Simplified Non-Perfect Reflection Model (SNPRM): pseudo-ideal model where the optical properties of the NPRM are simplified into a single coefficient.

In the IRM the force $\mathbf{F}_{SRP}$ applied by the photons incident at an angle α with the normal to a solar sail of area A is given by

$$\mathbf{F}_{SRP} = \left(2P_{SR}A\cos^2\alpha\right)\mathbf{n}, \tag{2.5}$$

as shown in Fig. 2.4.

The NPRM (Fig. 2.5) parametrizes the optical behaviour of the sail film by the optical coefficient set $\{\rho,\, s,\, \epsilon_f,\, \epsilon_b,\, B_f,\, B_b\}$, where ρ is the reflection coefficient, s is the specular reflection factor, ϵ_f and ϵ_b are the emission coefficients of the front and back side, respectively, and B_f and B_b are the non-Lambertian coefficients of the front and back side, respectively. For example, the optical coefficients for a solar sail with a highly reflective aluminum-coated front side and with a highly emissive chromium-coated back side are: ρ = 0.88, s = 0.94, ϵ_f = 0.05, ϵ_b = 0.55, B_f = 0.79, B_b = 0.55. In this case force has the following expression:

$$\mathbf{F}_{SRP} = 2P_{SR}A\cos\alpha\left[\left(a_1\cos\alpha + a_2\right)\mathbf{n} - a_3\sin\alpha\mathbf{t}\right], \tag{2.6}$$

with $\mathbf{t}$ the vector tangent to the sail and a_1, a_2 and a_3 the derived optical coefficients:

$$a_1 = \frac{1}{2}(1+s\rho), \tag{2.7}$$

$$a_2 = \frac{1}{2}\left[B_f(1-s)\rho + (1-\rho)\frac{\epsilon_f B_f - \epsilon_b B_b}{\epsilon_f + \epsilon_b}\right], \tag{2.8}$$

$$a_3 = \frac{1}{2}(1-s\rho). \tag{2.9}$$

Defining $\psi_n = a_1\cos\alpha + a_2$, $\psi_t = a_3\sin\alpha$ and $\psi = \sqrt{\psi_n^2 + \psi_t^2}$ allows to rewrite the magnitude of the force as follows

$$F_{SRP} = \left(2P_{SR}A\cos\alpha\right)\psi. \tag{2.10}$$

According to the SNPRM, s = 1 and $\epsilon_f B_f = \epsilon_b B_b$, which yields

$$\mathbf{F}_{SRP} = P_{SR} A \cos\alpha \left[(1+\rho)\cos\alpha \mathbf{n} - (1-\rho)\sin\alpha \mathbf{t}\right]. \tag{2.11}$$

The SNRPM reduces to the IRM when ρ = 1.

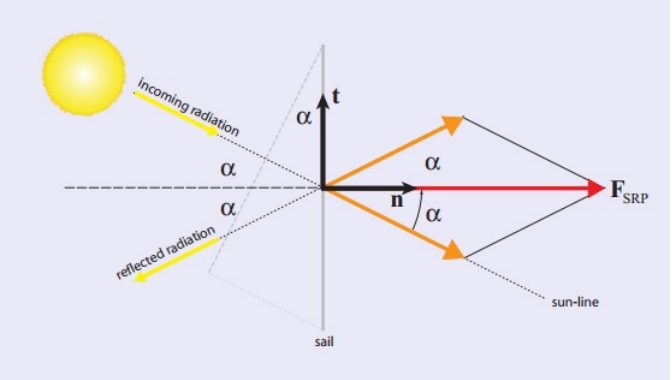

Figure 2.4: Ideal Reflection Model.

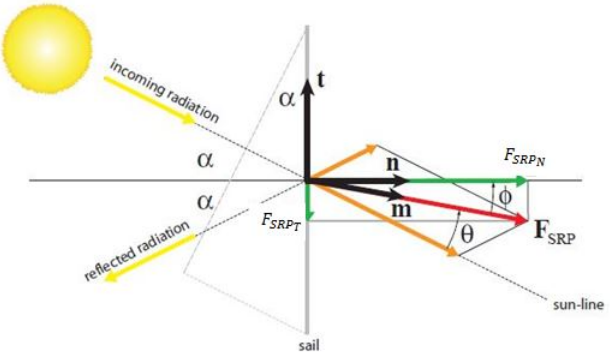

Figure 2.5: Non-Prefect Reflection Model: $\mathbf{m}$ is parallel to F_{SRP}, θ is the angle between the direction of sunlight and F_{SRP}, and ϕ is the angle between $\mathbf{n}$ and F_{SRP}.

The parameter called *characteristic acceleration* a_c is the acceleration imparted to a solar sail that is orthogonal ($\alpha = 0°$) to the direction of sunlight at 1 AU. For the IRM

$$a_{c,IRM} = \frac{2P_{SR}A}{m}, \tag{2.12}$$

whereas for the NPRM

$$a_{c,NPRM} = \frac{2P_{SR}A(a_1 + a_2)}{m}. \tag{2.13}$$

Defining the reflection efficiency η_{eff} as

$$\eta_{eff} = a_1 + a_2 = \frac{1}{2}\left[(1+s\rho) + B_f(1-s)\rho + (1-\rho)\left(\frac{\epsilon_f B_f - \epsilon_b B_b}{\epsilon_f + \epsilon_b}\right)\right], \tag{2.14}$$

allows to unify the expression of the characteristic acceleration for the three models:

$$a_c = \frac{2P_{SR}A\eta_{eff}}{m}. \tag{2.15}$$

For example, for a solar sail with a surface area of 50 m^2, η_{eff} = 1, $\alpha = 0^\circ$ at 1 AU from the Sun, F_{SRP} =$2P_{SR}A\eta_{eff}\cos^2\alpha$ = 456.3 μN.

The SNPRM is implemented in the trajectory analysis here presented, since this model is constrained to give the same characteristic acceleration modulus as the NPRM with η_{eff}. Given that the overall mass, m, of the s/c is 6 kgs, the acceleration of the s/c due to the solar radiation pressure in the body-fixed reference frame is

$$\mathbf{a}_{SRP} = \frac{\mathbf{F}_{SRP}}{m} = \frac{2P_{SR}A\eta_{eff}\cos^2\alpha}{m}\mathbf{n}. \tag{2.16}$$

Recalling Eq. 2.2 and coupling it with Eq. 2.16, the acceleration of the s/c in GEQ, $\mathbf{a}_{SRP}$ is:

$$\begin{pmatrix} a_{SRx} \\ a_{SRy} \\ a_{SRz} \end{pmatrix} = a_{SRP} \begin{bmatrix} \cos\psi & -\sin\psi & 0 \\ \sin\psi & \cos\psi & 0 \\ 0 & 0 & 1 \end{bmatrix} \cdot \begin{bmatrix} 1 & 0 & 0 \\ 0 & \cos\mu & -\sin\mu \\ 0 & \sin\mu & \cos\mu \end{bmatrix} \cdot \begin{pmatrix} 0 \\ 1 \\ 0 \end{pmatrix}. \tag{2.17}$$

2.3 The acceleration due to the terrestrial gravity field

In first approximation, the Earth can be treated as a homogeneous spherical body. As such, the gravitational potential U_{E0} that it produces at an external point P is the same as that due to a point with the same mass located at its center:

$$U_{E0}(P) = \frac{GM_E}{r}. \tag{2.18}$$

Here G is the gravitational constant, M_E is the mass of the Earth and r is the distance of P from the center. This potential is that which gives rise to two-body Keplerian orbits around the Earth. However, the Earth is a non-spherical, non-homogeneous body. And the closer we are to it the more important its deviations from sphericity and homogeneity become. The standard way to represent its potential at an external point is by the following expansion in spherical

harmonics ([22]):

$$U_E(P) = U_E(r,\phi,\lambda) = \frac{GM_E}{r}\left[1+\sum_{n=2}^{\infty}\left(\frac{R_E}{r}\right)^n\sum_{m=0}^{n}P_{nm}(\sin\phi)C_{nm}\cos m\lambda\right] + \frac{GM_E}{r}\sum_{n=2}^{\infty}\left(\frac{R_E}{r}\right)^n\sum_{m=0}^{n}P_{nm}(\sin\phi)S_{nm}\sin m\lambda, \quad (2.19)$$

where r, ϕ and λ are, respectively, the radial distance from the center, the latitude and the longitude of P in a body-fixed equatorial reference frame, the two series are sums over the degree n and the order m, respectively, P_{nm} are the associated Legendre functions of the second kind and C_{nm} and S_{nm} are the Stokes coefficients, functions of the mass distribution within the Earth:

$$P_{nm}(\sin\phi) = \frac{\cos^m\phi}{2^n n!}\frac{d^{n+m}}{d(\sin\phi)^{n+m}}(\sin^2\phi-1)^n, \quad (2.20)$$

$$C_{nm} = \frac{1}{M_E(R_E)^n}(2-\delta_{om})\frac{(n-m)!}{(n+m)!} \times \int (r')^n P_{nm}(\sin\phi')\cos m\lambda' dM_E, \quad (2.21)$$

$$S_{nm} = \frac{1}{M_E(R_E)^n}(2-\delta_{om})\frac{(n-m)!}{(n+m)!} \times \int (r')^n P_{nm}(\sin\phi')\sin m\lambda' dM_E. \quad (2.22)$$

Note that all the Stokes coefficients of the kind S_{n0} are null by construction, and the same holds for C_{10}, C_{11} and S_{11} which represent the coordinates of the centre of mass of the body (they are zero in a reference frame with origin in the center of mass of the Earth, such as GEQ), whereas C_{00} = 1.

The Stokes coefficients are measured by a wide range of terrestrial, airborne and spacecraft techniques. Global models exist such as EGM96[23], EGM2008[24], GRACE[25]. Table 2.1 lists the fully-normalized Stokes coefficients $\bar{C}_{nm}$, $\bar{S}_{nm}$ up to degree n = 3 and the associated standard deviations from the EGM96 model. The full normalization consists in multiplying each P_{nm} by the factor N_{nm},

$$N_{nm} = \sqrt{(2-\delta_{0m})(2n+1)\frac{(n-m)!}{(n+m)!}}, \quad (2.23)$$

and at the same time dividing each Stokes coefficient by the same factor.

The magnitude of the Stokes coefficients decreases as n increases. In general, the spherical harmonics decrease in magnitude as n increases and r increases.

n	m	$\bar{C}_{nm}$	$\bar{S}_{nm}$	$\Delta\bar{C}_{nm}$	$\Delta\bar{S}_{nm}$
0	0	1.000000000000E+00	0.000000000000E+00	0.00000000E+00	0.00000000E+00
1	0	0.000000000000E+00	0.000000000000E+00	0.00000000E+00	0.00000000E+00
1	1	0.000000000000E+00	0.000000000000E+00	0.00000000E+00	0.00000000E+00
2	0	-0.484165371736E-03	0.000000000000E+00	0.35610635E-10	0.00000000E+00
2	1	-0.186987635955E-09	0.119528012031E-08	0.10000000E-29	0.10000000E-29
2	2	0.243914352398E-05	-0.140016683654E-05	0.53739154E-10	0.54353269E-10
3	0	0.957254173792E-06	0.000000000000E+00	0.18094237E-10	0.00000000E+00
3	1	0.202998882184E-05	0.248513158716E-06	0.13965165E-09	0.13645882E-09
3	2	0.904627768605E-06	-0.619025944205E-06	0.10962329E-09	0.11182866E-09
3	3	0.721072657057E-06	0.141435626958E-05	0.95156281E-10	0.93285090E-10

Table 2.1: Fully-normalized EGM96 Stokes coefficients up to degree 3 and their standard deviations.

For practical applications, the series over the degree is truncated at a maximum index N which depends on the availability of the Stokes coefficients (see later) and must be appropriately determined on the basis of the accuracy sought and the relative importance of the neglected terms with respect to the level of the inaccuracies associated to other perturbations (such as atmospheric drag, solar radiation pressure, third-body accelerations, or even relativistic corrections to gravity) acting on the s/c.

For a trajectory starting at the radial distance of the geostationary orbit (GEO), approximately 42000 km from the Earth center, truncating the expansion Eq. 2.19 at the second zonal harmonic is satisfactory for our purposes. The corresponding potential at P looks like:

$$U_{2E}(P) = U_{2E}(r, \phi, \lambda) = \frac{GM_E}{r} + \frac{GM_E}{r}\left(\frac{R_E}{r}\right)^2 P_{20}(\sin\phi)C_{20}. \tag{2.24}$$

Upon substituting for $P_{20}(x)$ its expression $(3x^2 - 1)/2$,

$$P_{20} = \frac{3\sin^2\phi - 1}{2}, \tag{2.25}$$

and replacing C_{20} by the coefficient J_2 (see[26]),

$$J_2 = -\bar{C}_{20}\sqrt{5} = 1.08262668355 \cdot 10^{-3}, \tag{2.26}$$

Eq. 2.24 becomes

$$U_{2E}(P) = \frac{GM_E}{r}\left[1 - J_2\left(\frac{R_E}{r}\right)^2 \frac{(3\sin^2\phi - 1)}{2}\right]. \tag{2.27}$$

Later on, as the s/c crosses a pre-defined boundary (see Sec. 2.7.1), the zonal term can be neglected and Eq. 2.18 will be employed to determine the gravitational acceleration due to the Earth from there to the Moon. We recall that the second zonal harmonic describes the effect of the polar flattening of the Earth, responsible for an axially-symmetric perturbation. Eventually, the acceleration $\mathbf{a}_E$ of the s/c as produced by U_E (in any of its above-listed forms) is given by

$$\mathbf{a}_E(P) = \nabla U_E(P). \tag{2.28}$$

In particular,

$$\mathbf{a}_{0E}(P) = -\frac{GM_E}{r^3}\mathbf{r} \tag{2.29}$$

and

$$\mathbf{a}_{2E}(P) = -\frac{GM_E}{r^3}\begin{bmatrix} r_x - \frac{3}{2}J_2\left(\frac{R_E}{r}\right)^2 r_x\left(\frac{5r_x^2 - r^2}{r^2}\right) \\ r_y - \frac{3}{2}J_2\left(\frac{R_E}{r}\right)^2 r_y\left(\frac{5r_y^2 - r^2}{r^2}\right) \\ r_z - \frac{3}{2}J_2\left(\frac{R_E}{r}\right)^2 r_z\left(\frac{5r_z^2 - r^2}{r^2}\right) \end{bmatrix}, \tag{2.30}$$

where use has been made of the fact that

$$\sin\phi = \frac{r_z}{\sqrt{r_x^2 + r_y^2 + r_z^2}}. \tag{2.31}$$

2.4 The acceleration due to the lunar gravity field

The motion of the s/c in GEQ is perturbed by the lunar gravity field that, for our purposes, can be approximated with the field generated by a point of mass M_{Moon} located at its center. The corresponding acceleration is

$$\mathbf{a}_M(P) = GM_{Moon}\left(\frac{\mathbf{d}_M}{d_M^3} - \frac{\mathbf{r}_M}{r_M^3}\right), \tag{2.32}$$

where $\mathbf{d}_M$ is the position vector of the Moon relative to the s/c, $\mathbf{r}_M$ the position vector of the Moon in GEQ, and d_M and r_M the respective magnitude. Furthermore,

$$\mathbf{d}_M = \mathbf{r}_M - \mathbf{r}. \tag{2.33}$$

For the computation of Eq. 2.32 one needs to know the position of the Moon in GEQ as a function of time. Accurate ephemerides are available through, for example, the web site of the JPL Solar System's Dynamics group[27]. They can

be retrieved in the form of osculating elements or state vectors in the preferred reference frame at discrete time intervals. Then, such discrete data should be interpolated to obtain a continuous representation through time. Given that our study does not require such high accuracy, we resorted to the implementation of approximate formulas providing mean orbital parameters for the Moon[1]. The mean ecliptic orbital elements at the epoch 1 January 2000 at 12 TT are listed in Table 2.2. The table also explains the meaning of the symbols employed.

a_{M0}	e_{M0}	ω_{M0}	M_{M0}	i_{M0}	Ω_{M0}	n_{M0}	T_{M0}	$P_{\omega M0}$	$P_{\Omega M0}$
km	-	$^\circ$	$^\circ$	$^\circ$	$^\circ$	$^\circ$/day	days	years	years
384400	0.0554	318.15	135.27	5.16	125.08	13.176358	27.322	5.997	18.600

Table 2.2: Mean geocentric ecliptic orbital elements of the Moon at 1 January 2000, 12 TT[27]. From left to right: semimajor axis, eccentricity, argument of the perigee, mean anomaly, inclination, longitude of the ascending node, mean motion, orbital period, period of the perigee, nodal period.

For a given time t, the mean anomaly M_M, the longitude of the ascending node Ω_M and the argument of perigee ω_M are computed by the following linear relationships:

$$M_M = M_{M0} + n_{M0} \cdot t, \tag{2.34}$$

$$\Omega_M = \Omega_{M0} + P_{\Omega M0} \cdot t, \tag{2.35}$$

$$\omega_M = \omega_{M0} + P_{\omega M0} \cdot t. \tag{2.36}$$

Then, the eccentric anomaly E_M is approximated by solving Kepler's equation:

$$M_M = E_M - e_{M0} \sin E_M. \tag{2.37}$$

The perifocal coordinates of the Moon in its orbital plane are:

$$x_{Mp} = a_{M0}(\cos E_M - e_{M0}), \tag{2.38}$$

$$y_{Mp} = a_{M0}\sqrt{1 - e_{M0}^2} \sin E_M, \tag{2.39}$$

$$z_{Mp} = 0. \tag{2.40}$$

[1] It is worthwhile emphasizing that the modular structure of the code that implements the dynamical model allows to easily substitute this formulation with any other.

Next, the position of the Moon in ecliptic coordinates is given by

$$\begin{aligned} x_{Mec} &= (\cos\omega_M \cos\Omega_M - \sin\omega_M \sin\Omega_M \cos i)x_{Mp} \\ &- (\sin\omega_M \cos\Omega_M + \cos\omega_M \sin\Omega_M \cos i)y_{Mp}, \qquad (2.41) \\ y_{Mec} &= (\cos\omega_M \sin\Omega_M + \sin\omega_M \cos\Omega_M \cos i)x_{Mp} \\ &- (\sin\omega_M \sin\Omega_M - \cos\omega_M \cos\Omega_M \cos i)y_{Mp}, \qquad (2.42) \\ z_{Mec} &= (\sin\omega_M \sin i)x_{Mp} + (\cos\omega_M \sin i)y_{Mp}. \qquad (2.43) \end{aligned}$$

Eventually, a rotation around the x-axis of angle ϵ (the obliquity of the ecliptic, equal to 23.43928° at J2000.0) yields the equatorial coordinates sought:

$$\begin{aligned} x_M &= x_{Mec}, \qquad (2.44) \\ y_M &= y_{Mec}\cos\epsilon - z_{Mec}\sin\epsilon, \qquad (2.45) \\ z_M &= y_{Mec}\sin\epsilon + z_{Mec}\cos\epsilon. \qquad (2.46) \end{aligned}$$

Fig. 2.6 illustrates the orbit of the Moon computed for a time interval of one year since January 1st 2014.

2.5 The acceleration due to the solar gravity field

The motion of the s/c in GEQ is perturbed by the Sun's gravity field that, for our purposes, can be approximated with the field generated by a point of mass M_{Sun} located at its center. The corresponding acceleration is

$$\mathbf{a}_S(P) = GM_{Sun}\left(\frac{\mathbf{d}_S}{d_S^3} - \frac{\mathbf{r}_S}{r_S^3}\right), \qquad (2.47)$$

where $\mathbf{r}_S$ the position vector of the Sun in GEQ, $\mathbf{d}_S = \mathbf{r}_S - \mathbf{r}$ is the position vector of the Sun relative to the s/c and r_S and d_S the corresponding magnitudes. For the computation of Eq. 2.47, one also needs to know the position of the Sun in GEQ as a function of time. Accurate ephemerides can be found as well through the web site of the JPL Solar System's Dynamics group[28]. The mean ecliptic orbital elements of the Earth-to-Moon barycenter at the epoch 1 January 2000 at 12 TT are listed in Table 2.3. The table also explains the meaning of the symbols employed.

For a given time $t_S = \dfrac{JD - 2451545}{36525}$, where JD is the Julian Ephemeris Date, the semimajor axis a_S, the eccentricity e_S, the inclination i_S, the right ascension of the ascending node Ω_S, the longitude of the perihelion ϖ_S and the mean

a_{J2000}	$\dot{a}_{J2000}$	e_{J2000}	$\dot{e}_{J2000}$	i_{J2000}	$\dot{i}_{J2000}$
AU	AU/cty		1/cty	deg	deg/cty deg
1.00000261	0.00000562	0.01671123	-0.00004392	-0.00001531	-0.01294668
Ω_{J2000}	$\dot{\Omega}_{J2000}$	ϖ_{J2000}	$\dot{\varpi}_{J2000}$	L_{J2000}	$\dot{L}_{J2000}$
deg	deg/cty	deg	deg/cty	deg	deg/cty
0	0	102.93768193	0.32327364	100.46457166	35999.37244981

Table 2.3: Mean ecliptic orbital elements of the Earth-to-Moon barycenter at 1 January 2000, 12 TT[28]. From left to right and top to bottom: semimajor axis, rate of the semimajor axis, eccentricity, rate of the eccentricity, inclination, rate of the inclination, right ascension of the ascending node, rate of the right ascension of the ascending node, longitude of the perihelion, rate of the longitude of the perihelion, mean longitude, rate of the mean longitude (cty=century).

longitude L_S of the Earth-to-Moon barycenter are computed by the following linear relationships:

$$a_S = a_{J2000} + \dot{a}_{J2000} \cdot t_S, \tag{2.48}$$

$$e_S = e_{J2000} + \dot{e}_{J2000} \cdot t_S, \tag{2.49}$$

$$i_S = i_{J2000} + \dot{i}_{J2000} \cdot t_S, \tag{2.50}$$

$$\Omega_S = \Omega_{J2000} + \dot{\Omega}_{J2000} \cdot t_S, \tag{2.51}$$

$$\varpi_S = \varpi_{J2000} + \dot{\varpi}_{J2000} \cdot t_S, \tag{2.52}$$

$$L_S = L_{J2000} + \dot{L}_{J2000} \cdot t_S. \tag{2.53}$$

Therefore, the argument of the perihelion, ω_S, and the mean anomaly, M_S, are computed:

$$\omega_S = L_S - \omega_S, \tag{2.54}$$

$$M_S = L_S - \omega_S. \tag{2.55}$$

Then, the eccentric anomaly E_S is approximated by solving Kepler's equation:

$$M_S = E_S - e_S sin E_S. \tag{2.56}$$

The perifocal coordinates of the Earth-to-Moon barycenter in its orbital plane are:

$$x_{Sp} = a_S(\cos E_S - e_S), \tag{2.57}$$

$$y_{Sp} = a_S\sqrt{1 - e_S^2}\sin E_S, \tag{2.58}$$

$$z_{Sp} = 0. \tag{2.59}$$

Next, the position of the Sun with reference to the Earth-to-Moon barycenter in ecliptic coordinates is given by:

$$\begin{aligned} x_{Sec} &= (-\cos\omega_S\cos\Omega_S + \sin\omega_S\sin\Omega_S\cos i_S)x_{Sp} \\ &+ (\sin\omega_S\cos\Omega_S + \cos\omega_S\sin\Omega_S\cos i_S)y_{Sp}, \qquad (2.60) \\ y_{Sec} &= -(\cos\omega_S\sin\Omega_{SM} + \sin\omega_S\cos\Omega_S\cos i)x_{Sp} \\ &+ (\sin\omega_S\sin\Omega_S - \cos\omega_S\cos\Omega_S\cos i_S)y_{Sp}, \qquad (2.61) \\ z_{Sec} &= -(\sin\omega_M\sin i_S)x_{Mp} - (\cos\omega_M\sin i_S)y_{Mp}. \qquad (2.62) \end{aligned}$$

Finally, a rotation around the x-axis of angle ϵ (the obliquity of the ecliptic, equal to 23.43928° at J2000.0) yields the equatorial coordinates desired:

$$\begin{aligned} x_S &= x_{Sec}, \qquad (2.63) \\ y_S &= y_{Sec}\cos\epsilon - z_{Sec}\sin\epsilon, \qquad (2.64) \\ z_S &= y_{Sec}\sin\epsilon + z_{Sec}\cos\epsilon. \qquad (2.65) \end{aligned}$$

Fig. 2.7 illustrates the orbit of the Sun computed for a time interval of one year since January 1^{st} 2014.

2.6 Eclipse model

2.6.1 Solar eclipses due to the Earth

There are two different ways of calculating eclipses: the cylinder model and the double-cone model. The first one is not only much more simplified than the latter, but it also disregards the penumbra caused by the Earth. Consequently, in order to make the study more detailed, the best way to model the solar eclipses caused by the Earth is with a double-cone geometry (Fig. 2.8).

Knowing the average distance between the Earth and the Sun, $r_S = 150 \cdot 10^6$ km, the Earth radius, $R_E = 6378$ km, and the Sun radius, $R_S = 7 \cdot 10^5$ km, all the geometry parameters inside Fig. 2.8 are obtained by the following formulation:

$$\begin{cases} R_S = (L + r_S)\sin\alpha \\ R_E = L\sin\alpha \end{cases}, \qquad (2.66)$$

where L is the distance between the umbra cone vertex and the centre of the Earth. Then,

$$(L + r_S)R_E = LR_S, \qquad (2.67)$$

which yields

$$L = \frac{r_S R_E}{R_S - R_E} = 1.38 \cdot 10^6 \quad \text{km}. \tag{2.68}$$

As a result,

$$\alpha = \sin^{-1}\left(\frac{R_E}{L}\right) = 0.26^\circ, \tag{2.69}$$

where α is the semiaperture of the umbra cone. In the same way as above,

$$\begin{cases} R_S = (r_S - Q)\sin\beta, \\ R_E = Q\sin\beta, \end{cases}, \tag{2.70}$$

where Q is the distance between the penumbra cone vertex and the centre of the Earth. Then,

$$(r_S - Q)R_E = QR_S, \tag{2.71}$$

which yields

$$Q = \frac{r_S R_E}{(R_E + R_S} = 1.35 \cdot 10^6 \quad \text{km}, \tag{2.72}$$

Therefore,

$$\beta = \sin^{-1}(\frac{R_E}{Q}) = 0.27^\circ. \tag{2.73}$$

where β is the semiaperture of the penumbra cone. Finally,

$$h = (L + Q)\tan\beta = 1.29 \cdot 10^4 \quad \text{km}. \tag{2.74}$$

If the s/c is on the same side as the Sun with respect to the Earth, it is not in eclipse. Therefore, one should check if the s/c is inside the penumbra or umbra regions in order to know whether it is in eclipse or not. In Fig. 2.8, y is the height of the s/c on the antisun line, which is the axis of the umbra and penumbra cones, and x is the projection of the position of the s/c on the antisun line:

$$x = \mathbf{u}_{sun} \cdot \mathbf{r}. \tag{2.75}$$

where $\mathbf{u}_{sun}$ is the Sun-Earth's unit vector and $\mathbf{r}$ is the distance of the s/c from the centre of the Earth. Then, the size of the penumbra cone, d_1 in Fig. 2.8, is determined in the location of the s/c. Since the distance between T and U in Fig. 2.8 is very small, d_1 is calculated through geometry as follows:

$$d_1 = x\sin\beta \simeq x\beta \quad (\text{approximation of small angles}). \tag{2.76}$$

Note that $\beta \simeq \alpha$, besides

$$\alpha = \frac{R_S}{r_S} \tag{2.77}$$

assuming that r_S is much bigger than L. Consequently, d_2 (Fig. 2.8) equates to d_1 and both distances are called d from now onwards. The radius of the penumbra cone at the location of the s/c, r_p, is given by:

$$r_p = R_E + d. \tag{2.78}$$

Thus, if $y > r_p$, the s/c is not in eclipse. Taking into account that the two segments indicated with d in Fig. 2.8 are equal under the approximation $\beta \simeq \alpha$, the radius of the umbra cone at the location of the s/c, r_s, is given by:

$$r_s = r_p - 2d. \tag{2.79}$$

As a result, if $y < r_s$, the s/c is in total eclipse.

If the s/c is located between r_s and r_p, it is in partial eclipse. In this case, one proceeds to the computation of the circular segment of the disk of the sun that is visible: we assume that the cut produced by the Earth's disk is a line segment (see Fig. 2.9).

Let us call ξ the visible fraction of the angular diameter of the Sun:

$$\xi = \frac{y - r_s}{2d}. \tag{2.80}$$

As a matter of fact, if $y = r_s$, $\xi = 0$ and the s/c is on the surface of the umbra cone and hence in total eclipse, whereas if $y = 2d + r_s$, $\xi = 1$ and the s/c is located on the surface of the penumbra cone and thus it is not in eclipse. σ is the angle indicated in Fig. 2.9:

$$\sin\sigma = 2\xi - 1. \tag{2.81}$$

If $\xi = 0$ (total eclipse), $\sigma = -90°$, whereas if $\xi = 1$, $\sigma = +90°$ (no eclipse). Then,

$$\psi = \pi + 2\beta. \tag{2.82}$$

The fraction of the visible portion is given by the area of the circular segment subtended by ψ (=$\psi/2\pi$) and the area of the triangle OAB $(\psi/2 + \cos\sigma \sin\sigma)\pi$ (here one is treating the sun's disk as having unit radius).

2.6.2 Solar eclipses due to the Moon

The best way to model the solar eclipses caused by the Moon is with a double-cone geometry as well (Fig. 2.10).

Knowing the average distance between the Moon and the Sun, r_{SM}, the Moon radius, R_M, and the Sun radius, R_S, all the geometry parameters are obtained by the same formulation as for the Earth from Eq. 2.66 to 2.74:

$$L_M = \frac{r_{SM}R_M}{R_S - R_M} = 364232 \quad \text{km}, \tag{2.83}$$

$$\alpha_M = \sin^{-1}\left(\frac{R_m}{L_M}\right) = 0.27^\circ, \tag{2.84}$$

$$Q_M = \frac{r_{SM}R_M}{R_M + R_S} = 363713.21 \quad \text{km}, \tag{2.85}$$

$$\beta_M = \sin^{-1}(\frac{R_M}{Q_M}) = 0.27^\circ, \tag{2.86}$$

$$h_M = (L_M + Q_M)\tan\beta_M = 3430.39 \quad \text{km}. \tag{2.87}$$

As a result, since $\alpha_M \simeq \beta_M$ and the Sun is much bigger than the Moon, all the approximations carried out for the computation of Earth eclipses are also considered for the Moon eclipses. Consequently, knowing that y_M is the height of the s/c on the antisun line and x_M is the projection of the position of the s/c on the antisun line

$$x_M = \mathbf{u}_{sun-moon} \cdot \mathbf{r}_{M-S}. \tag{2.88}$$

where $\mathbf{u}_{sun-moon}$ is the Sun-Moon's unit vector and $\mathbf{r}_{M-S}$ is the distance of the s/c from the centre of the Moon. Then, the size of the penumbra cone, d_{1M} in Fig. 2.10, is determined in the location of the s/c. Since the distance between T and U in Fig. 2.10 is very small, d_{1M} is calculated through geometry as follows:

$$d_{1M} = x_M \sin\beta_M \simeq x_M\beta_M \quad (\text{approximation of small angles}). \tag{2.89}$$

Under the approximation aforementioned, one have

$$\alpha_M = \frac{R_S}{r_{SM}}, \tag{2.90}$$

$$d_{1M} = d_{2M} = d_M. \tag{2.91}$$

The radius of the penumbra cone at the location of the s/c, r_{pM}, is given by:

$$r_{pM} = R_M + d_M. \tag{2.92}$$

Thus, if $y_M > r_{pM}$, the s/c is not in eclipse. Taking into account that the two segments indicated with d_M in Fig. 2.10 are equal under the approximation $\beta_M \simeq \alpha_M$, the radius of the umbra cone at the location of the s/c, r_{sM}, is given by:

$$r_{sM} = r_{pM} - 2d_M. \tag{2.93}$$

As a result, if $y_M < r_{sM}$, the s/c is in total eclipse. If the s/c is located between r_{sM} and r_{pM}, it is in partial eclipse. In this case, one proceeds to the computation of the circular segment of the disk of the sun that is visible: we assume that the cut produced by the Moon's disk is a line segment (see Fig. 2.9). Let us call ξ the visible fraction of the angular diameter of the Sun:

$$\xi = \frac{y - r_s}{2d}. \tag{2.94}$$

As a matter of fact, if $y_M = r_{sM}$, $\xi = 0$ and the s/c is on the surface of the umbra cone and hence in total eclipse, whereas if $y_M = 2d_M + r_{sM}$, $\xi = 1$ and the s/c is located on the surface of the penumbra cone and thus it is not in eclipse. σ is the angle indicated in Fig. 2.9:

$$\sin\sigma = 2\xi - 1. \tag{2.95}$$

If $\xi = 0$ (total eclipse), $\sigma = -90°$, whereas if $\xi = 1$, $\sigma = +90°$ (no eclipse). Then,

$$\psi = \pi + 2\beta_M. \tag{2.96}$$

The fraction of the visible portion is given by the area of the circular segment subtended by ψ (=$\psi/2\pi$) and the area of the triangle OAB $(\psi/2 + \cos\sigma\sin\sigma)\pi$ (here one is treating the sun's disk as having unit radius).

2.6.3 Eclipses in geocentric orbits

In theory, there are two eclipse periods for GEO throughout a whole year. These periods happen some days before and after the fall and spring equinoxes, with a maximum eclipse duration of 1.2 hours the same day of the equinoxes. Consequently, looking into Fig. 2.11, one can see that the formulation is correct since the peak eclipse duration also happens the 21^{st} of March and September and is equal to 1.2 hours.

Now, the eclipses due to the Moon and the Earth are going to be compared between all the dynamical model programmed in Fortran and the STK when the s/c is located at an orbit with the following characteristics:

Perigee height: h_{pe} = 300 km,
apogee height: h_{ae} = 35786 km,
Inclination: i_e = 28.6^{o}.

Again, the computations are carried out throughout an entire year by means of the code and STK. Regarding the eclipses caused by the Earth, looking into Fig. 2.12 left, the maximum eclipse duration matches with the 21^{st} of March and has a maximum duration of 2.25 hours. On the other side, the minimum happens the 20^{th} of September with a duration of 0.4 hours. These results are similar to the ones obtained with the code (Fig. 2.12 right). Moreover, the duration of the eclipses computed with STK equate to the ones computed with the code as time passes. As far as the eclipses due to the Moon are concerned, a partial eclipse is produced the 23^{rd} of October with a maximum duration of 0.33 hours. Actually, this partial eclipse also happens with STK, but at the same time that an Earth eclipse occurs, thus it cannot be perceived in STK.

2.7 Equations of motion of the spacecraft

The motion of the spacecraft is determined by the forces described in the previous sections. An illustration of the dynamical model is shown in Fig. 2.14.

The acceleration of the satellite in the GEQ reference frame is composed by :

$$\mathbf{a} = \mathbf{a}_E + \mathbf{a}_M + \mathbf{a}_S + f \cdot \mathbf{a}_{SR} \tag{2.97}$$

where the factor f takes into account whether the s/c is in eclipse (f = 0) or not (f = 1).

2.7.1 Variation of the accelerations as a function of height

In Fig. 2.15 it is shown the resulting orbit trajectory of a s/c subjected to a thrust parallel to the velocity and equal to 16 mN throughout a period of 160 days in the dynamical model aforementioned (the spiralling in red).

where the blue line is the Moon trajectory. All the acceleration components that appear along all the above trajectory (and explained throughout the whole dynamical model chapter) are studied separately (Fig. 2.16) in order to understand the order of magnitude of each one. The aim is to find out when the perturbation due to Earth's J2 parameter can be considered null. Therefore, how the different accelerations in Eq. 2.97 vary whilst the distance of the s/c with respect to the Earth increases are shown in Fig. 2.16.

Firstly, looking into Fig. 2.16, one can perceive that the acceleration due to the solar radiation pressure does not vary whatsoever. One can also see that the closer the s/c is of the Moon and the Sun, the more significant their acceleration contributions become. On the other hand, it is easy to understand that the further the s/c is from the Earth, the less noticeable the acceleration due to it's gravity field is. Therefore, it can be concluded that from $1.5 \cdot 10^5$ km onwards, the acceleration due to the J2 parameter is several orders of magnitude smaller than the perturbation caused by the Moon, the Sun, F_{SRP} and the Earth's spherical gravity field. Thus, this parameter can be completely disregarded when the satellite reaches this distance.

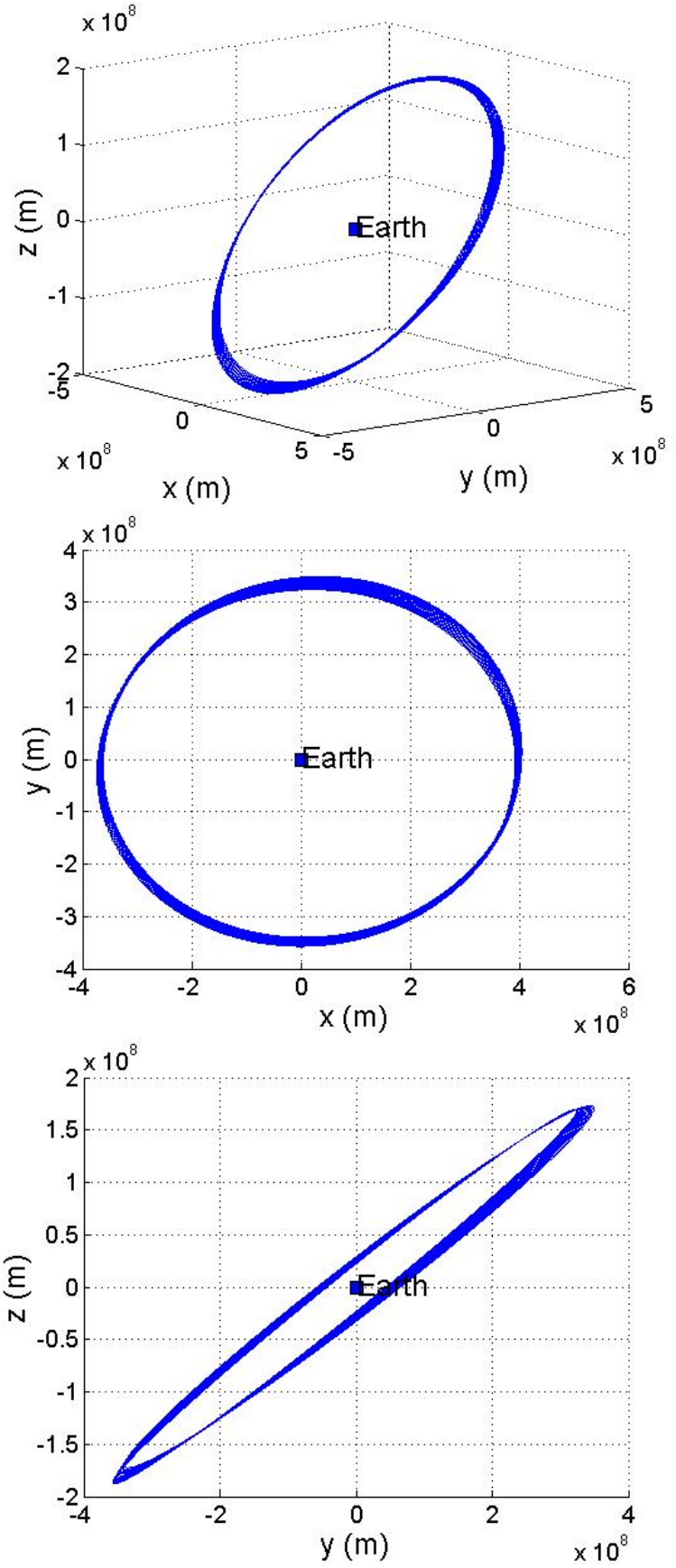

Figure 2.6: Approximate orbit of the Moon over one year: 3D view (top), xy-projection (middle), yz-projection (bottom).

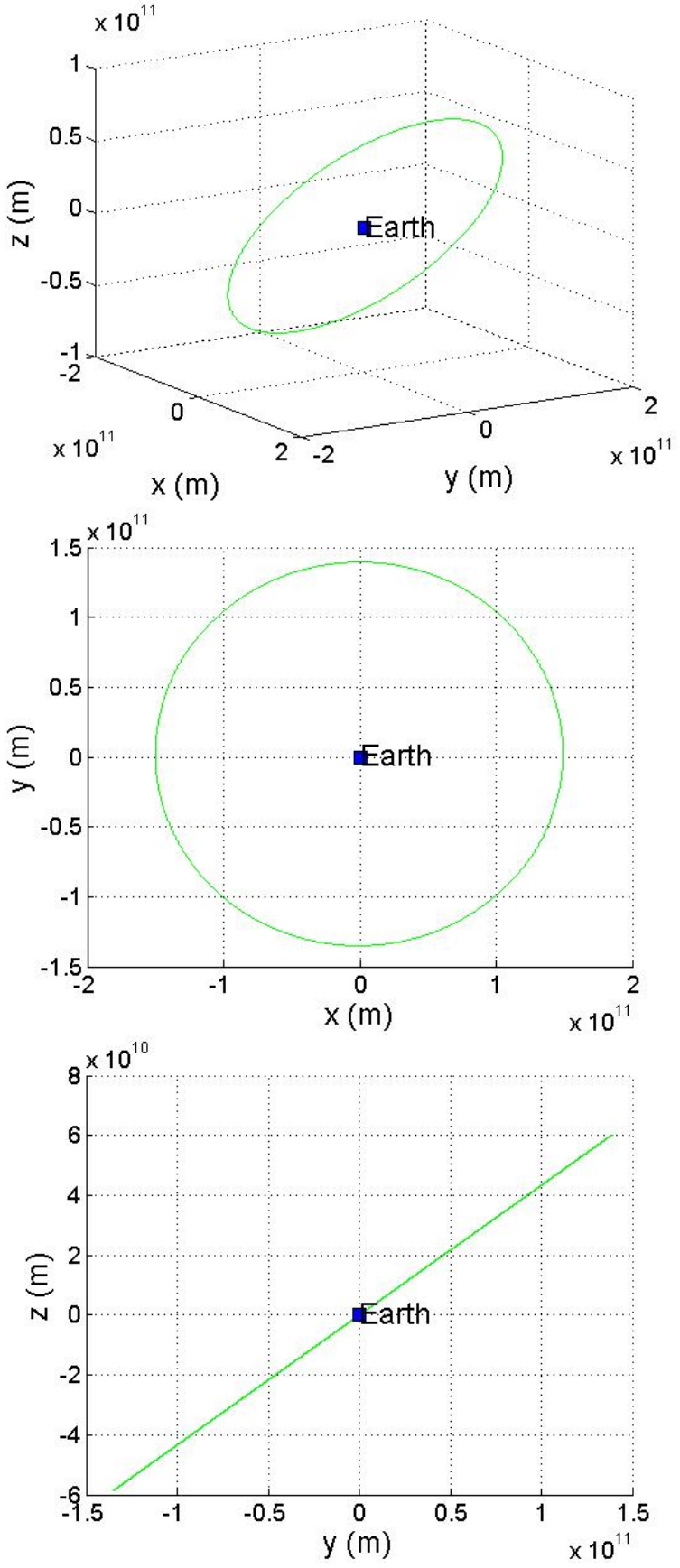

Figure 2.7: Approximate orbit of the Sun over one year: 3D (top), xy-projection (middle), yz-projection (bottom).

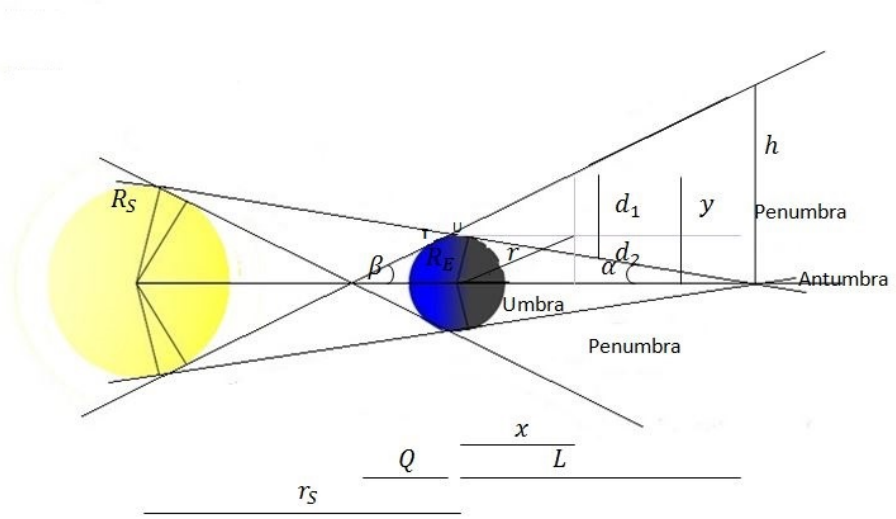

Figure 2.8: Double-cone Earth eclipse

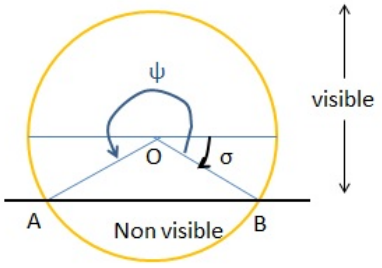

Figure 2.9: Partial eclipse model

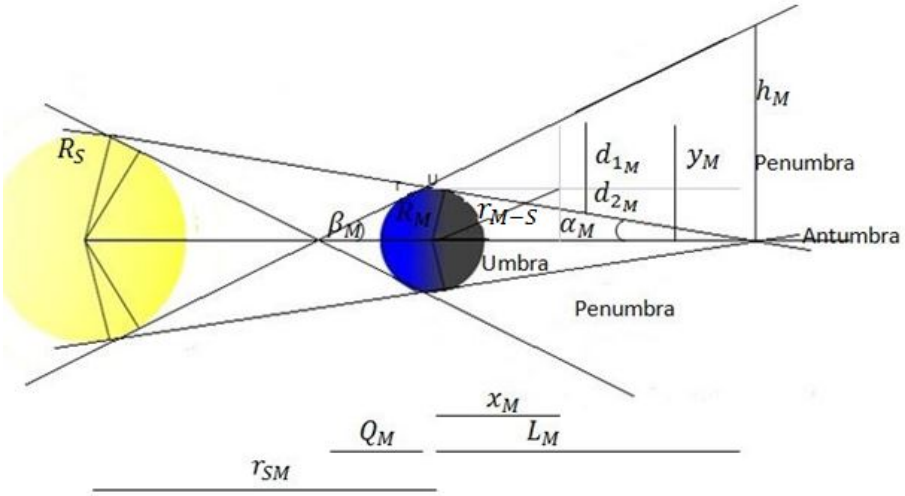

Figure 2.10: Double-cone Moon eclipse

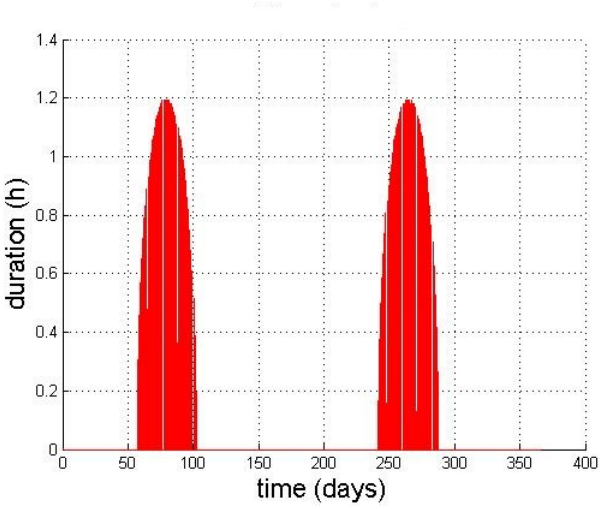

Figure 2.11: GEO eclipses by means of the code.

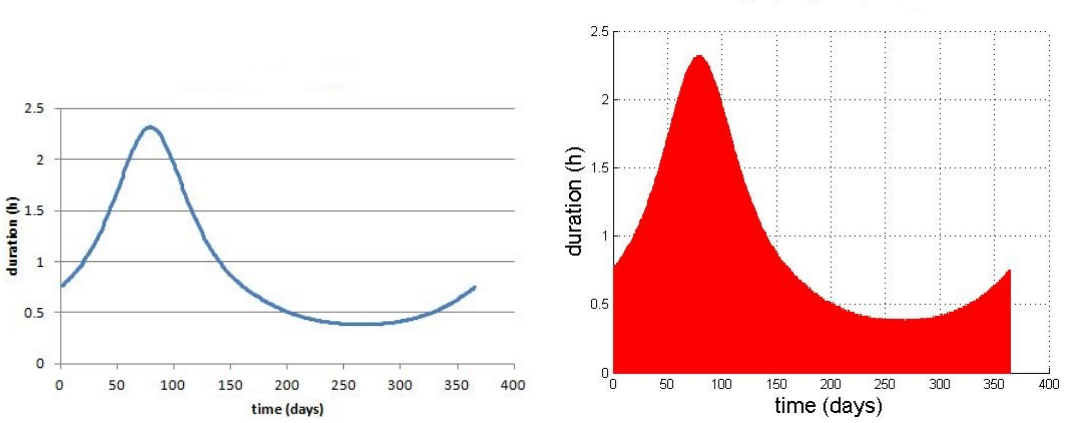

Figure 2.12: Duration of Earth eclipses: STK (left), code (right).

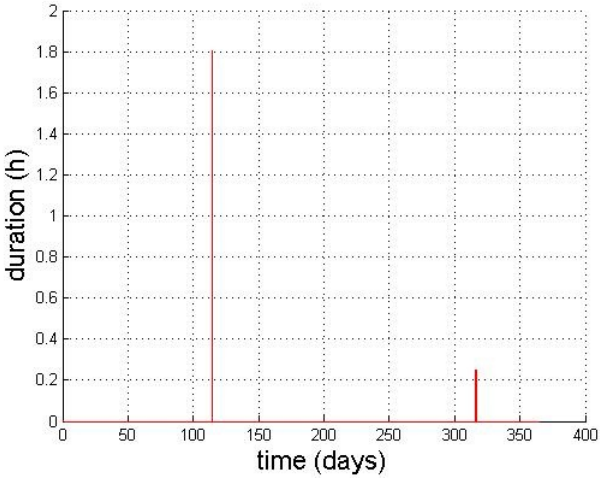

Figure 2.13: Duration of Moon eclipses.

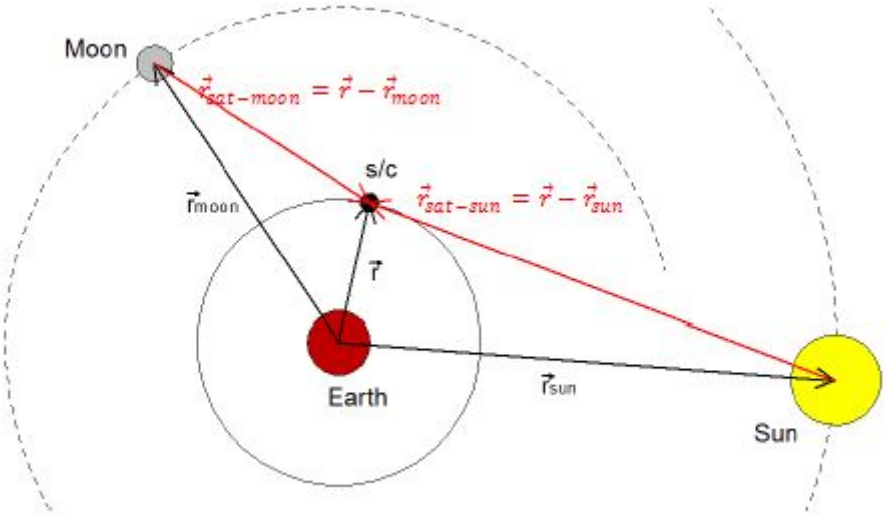

Figure 2.14: Dynamical model in the GEQ reference frame[10].

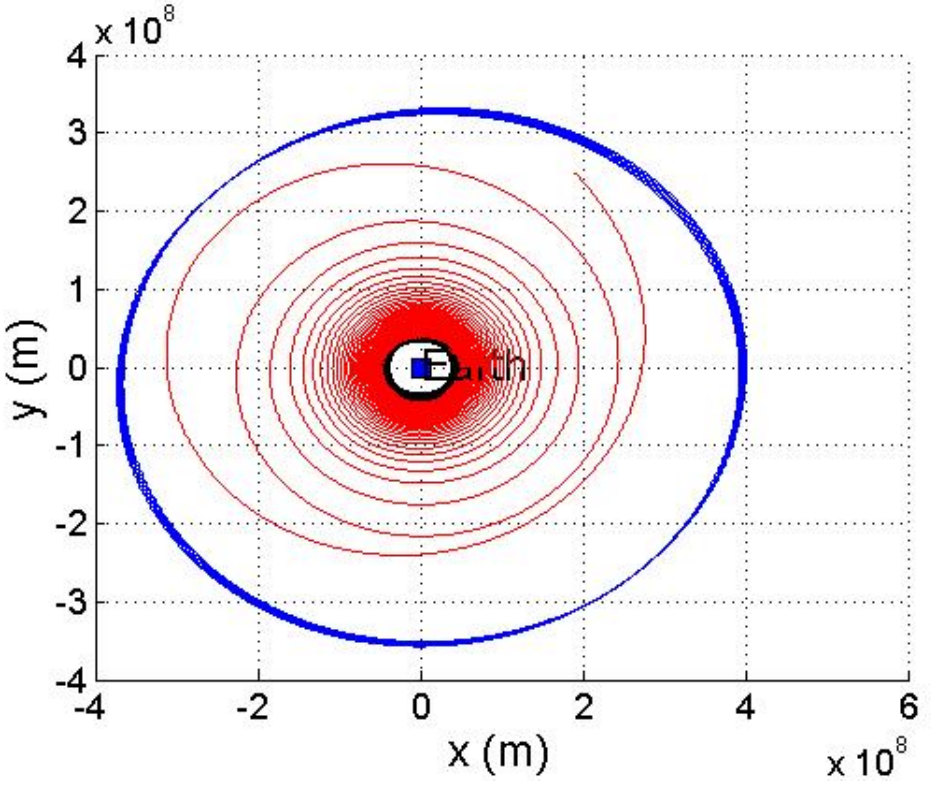

Figure 2.15: Trajectory for a period of 160 days,

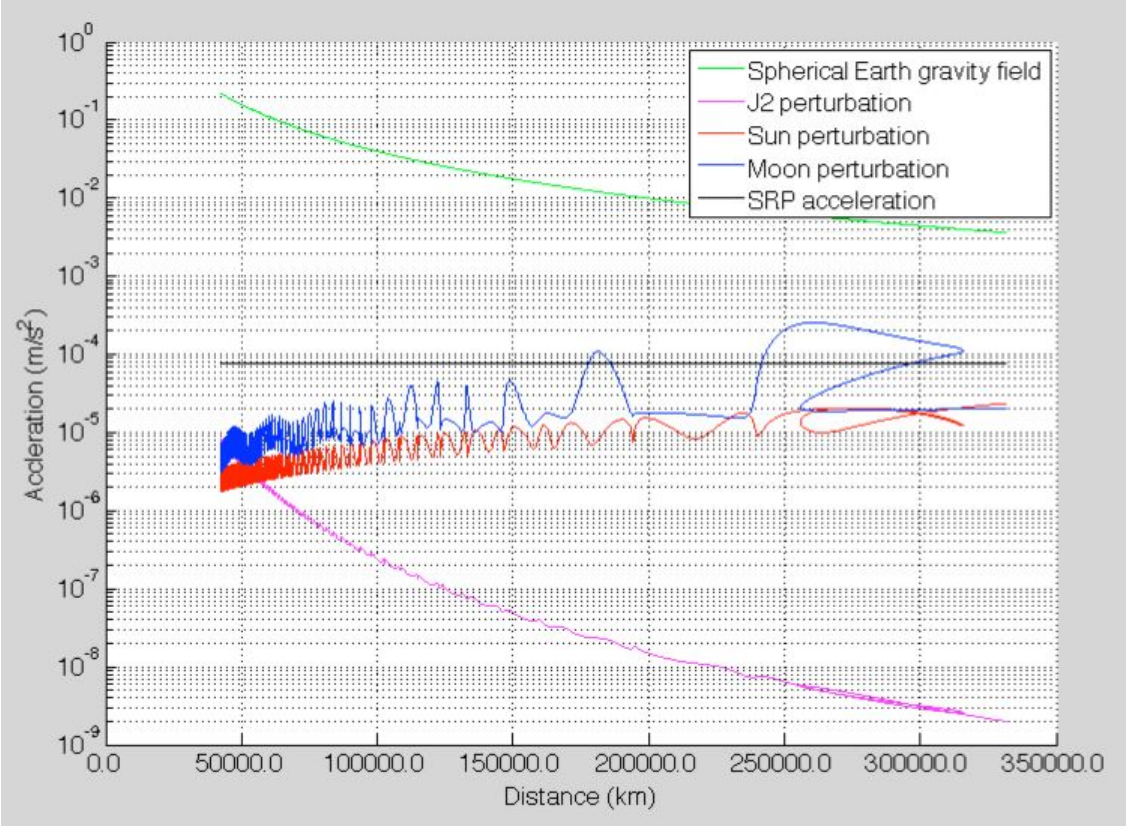

Figure 2.16: Variation of the accelerations of the s/c in a trajectory throughout 160 days.

Chapter 3

Solution of nonlinear problems

Nonlinear problems are similar to linear problems because they imply an objective function and general constraints. Nevertheless, unlike linear sytems, nonlinear systems do not satisfy the superposition principle, i.e., the output of this system is not directly proportional to the input. Given that the output of an optimal control problem is not directly proportional to the input parameters, optimal control problems are nonlinear. In order to face the problem presented in this dissertation, MINPACK-1 is used. MINPACK-1 includes Fortran subprograms for the numerical solution of systems of nonlinear equations. The subroutines used from this package are further explained later. Section 3.1 describes the difficulties of nonlinear programming and how to increase the probability of a successful solution. Section 3.2 explains how MINPACK-1 works and the different subroutines that it includes. Finally, the mathematical background of the subroutines used to solve our problem is explained in Section 3.3.

3.1 Nonlinear models

By means of the objective function, the state, the constraints and the Hessian matrix ([29]), nonlinear programs find out when and where there is a local maximum or minimum inside the problem. Yet, there is no way of knowing whether it is a global optimum or not. What is more, there can be optimum solutions anywhere in nonlinear problems: at an extreme point, along an edge or in inside of a feasible region. To make it worse, there could be many feasible regions that are not connected since nonlinear constraints can twist and lead to many

feasible regions where there could be a better optimal solution than in another region (see Fig. 3.1).

Figure 3.1: Left: feasible regions. Right: evaluation of a region.

Another distinctive feature of nonlinear programs is that different starting points may lead to different final solutions. This happens because the algorithm chooses a direction for searching the optimal value, and finds the best value of the objective function in that direction. This solution is inside a valley, and multiple starting points may end up in the same solution (peak of the valley). Nonetheless, if the starting point is inside another valley, the final solution would be obviously different. Therefore, the best way to solve the problem is **starting the problem from many different initial points**, despite being too much time consuming. It tends to be difficult to find a feasible starting point: in most cases, the problem does not converge and it is required to start the program again with another starting point. It is therefore impossible to know exactly if the model is unfeasible if no feasible solution is found because maybe the optimal solution is reached with another starting point. Given that equations are continuously twisting, finding a solution that satisfies the problem may be difficult, but even if a solution is found out, it may be violated when the algorithm moves to another point.

Choosing an algorithm to solve the problem may be also difficult given that there are some who work taking into account the algebraic structure of the problem (quadratic, polynomial, etc.) and others the shape of the problem (concavity and convexity). The main drawback is that it is often difficult to know, for example, whether the constraint is concave or not in the region of interest. Given that these algorithms work iteratively improving the initial guess until certain conditions are met, if the way the algorithm improves the initial point is different from another algorithm, these two may lead to different solutions.

There are some issues to bear in mind in order to increase the probability of a succesful solution:

- Use an existing nonlinear problem solver.
- Try a simpler formulation in order to increase the efficiency.
- Know the characteristics of your model before choosing a solution algorithm. MINPACK-1 is used in this thesis ([34]).
- Try to provide a good starting point. The best way is to solve a similar problem before and use this guess to solve the real problem.
- Put bounds on all variables.
- Try to make the most of the solver by setting its parameters into the ones that give the best performance.

If the reader is interested to know more about nonlinear programming, the reader can read[30] and[31].

3.2 MINPACK-1

MINPACK-1 is a fortran's package that solves nonlinear problems. MINPACK-1 finds values for x_1, x_2,..., x_n that solve the system of nonlinear equations formed by n functions:

$$f_i(x_1, x_2, ..., x_n) = 0, \qquad 1 \leq \mathrm{i} \leq n. \tag{3.1}$$

A modification of Powell's hybrid algorithm is used to solves the previous system, which is further explained later. This modification has two variants: one that requires the user to calculate the functions f_1,f_2,...,f_n and, next, the Jacobian matrix is then calculated by a forward differential approximation ([32]) or by an updated formula of Broyden ([33]); another one that requires the user to calculate the functions f_1,f_2,...,f_n and the Jacobian matrix:

$$\left(\frac{\delta f_i(x)}{\delta x_j}\right), \qquad 1 \leq \mathrm{i} \leq n, \qquad 1 \leq \mathrm{j} \leq n. \tag{3.2}$$

The main advantage of providing the Jacobian matrix is more reliability and therefore the program is much less sensitive to functions subject to errors. However, writing the Jacobian matrix may also lead to mistakes. Depending on whether the Jacobian matrix is available or not and if flexibility is required, four subroutines inside MINPACK-1 can be used (Fig. 3.2).

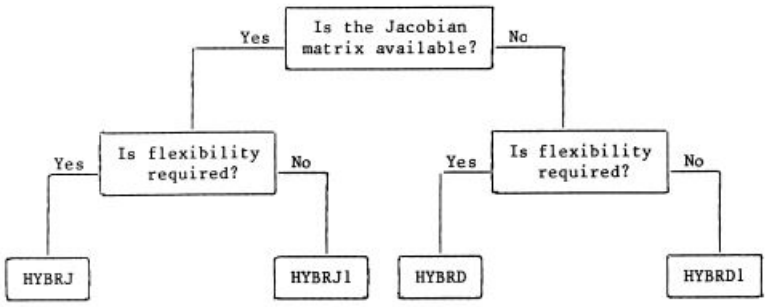

Figure 3.2: Decision tree for systems of nonlinear equations ([34]).

In order to solve our problem, given that the Jacobian matrix is not written and flexibility is always welcome, HYBRD1 subroutine is used. A mathematical background on how this subroutine works is presented in Section 3.3. Further information about MINPACK-1 and other subroutines can be found in[34].

3.3 Mathematical background of MINPACK-1

A n-dimensional Euclidean space is composed by the following real n-vectors:

$$\mathbf{x} = \begin{pmatrix} x_1 \\ x_2 \\ . \\ . \\ . \\ x_n \end{pmatrix}, \tag{3.3}$$

whose Euclidean norm is:

$$x = \left(\sum_{j=1}^{n} x_j^2 \right)^{\frac{1}{2}}. \tag{3.4}$$

A function vector, $\mathbf{F}(x)$, with domain, n, and range, m, can be denoted as:

$$\mathbf{F}(x) = \begin{pmatrix} F_1(x) \\ F_2(x) \\ . \\ . \\ . \\ F_m(x) \end{pmatrix}. \tag{3.5}$$

$m = n$ for systems of nonlinear equations. Knowing that the solution at the end of the computations (t_f) is previously known and measured, $\mathbf{y}$, and comparing it with the result obtained from the computations, $\mathbf{g}$, $\mathbf{F}$ is obtained:

$$\mathbf{F} = \mathbf{y} - \mathbf{g}. \tag{3.6}$$

HYBRD1 seeks a solution $\mathbf{x}*$ to the problem

$$min\left[||\mathbf{F}(x)|| : x\epsilon R^n\right], \tag{3.7}$$

being expected $\mathbf{F}(x*) = 0$ for problems where $m = n$.

Firstly, the user provides an initial guess $\mathbf{x} = \mathbf{x}_0$ to the solution of the problem. Next, the algorithm determines a correction $\mathbf{p}$ to $\mathbf{x}$ in order to decrease the residuals of $\mathbf{F}$ in the new point:

$$\mathbf{x}_+ = \mathbf{x} + \mathbf{p}, \tag{3.8}$$

and begins a new iteration with $\mathbf{x}_+$ replacing $\mathbf{x}$. Since the residuals are reduced,

$$||\mathbf{F}(x + p)|| < ||\mathbf{F}(x)||. \tag{3.9}$$

The correction $\mathbf{p}$ depends upon a diagonal scaling matrix, $\mathbf{D}$, a step bound, Δ, and an approximation $\mathbf{J}$ of the Jacobian matrix of $\mathbf{F}$ at $\mathbf{x}$. The first two parameters are set internally and the Jacobian matrix $\mathbf{J}_0$ is set by means of a forward differential approximation to $\mathbf{F}'(x_0)$. So, $\mathbf{p}$ is computed from

$$min\left[||\mathbf{f} + \mathbf{Jp}|| : ||\mathbf{Dp}|| \leq \Delta\right], \tag{3.10}$$

which is an approximate solution to $min\left[||\mathbf{F}(x + p)|| : ||\mathbf{Dp}|| \leq \Delta\right]$ and where $\mathbf{f}$ is the vector of residuals of $\mathbf{F}$ at $\mathbf{x}$. It works in such a way that if the problem does not give a suitable correction, Δ is decreased and $\mathbf{J}$ updated. Then, the problem

is solved again and this process is repeated until there is enough reduction of the residuals, and then $\mathbf{x}$ is replaced by $\mathbf{x}+\mathbf{p}$, and a new iteration starts with the new $\mathbf{D}$, Δ and $\mathbf{J}$. If there is a solution $\mathbf{x}*$ such that $||\mathbf{D}(\mathbf{x}-\mathbf{x}*)|| \leq \Delta$, $\mathbf{x}+\mathbf{p}$ is a better approximation to $\mathbf{x}*$ than $\mathbf{x}$.

It is important to point out that the algorithm is limited by the precision of the computations (better performance with higher precision) and the algorithm is designed to find only local solutions.

An important issue to deal with is how the convergence works. The criterion used is based on the estimation of the distance between the current approximation $\mathbf{x}$ and the current solution of the problem $\mathbf{x}*$:

$$||\mathbf{D}\left(\mathbf{x}-\mathbf{x}*\right)|| \leq xtol||\mathbf{D}\mathbf{x}*||, \tag{3.11}$$

where $xtol$ is the tolerance required for convergence. Nonetheless, since $\mathbf{x}*$ is unknown, the best criterion for the convergence of $\mathbf{x}$ is denoted by the following formulation:

$$\Delta \leq xtol||\mathbf{D}\mathbf{x}*||. \tag{3.12}$$

The convergence of $\mathbf{F}$ cannot be considered for systems of nonlinear equations where $\mathbf{F}(\mathbf{x}*)=0$ is the expected result, given that $||\mathbf{F}(\mathbf{x})|| \leq (1+ftol)||\mathbf{F}(\mathbf{x}*)||$ and the comparison would fail unless $\mathbf{F}(\mathbf{x})=0$.

In nonlinar equations, $\mathbf{J}$ is determined more often by an updated formula of Broyden rather than the forward difference approximation. The main disadvantage of the latter is that it requires a tolerance ϵ_{fcn}, which is 0 in HYBRD1 subroutine and therefore it is useless (see Section 2.4 in[34] for further information). Hence, an overview of the updated formula of Broyden is explained next.

The updated formula of Broyden depends on the current approximation of $\mathbf{x}$, $\mathbf{p}$ and $\mathbf{J}$:

$$\mathbf{F}(x+p)-\mathbf{F}(x)=\left[\int_0^1 \mathbf{F}'(x+\theta p)d\theta\right]\mathbf{p}, \tag{3.13}$$

fulfilling $\mathbf{J}_+$ the following equation at $\mathbf{x}+\mathbf{p}$:

$$\mathbf{J}_+\mathbf{p}=\mathbf{F}(x+p)-\mathbf{F}(x). \tag{3.14}$$

Finally, the solution of the problem

$$min\left[||\mathbf{J}'-\mathbf{J}||\mathbf{D}:\mathbf{J}'\mathbf{p}=\mathbf{F}(x+p)-\mathbf{F}(x)\right], \tag{3.15}$$

is given by

$$\mathbf{J}_+ = \mathbf{J} + \frac{[\mathbf{F}(x+p) - \mathbf{F}(x) - \mathbf{J}\mathbf{p}]\left(\mathbf{D}^T\mathbf{D}\mathbf{p}\right)^T}{||\mathbf{D}\mathbf{p}||^2}. \tag{3.16}$$

The reasons why the latter formula is used in the algorithm is beyond scope of this work.

Scale invariance plays an important role in MINPACK-1. Scale invariance applies to the invariance of individual functions and it is a desirable feature for optimization problems. Hence, one can work with either problem and obtain equivalent results. Algorithms of nonlinear equations are scale invariant if, given problems related by the change of scale such as

$$\mathbf{F}'(x) = \alpha\mathbf{F}(D_V\mathbf{x}), \tag{3.17}$$

$$\mathbf{x}'_0 = \mathbf{D}_V^{-1}\mathbf{x}_0, \tag{3.18}$$

being α a positive scalar and $\mathbf{D}_V$ a diagonal matrix with positive entries, $\mathbf{x}$ and $\mathbf{x}'$ generally satisfy

$$\mathbf{x}' = \mathbf{D}_V^{-1}\mathbf{x}. \tag{3.19}$$

HYBRD1 is scale invariant if, and only if, the scaling matrix satisfies:

$$\mathbf{D}'_0 = \alpha\mathbf{D}_V\mathbf{D}_0. \tag{3.20}$$

where $\mathbf{D}_0$ and $\mathbf{D}'_0$ are the initial scaling matrices of the respective problems defined by $\mathbf{F}$ and $\mathbf{x}_0$ and by $\mathbf{F}'$ and $\mathbf{x}'_0$, respectively. In HYBRD1 subroutine, since it deals with nonlinear problems, the initial scaling matrix is specified by the contents of the array $DIAG$ and scale invariance is achieved if only Eq. 3.20 is satisfied. HYBRD1 is coded so as to never losing the scale invariance by changing the elements that are 0 to 1 at the starting point.

Finally, all the information about HYBRD1 subroutine together with an example is provided in[34].

Chapter 4

Simulations Setup

In this chapter, we present the TPBVP for a trajectory from GEO to the Moon using a sail driven by solar radiation pressure and controlled by two angles, i.e., the yaw angle, ψ, and the pitch angle, μ. The dynamical model as presented in Chapter 2 includes all the accelerations acting on the s/c. However, when dealing with optimization problems, it is never a good idea to start the computations with the full dynamical equations. Rather, a simplified, approximated model is first solved and then used as initial guess for the complete model. In addition, a good integrator should be chosen to guarantee a good orbit propagation and a correct solution of the problem. By means of using the dynamical and conjugate equations of the simplified model, some simulations of the resulting non-optimal trajectory are also carried out in order to check if the results are reasonable. We start this chapter by presenting the problem in conjunction with all the assumptions required to solve it (Section 4.1). Section 4.2 shows the TPBVP of the problem stated in Section 4.1. This TPBVP is found out taking into account the optimal control theory. Section 4.3 explains the integrator used to perform the orbit propagation together with a detailed study of the chosen tolerance and step size.

4.1 Statement of the problem

As far as this study is concerned, it is senseless to set a problem where all the perturbations and forces are taken into account on the grounds that there would be much more difficulties in the convergence of the final results. Moreover, if one sets out a problem where all the perturbations are taken into account, it is easier

to make mistakes in the formulation since there are much more parameters to take into account.

Therefore, a simplified dynamical model governed by the Kepler's law of motion around a central body without perturbations is going to be assumed. This central body changes depending on if the s/c is under the gravity field of the Earth or of the Moon. Besides, the perturbation upon the s/c due to the solar radiation pressure plays the role of the propulsion system. This perturbation exerted upon a solar sail of 50 m^2 and with a weight, m, of 6 kg is considered to have a constant value of 456.3 μN throughout all the study. The GEQ reference frame is chosen for carrying out the study. As a result, the dynamical equations are simplified into:

$$\ddot{\mathbf{r}} = -\frac{\mu \mathbf{r}}{r^3} + \frac{\mathbf{F}_{SRP}}{m}, \tag{4.1}$$

where μ is the gravitational parameter of either the Earth ($\mu_E = 398600.4418$ km^3s^{-2}) or the Moon ($\mu_M = 4902.8000$ km^3s^{-2}).

Inside the Earth-Moon system, there are five points of equilibrium (Lagrangian points) where a third body of negligible mass compared to the other two can remind still if its velocity is null ([35]). The main reason for that is because the gravitational forces between the three bodies cancel out at these points in an inertial frame and, therefore, there is an equilibrium of accelerations. The Lagrangian point of interest for our problem is L1, which lies on the line between the Earth and the Moon (see Fig. 4.1). As a result, one can design a mission taking advantage of the L1 Lagrangian point, given that if the s/c reaches this point with the required velocity, it can be captured by the Moon's gravity field more easily.

In optimal control problems, the convergence of the results becomes a serious issue to deal with. Looking into several papers devoted to optimization of Earth-to-Moon trajectories, such as[36],[3],[6] and[37], or Bruce Conway's book devoted to trajectory optimization,[38], the convergence of the results of a problem where the initial boundary conditions are in GEO and the final boundary conditions are in a Low-Lunar Orbit (LLO) is almost impossible given that there are a huge amount of computations in a trajectory of such dimensions. Consequently, the problem is divided into two segments: one segment consists of the optimal trajectory of the s/c from GEO until the L1 Lagrangian point, where the main motion of the s/c is governed by the Earth's gravity field; the other segment consists of the optimal trajectory of the s/c from the L1 Lagrangian point until a LLO, where the main motion of the s/c is governed by the Moon's gravity field.

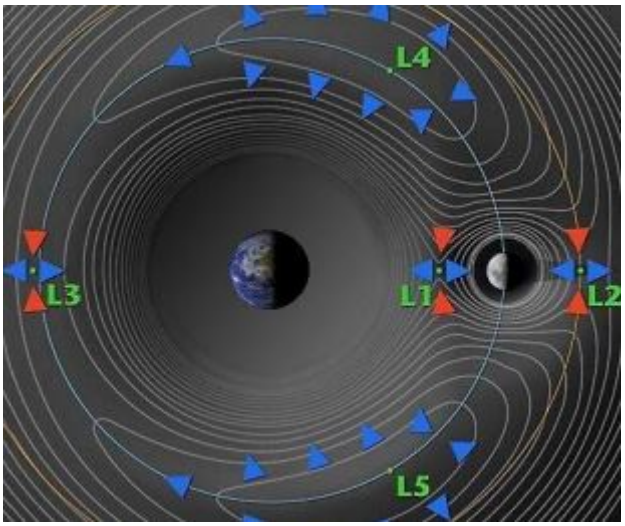

Figure 4.1: Effective potentials in the Earth-to-Moon system.

The orbit of the Moon is computed in order to know where it is at the current position of the s/c and, consequently, where the L1 Lagrangian point is (as it can be seen in Section 4.2.1). Besides, the orbit of the Sun is also computed in order to know the direction of the solar radiation pressure at the position of the s/c.

4.2 The two-point boundary value problem

Given that the problem is going to be divided into two parts, two TPBVP are required, one for each segment.

4.2.1 TPBVP from a GEO to the L1 Lagrangian Point

From the dynamical model, the following equations of motion are obtained:

$$\dot{r}_x = v_x, \tag{4.2}$$

$$\dot{r}_y = v_y, \tag{4.3}$$

$$\dot{r}_z = v_z, \tag{4.4}$$

$$\dot{v}_x = -\frac{\mu_e r_x}{r^3} + \frac{2P_{SR}A\eta_{eff}}{m}\cos^2\left(\arccos\left(\mathbf{d}_{Su}\cdot\mathbf{n}\right)\right)n_x, \tag{4.5}$$

$$\dot{v}_y = -\frac{\mu_e r_y}{r^3} + \frac{2P_{SR}A\eta_{eff}}{m}\cos^2\left(\arccos\left(\mathbf{d}_{Su}\cdot\mathbf{n}\right)\right)n_y, \tag{4.6}$$

$$\dot{v}_z = -\frac{\mu_e r_z}{r^3} + \frac{2P_{SR}A\eta_{eff}}{m}\cos^2\left(\arccos\left(\mathbf{d}_{Su}\cdot\mathbf{n}\right)\right)n_z, \tag{4.7}$$

where $\mathbf{d}_{Su}$ is the unit vector from the Sun to the s/c ($\mathbf{d}_{Su} = (\mathbf{r} - \mathbf{r}_S)/|\mathbf{r} - \mathbf{r}_S|$) ; P_{SR} is the solar radiation pressure; A is the area of the solar sail; η_{eff} is the reflection efficiency of the solar sail; m is the mass of the s/c; $\mathbf{n}$ is the normal direction of the solar sail in the GEQ frame:

$$\mathbf{n} = \begin{bmatrix} n_x \\ n_y \\ n_z \end{bmatrix} = \begin{bmatrix} -\cos\mu\sin\psi \\ \cos\mu\cos\psi \\ \sin\mu \end{bmatrix}, \tag{4.8}$$

where ψ and μ are the yaw and pitch angle, respectively. From now on, $k_{sun} = \dfrac{2P_{SR}A\eta_{eff}}{m}$.

For our study, the optimal control problem consists in finding an optimum-time solution. Therefore, the final time t_f has to be minimized. Following the theory of optimal control, a general performance index, J, can be given in terms of the final time:

$$J = t_f - t_0. \tag{4.9}$$

The previous equation implies that $\phi[\mathbf{r}(t_f), \mathbf{v}(t_f), t_f] = 0$ and $L[\mathbf{r}(t), \mathbf{v}(t), t] = 1$. The mass of the s/c is fixed, given that solar sails are propelled by solar radiation pressure and not by fuel. The initial state is also fixed:

$$\mathbf{r}(t_0) = \mathbf{r}_0, \qquad \mathbf{v}(t_0) = \mathbf{v}_0. \tag{4.10}$$

Here, $\mathbf{r}_0$ is the initial position of the s/c in GEO and $\mathbf{v}_0$ is the velocity of the s/c in such position.

The optimal control problem can be transformed into a TPBVP by means of the Pontryagin's Maximum Principle (PMP). The Hamiltonian, H, of the problem only depends upon the equations of motion of the s/c:

$$\begin{aligned} H &= \lambda_{rx}v_x + \lambda_{ry}v_y + \lambda_{rz}v_z + \lambda_{vx}\left[-\frac{\mu_e r_x}{r^3} + k_{sun}\left(\mathbf{d}_{Su}\cdot\mathbf{n}\right)^2 n_x\right] \\ &+ \lambda_{vy}\left[-\frac{\mu_e r_y}{r^3} + k_{sun}\left(\mathbf{d}_{Su}\cdot\mathbf{n}\right)^2 n_y\right] + \lambda_{vz}\left[-\frac{\mu_e r_z}{r^3} + k_{sun}\left(\mathbf{d}_{Su}\cdot\mathbf{n}\right)^2 n_z\right] \\ &+ 1, \end{aligned} \tag{4.11}$$

where λ_{rx}, λ_{ry} , λ_{rz} and λ_{vx}, λ_{vy}, λ_{vz} are the Lagrangian multipliers (costates) associated with the states $\mathbf{r}$ and $\mathbf{v}$. The derivative of the costates, that are termed Euler-Lagrange equations, are :

$$\dot{\lambda}_{rx} = -\frac{\delta H}{\delta r_x} = \lambda_{vx}\frac{\mu_e}{r^3} - \frac{3\mu_e r_x}{r^5}\left(\lambda_{vx}r_x + \lambda_{vy}r_y + \lambda_{vz}r_z\right) - 2k_{sun}\left(\lambda_{vx}n_x + \lambda_{vy}n_y + \lambda_{vz}n_z\right)$$
$$\times \left(\mathbf{d}_{Su}\cdot\mathbf{n}\right)\times\left(\frac{n_x}{|\mathbf{r}-\mathbf{r}_S|} - \frac{(\mathbf{r}-\mathbf{r}_S)\cdot\mathbf{n}\,(r_x - r_{Sx})}{|\mathbf{r}-\mathbf{r}_S|^3}\right), \quad (4.12)$$

$$\dot{\lambda}_{ry} = -\frac{\delta H}{\delta r_y} = \lambda_{vy}\frac{\mu_e}{r^3} - \frac{3\mu_e r_y}{r^5}\left(\lambda_{vx}r_x + \lambda_{vy}r_y + \lambda_{vz}r_z\right) - 2k_{sun}\left(\lambda_{vx}n_x + \lambda_{vy}n_y + \lambda_{vz}n_z\right)$$
$$\times \left(\mathbf{d}_{Su}\cdot\mathbf{n}\right)\times\left(\frac{n_y}{|\mathbf{r}-\mathbf{r}_S|} - \frac{(\mathbf{r}-\mathbf{r}_S)\cdot\mathbf{n}\,(r_y - r_{Sy})}{|\mathbf{r}-\mathbf{r}_S|^3}\right), \quad (4.13)$$

$$\dot{\lambda}_{rz} = -\frac{\delta H}{\delta r_z} = \lambda_{vz}\frac{\mu_e}{r^3} - \frac{3\mu_e r_z}{r^5}\left(\lambda_{vx}r_x + \lambda_{vy}r_y + \lambda_{vz}r_z\right) - 2k_{sun}\left(\lambda_{vx}n_x + \lambda_{vy}n_y + \lambda_{vz}n_z\right)$$
$$\times \left(\mathbf{d}_{Su}\cdot\mathbf{n}\right)\times\left(\frac{n_z}{|\mathbf{r}-\mathbf{r}_S|} - \frac{(\mathbf{r}-\mathbf{r}_S)\cdot\mathbf{n}\,(r_z - r_{Sz})}{|\mathbf{r}-\mathbf{r}_S|^3}\right), \quad (4.14)$$

$$\dot{\lambda}_{vx} = -\frac{\delta H}{\delta v_x} = -\lambda_{rx}, \quad (4.15)$$

$$\dot{\lambda}_{vy} = -\frac{\delta H}{\delta v_y} = -\lambda_{ry}, \quad (4.16)$$

$$\dot{\lambda}_{vz} = -\frac{\delta H}{\delta v_z} = -\lambda_{rz}. \quad (4.17)$$

In order to reach the optimality condition, $\frac{\delta H}{\delta u} = 0$ must be satisfied for $t_0 < t < t_f$, $u(t)$ being the control parameter. The optimal $\mathbf{n}$ that can minimize H is sought. Given that the term inside H (Eq. 4.11) that must be minimized is $k_{sun}(\mathbf{d}_{Su}\cdot\mathbf{n})^2(\lambda_{vx}n_x + \lambda_{vy}n_y + \lambda_{vz}n_z)$, $\mathbf{n}$ should be based on $\mathbf{d}_{Su}$ and λ_v. The problem at hand is illustrated in Fig. 4.2.

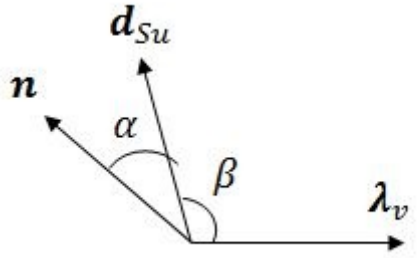

Figure 4.2: Direction of $\mathbf{n}$, $\mathbf{d}_{Su}$ and λ_v.

One should notice in Fig. 4.2 that $\mathbf{n}$ is in the same plane as $\mathbf{d}_{Su}$ and λ_v. In Fig. 4.2, β is the angle between $\mathbf{d}_{Su}$ and λ_v:

$$\beta = \arccos\left(\frac{\mathbf{d}_{Su}\cdot\lambda_v}{d_{Su}\lambda_v}\right). \tag{4.18}$$

Since $\mathbf{d}_{Su}$, λ_v and β are known, α must be minimized in order to minimize H. Given that $\mathbf{n}$ only multiplies k_{sun} in Eq. 4.11, the following is only considered when minimizing H:

$$\begin{aligned} H' &= k_{sun}(\mathbf{d}_{Su}\cdot\mathbf{n})^2(\lambda_v\cdot\mathbf{n}) = -d^2\cos^2(\alpha)\lambda_v\cos(\pi-\alpha-\beta) \\ &= -k_{sun}d^2\lambda_v\cos^2(\alpha)\cos(\pi-\alpha-\beta), \end{aligned} \tag{4.19}$$

being $n=1$ and $d=1$. Therefore:

$$\begin{aligned} \frac{\delta H'}{\delta\alpha} &= -2k_{sun}\cos\alpha\sin\alpha\cos(\pi-\alpha-\beta) + k_{sun}\cos^2\alpha\sin(\pi-\alpha-\beta) \\ &= -2\sin\alpha\cos(\pi-\alpha-\beta) + \cos\alpha\sin(\pi-\alpha-\beta) = 0, \end{aligned} \tag{4.20}$$

where the trivial solution $\cos\alpha = 0$ is obtained when $\alpha = \frac{\pi}{2}$. Nevertheless, this solution is meaningless. Simplifying Eq. 4.20 yields:

$$2\tan\alpha = \tan(\pi-\alpha-\beta) = -\tan(\alpha+\beta), \tag{4.21}$$

$$-2\tan\alpha = \frac{\tan\alpha+\tan\beta}{1-\tan\alpha\tan\beta}, \tag{4.22}$$

$$-2\tan\alpha + 2\tan^2\alpha\tan\beta = \tan\alpha+\tan\beta, \tag{4.23}$$

$$2\tan^2\alpha\tan\beta - 3\tan\alpha - \tan\beta = 0, \tag{4.24}$$

$$\tan\alpha = \frac{3\pm\sqrt{9+8\tan^2\beta}}{4\tan\beta}. \tag{4.25}$$

From Eq. 4.25, one obtains 2 possible solutions of α and their resulting conjugates, given that α is obtained by means of a tangent. However, these conjugates are excluded because the arrangement of the vectors in Fig. 4.2 would not be achieved with them. As a result, since we are minimizing the time, the α that gives the minimum H in Eq. 4.19 is chosen.

Once α is obtained, one should proceed to the computation of $\mathbf{n}$. In order to do this, firstly one should compute the following normal vector, $\mathbf{norm}$, with λ_{vu} and $\mathbf{d}_{Su}$:

$$\mathbf{norm} = \mathbf{d}_{Su}\times\lambda_{vu}, \tag{4.26}$$

where $\lambda_{vu} = \dfrac{\lambda_v}{|\lambda_v|}$. Then, by means of $\mathbf{d}_{Su}$ and $\mathbf{norm}$, the following normal vector, $\mathbf{r}_{norm}$, is computed:

$$\mathbf{r}_{norm} = \mathbf{norm} \times \mathbf{d}_{Su}. \tag{4.27}$$

Finally, an α rotation of $\mathbf{d}_{Su}$ and $\mathbf{r}_{norm}$ about $\mathbf{norm}$ vector leads to the normal vector of the solar sail, $\mathbf{n}$:

$$\mathbf{n} = \mathbf{d}_{Su}\cos(\alpha) + \mathbf{r}_{norm}\sin(\alpha). \tag{4.28}$$

The s/c must reach the L1 Lagrangian Point of the Earth-to-Moon system. One should pay attention that the Moon moves on its orbit and, given that L1 position depends on the position of the Moon, L1 moves as well. Taking into account the latter, the final state of the s/c can be defined by the following boundary conditions, which must be satisfied for any feasible solution:

$$\psi_1 = \mathbf{r}(t_f) - K_{L1}\mathbf{r}_{Moon}(t_f) = 0, \tag{4.29}$$

$$\psi_2 = \mathbf{v}(t_f) - K_{L1}\mathbf{v}_{Moon}(t_f) = 0, \tag{4.30}$$

where $K_{L1} = 0.828125$ and represents the fraction of the average distance between the Earth and the L1 Lagrangian Point; $\mathbf{r}_{Moon}(t_f)$ is the position of the Moon at the final state; $\mathbf{v}_{Moon}(t_f)$ is the velocity of the Moon at the final state. One should know that L1's position varies along the line between the Earth and the Moon since the orbit of the Moon is not circular whatsoever. However, this assumption is correct for a first approximation. As a result, being $\phi[\mathbf{r}(t_f), \mathbf{v}(t_f), t_f] = 0$ given that it is a minimum-time optimization problem, one obtains the following final boundary condition:

$$\Phi = \nu_1^T\left[\mathbf{r}(t_f) - K_{L1}\mathbf{r}_{Moon}(t_f)\right] + \nu_2^T\left[\mathbf{v}(t_f) - K_{L1}\mathbf{r}_{Moon}(t_f)\Omega_{Moon}(t_f)\right], \tag{4.31}$$

where ν_1^T and ν_2^T are the chosen Lagrangian parameters to satisfy Eq. 4.29 and Eq. 4.30. Hence, following the optimal control theory, the costates in the final

state are:

$$\lambda_{rx}(t_f) = \left.\frac{\delta\Phi}{\delta r_x}\right|_{t=t_f} = \nu_{1x}, \tag{4.32}$$

$$\lambda_{ry}(t_f) = \left.\frac{\delta\Phi}{\delta r_y}\right|_{t=t_f} = \nu_{1y}, \tag{4.33}$$

$$\lambda_{rz}(t_f) = \left.\frac{\delta\Phi}{\delta r_z}\right|_{t=t_f} = \nu_{1z}, \tag{4.34}$$

$$\lambda_{vx}(t_f) = \left.\frac{\delta\Phi}{\delta v_x}\right|_{t=t_f} = \nu_{2x}, \tag{4.35}$$

$$\lambda_{vy}(t_f) = \left.\frac{\delta\Phi}{\delta v_y}\right|_{t=t_f} = \nu_{2y}, \tag{4.36}$$

$$\lambda_{vz}(t_f) = \left.\frac{\delta\Phi}{\delta v_z}\right|_{t=t_f} = \nu_{2z}. \tag{4.37}$$

Finally, considering a free time transfer, the following additional equation has to be added:

$$\Omega = \left[\frac{d\Phi}{dt} + 1\right]_{t_f} = 0, \tag{4.38}$$

where,

$$\frac{d\Phi}{dt} = \frac{\delta\Phi}{\delta t} + \frac{\delta\Phi}{\delta x}\dot{x}. \tag{4.39}$$

For each equation of motion, Eq. 4.38 turns into:

$$\left[\frac{\delta\Phi}{\delta t}\right]_{t_f} + \nu_{1x}v_{xf} + 1 = 0, \tag{4.40}$$

$$\left[\frac{\delta\Phi}{\delta t}\right]_{t_f} + \nu_{1y}v_{yf} + 1 = 0, \tag{4.41}$$

$$\left[\frac{\delta\Phi}{\delta t}\right]_{t_f} + \nu_{1z}v_{zf} + 1 = 0, \tag{4.42}$$

$$\left[\frac{\delta\Phi}{\delta t}\right]_{t_f} + \nu_{2x}\left[-\frac{\mu_e r_{xf}}{r^3} - k_{sun}\left(\mathbf{d}_{Su-f}\cdot\mathbf{n}\right)^2 n_x\right] + 1 = 0, \tag{4.43}$$

$$\left[\frac{\delta\Phi}{\delta t}\right]_{t_f} + \nu_{2y}\left[-\frac{\mu_e r_{yf}}{r^3} + k_{sun}\left(\mathbf{d}_{Su-f}\cdot\mathbf{n}\right)^2 n_y\right] + 1 = 0, \tag{4.44}$$

$$\left[\frac{\delta\Phi}{\delta t}\right]_{t_f} + \nu_{2z}\left[-\frac{\mu_e r_{zf}}{r^3} + k_{sun}\left(\mathbf{d}_{Su-f}\cdot\mathbf{n}\right)^2 n_z\right] + 1 = 0. \tag{4.45}$$

$\left[\frac{\delta\Phi}{\delta t}\right]_{t_f}$ can be considered null since Φ does not depend implicitly on the time.

The differential Eq. 4.2- 4.7 and Eq. 4.12-4.17 are solved subject to the boundary conditions of Eq. 4.10 and Eq. 4.32-4.37, with the choice of the parameters

ν_1^T, ν_2^T and t_f available to satisfy the boundary conditions (Eq. 4.29, Eq. 4.30, Eq. 4.38).

4.2.2 TPBVP from the L1 Lagrangian Point to a LLO

The following equations of motion are obtained when the s/c's motion is governed by the Moon's potential gravity field:

$$\dot{r}_x = v_x, \tag{4.46}$$

$$\dot{r}_y = v_y, \tag{4.47}$$

$$\dot{r}_z = v_z, \tag{4.48}$$

$$\dot{v}_x = -\frac{\mu_M d_{Mx}}{d_M^3} + k_{sun}\left(\mathbf{d}_{SuM}\cdot\mathbf{n}\right)^2 n_x, \tag{4.49}$$

$$\dot{v}_y = -\frac{\mu_M d_{My}}{d_M^3} + k_{sun}\left(\mathbf{d}_{SuM}\cdot\mathbf{n}\right)^2 n_y, \tag{4.50}$$

$$\dot{v}_z = -\frac{\mu_M d_{Mz}}{d_M^3} + k_{sun}\left(\mathbf{d}_{SuM}\cdot\mathbf{n}\right)^2 n_z, \tag{4.51}$$

where $\mathbf{d}_{SuM}$ is the unit vector from the Sun to the s/c ($\mathbf{d}_{SuM} = (\mathbf{d}_M - \mathbf{r}_{SM})/|\mathbf{d}_M - \mathbf{r}_{SM}|$) ; $\mathbf{d}_M$ is the position of the s/c relative to the Moon ($\mathbf{d}_M = \mathbf{r} - \mathbf{r}_M$); $\mathbf{r}_{SM}$ is the position of the Sun relative to the Moon ($\mathbf{r}_{SM} = \mathbf{r}_S - \mathbf{r}_M$); μ_M is the Moon's gravitational parameter; P_{SR} is the solar radiation pressure; A is the area of the solar sail; η_{eff} is the reflection efficiency of the solar sail; m is the mass of the s/c; $\mathbf{n}$ is the normal direction of the solar sail in the GEQ frame:

$$\mathbf{n} = \begin{bmatrix} n_x \\ n_y \\ n_z \end{bmatrix} = \begin{bmatrix} -\cos\mu\sin\psi \\ \cos\mu\cos\psi \\ \sin\mu \end{bmatrix}, \tag{4.52}$$

where ψ and μ are the yaw and pitch angle, respectively.

The optimal control problem also consists in finding an optimum-time solution and the final time t_f has to be minimized. Therefore, the performance index, J, is again:

$$J = t_f - t_0. \tag{4.53}$$

The previous equation implies that $\phi[\mathbf{r}(t_f), \mathbf{v}(t_f), t_f] = 0$ and $L[\mathbf{r}(t), \mathbf{v}(t), t] = 1$. The mass of the s/c is fixed, as the initial state also is:

$$\mathbf{r}(t_0) = K_{L1}\mathbf{r}_{Moon}(t_0), \qquad \mathbf{v}(t_0) = K_{L1}\mathbf{r}_{Moon}(t_0)\Omega_{Moon}. \tag{4.54}$$

Here, t_0 is the final time when the s/c arrived to the L1 Lagrangian point in segment 1 and, therefore, $\mathbf{r}(t_0)$ and $\mathbf{v}(t_0)$ is the position and velocity of the s/c at L1, respectively.

The optimal control problem can be transformed into a TPBVP by means of the PMP. The Hamiltonian, H, of the problem only depends upon the equations of motion of the s/c:

$$\begin{aligned} H &= \lambda_{rx} v_{Mx} + \lambda_{ry} v_{My} + \lambda_{rz} v_{Mz} + \lambda_{vx} \left[-\frac{\mu_M d_{Mx}}{d_M^3} + k_{sun} \left(\mathbf{d}_{SuM} \cdot \mathbf{n} \right)^2 n_x \right] \\ &+ \lambda_{vy} \left[-\frac{\mu_M d_{My}}{d_M^3} + k_{sun} \left(\mathbf{d}_{SuM} \cdot \mathbf{n} \right)^2 n_y \right] + \lambda_{vz} \left[-\frac{\mu_M d_{Mz}}{d_M^3} + k_{sun} \left(\mathbf{d}_{SuM} \cdot \mathbf{n} \right)^2 n_z \right] \\ &+ 1, \end{aligned} \tag{4.55}$$

where λ_{rx}, λ_{ry} , λ_{rz} and λ_{vx}, λ_{vy}, λ_{vz} are the Lagrangian multipliers (costates) associated with the states $\mathbf{r}$ and $\mathbf{v}$. The Euler-Lagrange equations are:

$$\begin{aligned} \dot{\lambda}_{rx} &= -\frac{\delta H}{\delta d_{Mx}} = \lambda_{vx} \frac{\mu_M}{d_M^3} - \frac{3\mu_M d_{Mx}}{d_M^5} \left(\lambda_{vx} d_{Mx} + \lambda_{vy} d_{My} + \lambda_{vz} d_{Mz} \right) - 2k_{sun} \\ &\times \left(\lambda_{vx} n_x + \lambda_{vy} n_y + \lambda_{vz} n_z \right) \left(\mathbf{d}_{SuM} \cdot \mathbf{n} \right) \\ &\times \left(\frac{n_x}{|\mathbf{d}_M - \mathbf{r}_{SM}|} - \frac{\left(\mathbf{d}_M - \mathbf{r}_{SM} \right) \cdot \mathbf{n} \left(d_{Mx} - r_{SMx} \right)}{|\mathbf{d}_M - \mathbf{r}_{SM}|^3} \right), \end{aligned} \tag{4.56}$$

$$\begin{aligned} \dot{\lambda}_{ry} &= -\frac{\delta H}{\delta d_{My}} = \lambda_{vy} \frac{\mu_M}{d_M^3} - \frac{3\mu_M d_{My}}{d_M^5} \left(\lambda_{vx} d_{Mx} + \lambda_{vy} d_{My} + \lambda_{vz} d_{Mz} \right) - 2k_{sun} \\ &\times \left(\lambda_{vx} n_x + \lambda_{vy} n_y + \lambda_{vz} n_z \right) \left(\mathbf{d}_{SuM} \cdot \mathbf{n} \right) \\ &\times \left(\frac{n_y}{|\mathbf{d}_M - \mathbf{r}_{SM}|} - \frac{\left(\mathbf{r}_M - \mathbf{r}_{SM} \right) \cdot \mathbf{n} \left(d_{My} - r_{SMy} \right)}{|\mathbf{d}_M - \mathbf{r}_{SM}|^3} \right), \end{aligned} \tag{4.57}$$

$$\begin{aligned} \dot{\lambda}_{rz} &= -\frac{\delta H}{\delta d_{Mz}} = \lambda_{vz} \frac{\mu_M}{d_M^3} - \frac{3\mu_M d_{Mz}}{d_M^5} \left(\lambda_{vx} d_{Mx} + \lambda_{vy} d_{My} + \lambda_{vz} d_{Mz} \right) - 2k_{sun} \\ &\times \left(\lambda_{vx} n_x + \lambda_{vy} n_y + \lambda_{vz} n_z \right) \left(\mathbf{d}_{SuM} \cdot \mathbf{n} \right) \\ &\times \left(\frac{n_z}{|\mathbf{d}_M - \mathbf{r}_{SM}|} - \frac{\left(\mathbf{d}_M - \mathbf{r}_{SM} \right) \cdot \mathbf{n} \left(d_{Mz} - r_{SMz} \right)}{|\mathbf{d}_M - \mathbf{r}_{SM}|^3} \right), \end{aligned} \tag{4.58}$$

$$\dot{\lambda}_{vx} = -\frac{\delta H}{\delta v_{Mx}} = -\lambda_{rx}, \tag{4.59}$$

$$\dot{\lambda}_{vy} = -\frac{\delta H}{\delta v_{My}} = -\lambda_{ry}, \tag{4.60}$$

$$\dot{\lambda}_{vz} = -\frac{\delta H}{\delta v_{Mz}} = -\lambda_{rz}. \tag{4.61}$$

The optimal $\mathbf{n}$ that can minimize H is sought. Given that the term inside H (Eq. 4.55) that must be minimized is $k_{sun}(\mathbf{d}_{SuM} \cdot \mathbf{n})^2(\lambda_{vx} n_x + \lambda_{vy} n_y + \lambda_{vz} n_z)$, $\mathbf{n}$

should be based on $\mathbf{d}_{Su}$ and λ_v. The problem at hand is illustrated in Fig. 4.3.

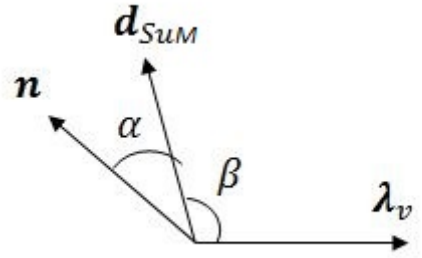

Figure 4.3: Direction of $\mathbf{n}$, $\mathbf{d}_{SuM}$ and λ_v.

In Fig. 4.3, β is the angle between $\mathbf{d}_{SuM}$ and λ_v:

$$\beta = \arccos\left(\frac{\mathbf{d}_{SuM}\cdot\lambda_v}{d_{SuM}\lambda_v}\right). \tag{4.62}$$

Since $\mathbf{d}_{SuM}$, λ_v and β are known, α must be minimized in order to minimize H. Given that $\mathbf{n}$ only multiplies k_{sun} in Eq. 4.55, the following is only considered when minimizing H:

$$\begin{aligned} H' &= k_{sun}(\mathbf{d}_{SuM}\cdot\mathbf{n})^2(\lambda_v\cdot\mathbf{n}) = -d^2\cos^2(\alpha)\lambda_v\cos(\pi-\alpha-\beta) \\ &= -k_{sun}d^2\lambda_v\cos^2(\alpha)\cos(\pi-\alpha-\beta), \end{aligned} \tag{4.63}$$

being $n=1$ and $d=1$. Therefore:

$$\begin{aligned} \frac{\delta H'}{\delta\alpha} &= -2k_{sun}\cos\alpha\sin\alpha\cos(\pi-\alpha-\beta) + k_{sun}\cos^2\alpha\sin(\pi-\alpha-\beta) \\ &= -2\sin\alpha\cos(\pi-\alpha-\beta) + \cos\alpha\sin(\pi-\alpha-\beta) = 0, \end{aligned} \tag{4.64}$$

where the trivial solution $\cos\alpha = 0$ is obtained when $\alpha = \frac{\pi}{2}$. Nevertheless, this solution is again meaningless. Simplifying Eq. 4.64, one reaches the following equation to compute α as a function of β.

$$\tan\alpha = \frac{3 \pm \sqrt{9+8\tan^2\beta}}{4\tan\beta}. \tag{4.65}$$

Again, the conjugate angles of Eq. 4.65 are excluded and the chosen α is the one that minimizes H.

Once α is obtained, one should proceed to the computation of $\mathbf{n}$. In order to do this, firstly one should compute the following normal vector, $\mathbf{norm}$, with λ_{vu} and

$\mathbf{d}_{SuM}$:

$$\mathbf{norm} = \mathbf{d}_{SuM} \times \lambda_{vu}, \tag{4.66}$$

where $\lambda_{vu} = \dfrac{\lambda_v}{|\lambda_v|}$. Then, by means of $\mathbf{d}_{SuM}$ and $\mathbf{norm}$, the following normal vector, $\mathbf{r}_{norm}$, is computed:

$$\mathbf{r}_{norm} = \mathbf{norm} \times \mathbf{d}_{SuM}. \tag{4.67}$$

Finally, an α rotation of $\mathbf{d}_{Su}$ and $\mathbf{r}_{norm}$ about $\mathbf{norm}$ vector leads to $\mathbf{n}$:

$$\mathbf{n} = \mathbf{d}_{SuM} \cos(\alpha) + \mathbf{r}_{norm} \sin(\alpha). \tag{4.68}$$

Taking into account that the s/c must reach a LLO, the final state of the s/c can be defined by the following boundary conditions, which must be satisfied for any feasible solution:

$$\psi_1 = \mathbf{r}(t_f) - \mathbf{r}_{LLO}(t_f) = 0, \tag{4.69}$$

$$\psi_2 = \mathbf{v}(t_f) - \mathbf{v}_{LLO}(t_f) = 0, \tag{4.70}$$

where $r_{LLO} = 300$ metres above the surface of the Moon and v_{LLO} is the velocity of the s/c in such position. As a result, being $\phi[\mathbf{r}(t_f), \mathbf{v}(t_f), t_f] = 0$ given that it is a minimum-time optimization problem,

$$\Phi = \nu_1^T \left[\mathbf{r}(t_f) - \mathbf{r}_{LLO}(t_f)\right] + \nu_2^T \left[\mathbf{v}(t_f) - \mathbf{v}_{LLO}(t_f)\right], \tag{4.71}$$

where ν_1^T and ν_2^T are the chosen Lagrangian parameters to satisfy Eq. 4.69 and Eq. 4.70. Hence, following the theory of optimal control, the costates in the final states are:

$$\lambda_{rx}(t_f) = \left.\frac{\delta\Phi}{\delta d_{Mx}}\right|_{t=t_f} = \nu_{1x}, \tag{4.72}$$

$$\lambda_{ry}(t_f) = \left.\frac{\delta\Phi}{\delta d_{My}}\right|_{t=t_f} = \nu_{1y}, \tag{4.73}$$

$$\lambda_{rz}(t_f) = \left.\frac{\delta\Phi}{\delta d_{Mz}}\right|_{t=t_f} = \nu_{1z}, \tag{4.74}$$

$$\lambda_{vx}(t_f) = \left.\frac{\delta\Phi}{\delta v_{Mx}}\right|_{t=t_f} = \nu_{2x}, \tag{4.75}$$

$$\lambda_{vy}(t_f) = \left.\frac{\delta\Phi}{\delta v_{My}}\right|_{t=t_f} = \nu_{2y}, \tag{4.76}$$

$$\lambda_{vz}(t_f) = \left.\frac{\delta\Phi}{\delta v_{Mz}}\right|_{t=t_f} = \nu_{2z}. \tag{4.77}$$

Finally, considering a free time transfer, the following additional equation has to be added:

$$\Omega = \left[\frac{d\Phi}{dt} + 1\right]_{t_f} = 0, \tag{4.78}$$

where,

$$\frac{d\Phi}{dt} = \frac{\delta\Phi}{\delta t} + \frac{\delta\Phi}{\delta x}\dot{x}. \tag{4.79}$$

For each equation of motion, Eq. 4.78 turns into:

$$\nu_{1x} v_{LLOx} + 1 = 0, \tag{4.80}$$

$$\nu_{1y} v_{LLOy} + 1 = 0, \tag{4.81}$$

$$\nu_{1z} v_{LLOz} + 1 = 0, \tag{4.82}$$

$$\nu_{2x}\left[-\frac{\mu_M r_{LLOx}}{r_{LLO}^3} - k_{sun}\left(\mathbf{d}_{SuM-f}\cdot\mathbf{n}\right)^2 n_x\right] + 1 = 0, \tag{4.83}$$

$$\nu_{2y}\left[-\frac{\mu_M r_{LLOy}}{r_{LLO}^3} + k_{sun}\left(\mathbf{d}_{SuM-f}\cdot\mathbf{n}\right)^2 n_y\right] + 1 = 0, \tag{4.84}$$

$$\nu_{2z}\left[-\frac{\mu_M r_{LLOz}}{r_{LLO}^3} + k_{sun}\left(\mathbf{d}_{SuM-f}\cdot\mathbf{n}\right)^2 n_z\right] + 1 = 0. \tag{4.85}$$

The differential Eq. 4.46- 4.51 and Eq. 4.56-4.61 are solved subject to the boundary conditions of Eq. 4.54 and Eq. 4.72-4.77, with the choice of the parameters ν_1^T, ν_2^T and t_f available to satisfy the boundary conditions (Eq. 4.69, Eq. 4.70, Eq. 4.78).

4.3 Orbit propagation

In order to obtain the position and velocity of the s/c along the transfer orbit, the s/c's velocity and acceleration must be integrated. In order to do this, an existing numerical integrator is used. The integrator model mainly used to solve space trajectories is the Runge-Kutta-Fehlberg (RKF) method. Numerical methods are used to guarantee an accurate numerical integrator. A description of the numerical methods used by a RKF integrator applied to our problem is going to be explained in Section 4.3.1. Nonetheless, for further information about this method, the reader can go through[39],[40] or[41].

4.3.1 Runge-Kutta-Fehlberg 7(8)

RKF of 8^{th} order (RKF 7(8)) is more accurate than RKF of either 4^{th} or 5^{th} order given that it is able to update the step of the computations, h, automatically. This step is updated in such a way that if the changes in the computations are big, the step size becomes larger, but if these changes are small, the step size becomes shorter. This ability to automatically modify the step is called the *embedded method*.

In order to know the time discretization of the integrator, the following is used:

$$t = t_i + \alpha_n h, \tag{4.86}$$

where t_i is the time when the calculations are performed (current state of the s/c), h is the chosen step and α_n is a vector with 13 coefficients (see Appendix A).

The aim of the integrator is to create a matrix, f, with 13 columns ($m = 13$), each of which includes the derivatives of the dynamical and conjugate equations. That is to say, each column will be filled by the following differential equations:

$$\mathbf{dif} = \begin{pmatrix} \dot{r}_x \\ \dot{r}_y \\ \dot{r}_z \\ \dot{v}_x \\ \dot{v}_y \\ \dot{v}_z \\ \dot{\lambda}_{rx} \\ \dot{\lambda}_{ry} \\ \dot{\lambda}_{rz} \\ \dot{\lambda}_{vx} \\ \dot{\lambda}_{vy} \\ \dot{\lambda}_{vz} \end{pmatrix}, \tag{4.87}$$

where $\dot{\mathbf{r}}$, $\dot{\mathbf{v}}$, $\dot{\lambda}_r$ and $\dot{\lambda}_v$ are the equations of the TPBVP. $\mathbf{dif}$ changes in each column given that $\mathbf{x}_i$ is modified every iteration using the following formulation:

$$\mathbf{x}_i = \mathbf{x}_i + \beta_{m,n} h \mathbf{f}_{12,n}, \tag{4.88}$$

where $\beta_{m,n}$ is a matrix that includes the coupling coefficients of the RKF 7(8) (see Appendix A), $n = m - 1$, h is the stepsize of the integrator and $\mathbf{x}_i$ is:

$$\mathbf{x}_i = \begin{pmatrix} r_x \\ r_y \\ r_z \\ v_x \\ v_y \\ v_z \\ \lambda_{rx} \\ \lambda_{ry} \\ \lambda_{rz} \\ \lambda_{vx} \\ \lambda_{vy} \\ \lambda_{vz} \end{pmatrix}, \tag{4.89}$$

where $\mathbf{r}$, $\mathbf{v}$, λ_r and λ_v are the equations of the TPBVP.

In the first iteration, $\mathbf{x}_i$ matches with the current state of the s/c in the transfer orbit. Next, for $m = 1$, Eq. 4.87 is obtained by means of the TPBVP. Then, the first column of $f_{13,1}$ is filled with Eq. 4.87. In the next iteration, for $m = 2$, the new $\mathbf{x}_i$ is obtained thanks to Eq. 4.88. Therefore, the new derivatives are obtained by means of the TPBVP and the second column of $\mathbf{f}_{12,2}$ is filled with them. The same procedure is carried out from $m = 3$ to $m = 13$ until matrix $\mathbf{f}$ is totally filled.

Once matrix $\mathbf{f}$ is obtained, two estimations of $\mathbf{x}$ are obtained from the 7^{th} and 8^{th} order of the integrator:

$$\mathbf{x}_7 = h\mathbf{f}\mathbf{c}_7, \tag{4.90}$$

$$\mathbf{x}_8 = h\mathbf{f}\mathbf{c}_8, \tag{4.91}$$

being $\mathbf{c}_7$ and $\mathbf{c}_8$ two vectors with 13 coefficients (see Appendix A). The maximum truncation error, e_{max}, is obtained from both previous equations:

$$e'_{max} = |\mathbf{x}_7 - \mathbf{x}_8| = |e_1\ e_2\ ...\ e_{11}\ e_{12}|\,, \tag{4.92}$$

$$e_{max} = \frac{e_1 + e_2 + ... + e_{11} + e_{12}}{12}. \tag{4.93}$$

Then, the allowable truncation error, e_{allow}, is obtained by:

$$dd = \sum_{i=1}^{12} |\mathbf{x}_8(i)|, \tag{4.94}$$

$$e'_{allow} = 1 + 0.01dd, \tag{4.95}$$

$$e_{allow} = \epsilon e'_{allow}, \tag{4.96}$$

being ϵ a tolerance selected by the user. Finally, the updated step, h', is given by:

$$h' = 0.9h \left(\frac{e_{allow}}{e_{max}} \right)^{\frac{1}{8}}, \tag{4.97}$$

being 8 the order of the RKF integrator. A maximum and minimum step, h_{max} and h_{min} respectively, are defined so as to guarantee that h is inside a reasonable interval when carrying out the computations.

Finally, when $e_{max} < e_{allow}$, the new state of the s/c inside the transfer orbit is defined by $\mathbf{x}_8$. Then, the orbit keeps propagating until the time reaches the final time, t_f.

4.3.2 Setting the error tolerance for the integrator

If the tolerance, ϵ, is very small, the computations may take an unnecessary and probably huge amount of time; on the other hand, if ϵ is very high, the resulting position and velocity of the s/c may not be as accurate as if ϵ was smaller. Consequently, an optimal value of ϵ should be found out so as to reach an agreement between an accurate result and the time employed to perform the computations.

In order to do this, a simplified problem is studied. The starting point of this transfer orbit is a Geostationary Transfer Orbit (GTO) with a perigee height of 6671 meters, and the orbit is going to be propagated throughout 1 period of the GTO ($10^h 33^{min}$). The thrust of the s/c is always constant and parallel to the velocity (456.3 μN). At the end of this transfer, the variation of the position and velocity as a function of ϵ is studied. ϵ is modified from $\epsilon = 1 \cdot 10^{-5}$ to $\epsilon = 1 \cdot 10^{-13}$. Fig. 4.4 shows the resulting transfer orbit throughout this period.

Fig. 4.5 and 4.6 show the variation of the position and velocity of the s/c as a function of ϵ. When the tolerance reaches $\epsilon = 1 \cdot 10^{-9}$, both components of

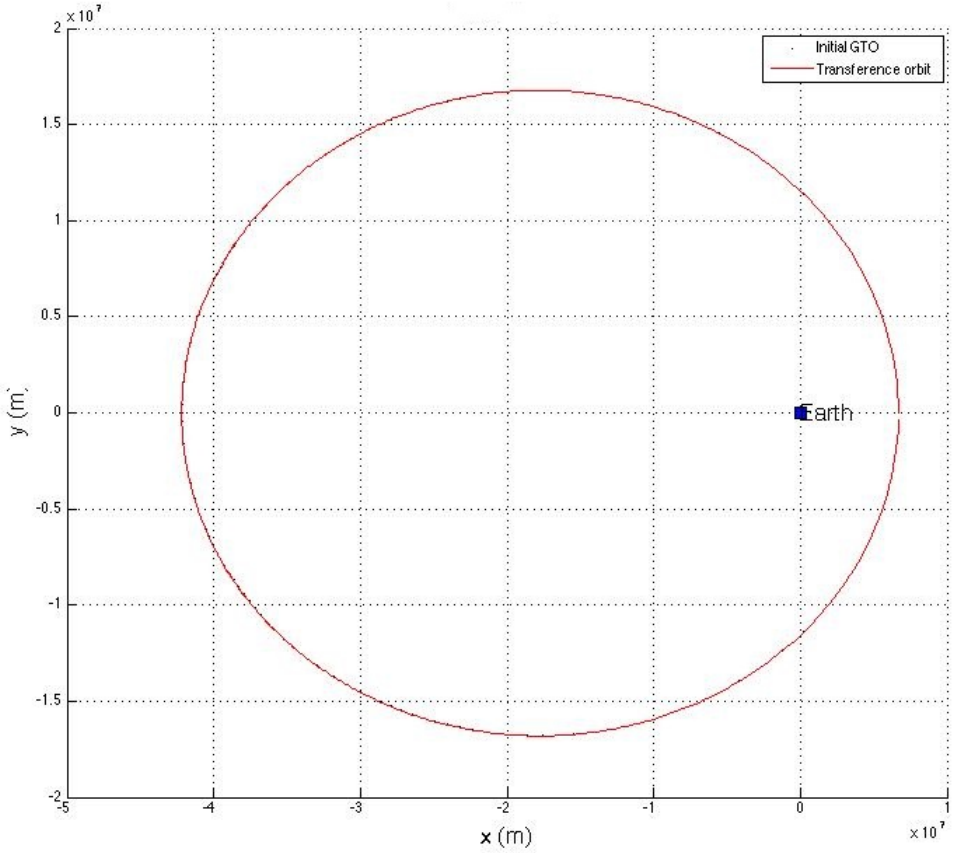

Figure 4.4: Orbit propagation for studying the tolerance.

either the position and velocity tend to an asymptotic value. The behaviour of each component is carefully assessed:

- r_x varies from 6688768 meters to 6688772 meters. A variation of 4 meters can be considered negligible.
- r_y varies from -351620 meters to -351500 meters. 120 meters in an orbit can be also considered insignificant.
- v_x varies from 308.32 m/s to 308.22 m/s. The total variation is 0.1 m/s, which is very small.
- v_y varies from 10130.325 m/s to almost 10130.33 m/s. A variation of 0.01 m/s is almost null.

As a result, the best tolerance to choose is $\epsilon = 1 \cdot 10^{-7}$.

4.3.3 Setting the step size

The maximum and minimum step, h_{max} and h_{min} respectively, are defined in order to guarantee that a certain accuracy in the computations is always maintained. In order to do this, using the same simplified problem as in Sec. 4.3.2, the variation of the step throughout a transfer of 20 days is studied. The resulting transfer orbit can be seen in Fig. 4.7.

The parabolic variation of h in Fig. 4.8 shows that, when the s/c is close again to the perigee of the initial GTO, the required h for the integrator to perform the computations is smaller given that the velocity of the s/c is bigger here than when it is next to the apogee of the initial GTO. Therefore, the integrator requires less time to perform the calculations. The further the s/c is from the Earth, the more time the integrator requires to perform all the computations given that the velocity of the s/c is smaller. Thus, h_{max} is taken as 400 seconds. On the other hand, h_{min} is chosen of 10 seconds because it would be very unusual a lower stepsize.

4.3.4 Non-dimensional units

The time that the code takes to finish all the computations is very large given that the orbit integrator performs multiple iterations in order to propagate all the transfer orbit of our problem. One reason why it takes so long is because the parameters and equations are working with dimensions. As a result, an optimum solution to decrease the time of the computations would be setting without dimensions the position, the acceleration, the velocity, the time and the thrust. All the previous parameters are respectively non-dimensioned with the following:

$$d_{adm} = 6378145 \quad \mathrm{m}, \tag{4.98}$$

$$a_{adm} = 9.80655 \quad \mathrm{m/s^2}, \tag{4.99}$$

$$v_{adm} = \sqrt{d_{adm} a_{adm}} \quad \mathrm{m/s}, \tag{4.100}$$

$$t_{adm} = \frac{d_{adm}}{v_{adm}} \quad \mathrm{s}, \tag{4.101}$$

$$F_{adm} = m a_{adm} \quad \mathrm{N}. \tag{4.102}$$

4.3.5 Trajectory simulations from the Earth to L1

Once ϵ, h_{max} and h_{min} of the integrator are established, it is time to test if the dynamical and conjugate equations work properly. In order to do this, the TPBVP of the first segment (Sec. 4.2.1) is studied.

One can see in Eq. 4.25 that α and, therefore, n depend upon the initial values of λ_r and λ_v. Hence, the resulting orbit may vary depending on these parameters. In order to see if the dynamical model and the TPBVP is properly coded, two different tests with different values of λ_r and λ_v are carried out. The orbits are propagated throughout 40 days.

The first orbit propagation (Fig. 4.9) is obtained with the following random values of λ_r and λ_v:

$$\lambda_r = \begin{pmatrix} 6.2490750 \\ 0.5814762 \\ 7.0112307 \end{pmatrix}, \qquad \lambda_v = \begin{pmatrix} -4.8332992 \\ 1.8523355 \\ 4.2072336 \end{pmatrix}. \tag{4.103}$$

One can see in Fig. 4.9 that, with the values of Eq. 4.103, the s/c's trajectory is decreasing towards the Earth. A clean orbit propagation is obtained and therefore, the code works properly.

The second orbit propagation (Fig. 4.10) is obtained with the following random values of λ_r and λ_v:

$$\lambda_r = \begin{pmatrix} 5.2450419 \\ -9.8397239 \\ -4.0788961 \end{pmatrix}, \qquad \lambda_v = \begin{pmatrix} 4.5592717 \\ 1.1610007 \\ 9.4155392 \end{pmatrix}. \tag{4.104}$$

One can see in Fig. 4.10 that, with the values of Eq. 4.104, the s/c's trajectory is now increasing. A clean orbit propagation is obtained and, therefore, the code works properly.

One should bear in mind that the axes of the both figures are non-dmiensioned with the parameters of Sec. 4.3.4.

4.4 TPBVP solution by means of HYBRD1

The problem consists of finding which are the optimal initial λ_{r0} and λ_{v0} that fulfil the boundary conditions imposed in the TPBVP. Given that it is impossible to know an initial approximation of λ_{r0} and λ_{v0} for the starting point of the nonlinear problem, random numbers are going to be chosen to fill the two vectors.

Random numbers are commonly used in optimization and integration problems, and these are randomly chosen by means of Montecarlo's method ([42]). This method relies on repeated random sampling to obtain numerical results and this simulation is repeated many times in order to obtain a distribution of an unknown probabilistic entity. The interval of the random numbers that are going to be used for λ_{r0} and λ_{v0} in this problem is between -10 and 10.

The final time of the orbit propagation, t_f, is free and unknown. Therefore, an approximate t_f should be also guessed to start the computations. In order to guess this t_f, a s/c with a constant thrust of 456.3 μN parallel to the velocity is propagated from GEO towards an approximated distance to L1 (318000 km). One can see in Fig. 4.11 the final orbit propagation from GEO to 318000 km. This s/c takes 297 days to reach that distance. As a result, one should take into account that the s/c will take longer to reach L1 with a solar sail than with a constant thrust parallel to the velocity. Looking into[10], it has been demonstrated that a non-optimal trajectory lasts 2.9 years to reach the Moon. Therefore, taking into account that the trajectory is optimum in our project, t_f is chosen randomly between 400 days to 600 days in order to carry out the computations with HYBRD1.

Therefore, when the compilation of the program starts, a set of 7 random numbers are chosen, three for λ_{r0}, three for λ_{v0} and another one for t_f. Then, the main code calls HYBRD1. In order to work properly, the user must provide to HYBRD1 a subroutine, called FCN, to calculate the residuals of the function $\mathbf{F}$. This subroutine shall be as efficient as possible, since the time spent by the algorithm is strongly influenced by the time spent in FCN.

Inside FCN, firstly the departure point of the s/c is computed, just as the Julian Date in order to precisely locate the Moon and the Sun at the moment of the departure. At the starting point of the transfer orbit, the position and the velocity of the s/c is computed, $\mathbf{r}_0$ and $\mathbf{v}_0$, and these are included in conjunction with the

random λ_{r0} and λ_{v0} into:

$$\mathbf{x}_0 = \begin{pmatrix} r_{x0} \\ r_{y0} \\ r_{z0} \\ v_{x0} \\ v_{y0} \\ v_{z0} \\ \lambda_{rx0} \\ \lambda_{ry0} \\ \lambda_{rz0} \\ \lambda_{vx0} \\ \lambda_{vy0} \\ \lambda_{vz0} \end{pmatrix}. \tag{4.105}$$

Next, the orbit is propagated throughout the period of time t_f by means of the RKF 7(8) integrator, and, when the s/c reaches the final point, the position at this point is compared with the position of L1, $\mathbf{r}_{L1}$, at t_f:

$$\mathbf{F}_1 = \mathbf{r}_{xL1}(t_f) - \mathbf{r}_x(t_f), \tag{4.106}$$
$$\mathbf{F}_2 = \mathbf{r}_{yL1}(t_f) - \mathbf{r}_y(t_f), \tag{4.107}$$
$$\mathbf{F}_3 = \mathbf{r}_{zL1}(t_f) - \mathbf{r}_z(t_f). \tag{4.108}$$
$$\tag{4.109}$$

The s/c's velocity at the end of the orbit propagation is also compared with the required for the s/c in order to be captured by the Moon's sphere of influence, $\mathbf{v}_{capt}$.

$$\mathbf{F}_4 = \mathbf{v}_{xcapt}(t_f) - \mathbf{v}_x(t_f), \tag{4.110}$$
$$\mathbf{F}_5 = \mathbf{v}_{ycapt}(t_f) - \mathbf{v}_y(t_f), \tag{4.111}$$
$$\mathbf{F}_6 = \mathbf{v}_{zcapt}(t_f) - \mathbf{v}_z(t_f). \tag{4.112}$$
$$\tag{4.113}$$

Finally, since it is a free time problem, the Hamiltonian, H, at the end of the propagation must be 0:

$$\mathbf{F}_7 = H(t_f). \tag{4.114}$$

Given that a nonlinear system with 7 inputs (λ_{r0}, λ_{v0} and t_f) and 7 outputs ($\mathbf{F}$) is obtained, it can be solved with HYBRD1 without any problem. By means of the residuals of $\mathbf{F}$, by using all the mathematical background explained in Sec. 3.3,

HYBRD1 is in charge of finding a correction $\mathbf{p}$, and hence iterating with the aim of finding an optimal solution. HYBRD1 stops working when:

- The problem has converged.
- The tolerance is too small and there is no further improvement in the approximate solution of $\mathbf{x}$.
- Iteration is not making good progress because the last five jacobian evaluations have not improved.
- Iteration is not making good progress because the last ten iterations are not improving.

Once HYBRD1 has finished, then another set of random numbers are used for λ_{r0}, λ_{v0} and t_f and the procedure starts again. This procedure is repeated until two solutions that have converged to the same result are found out in order to reassure that this solution is correct.

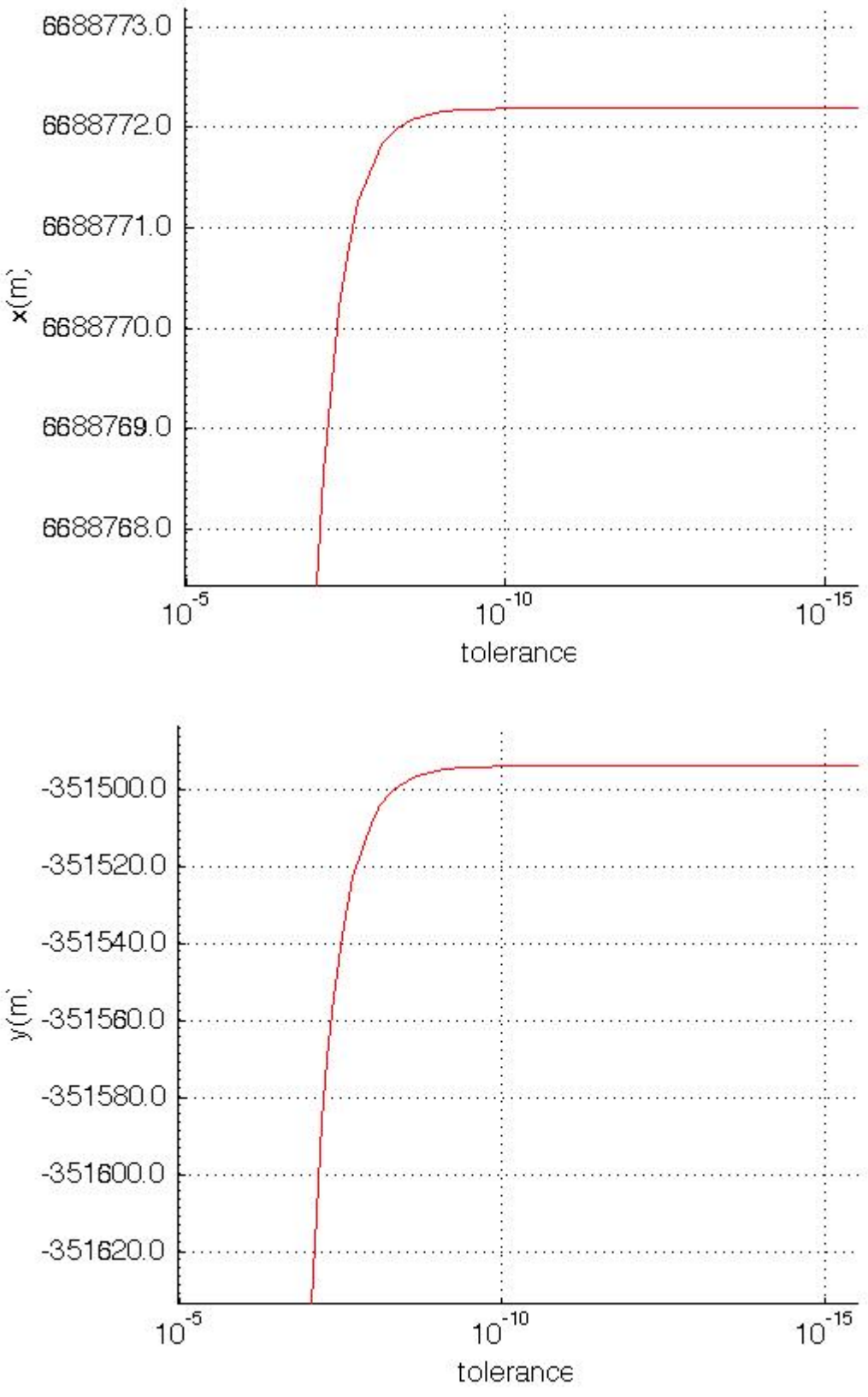

Figure 4.5: Variation as a function of the tolerance of: r_x (top), r_y (bottom).

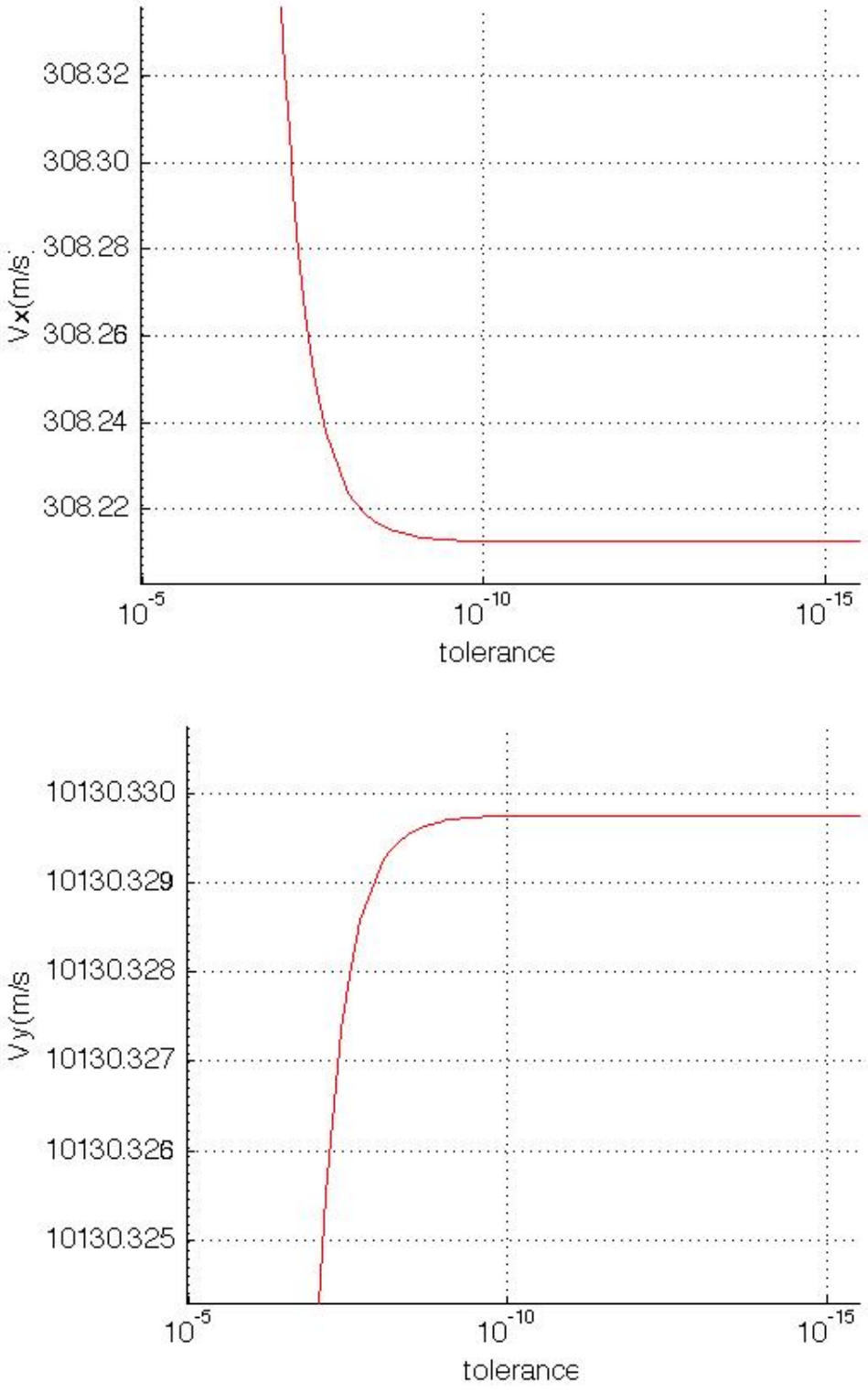

Figure 4.6: Variation as a function of the tolerance of: v_x (top), v_y (bottom).

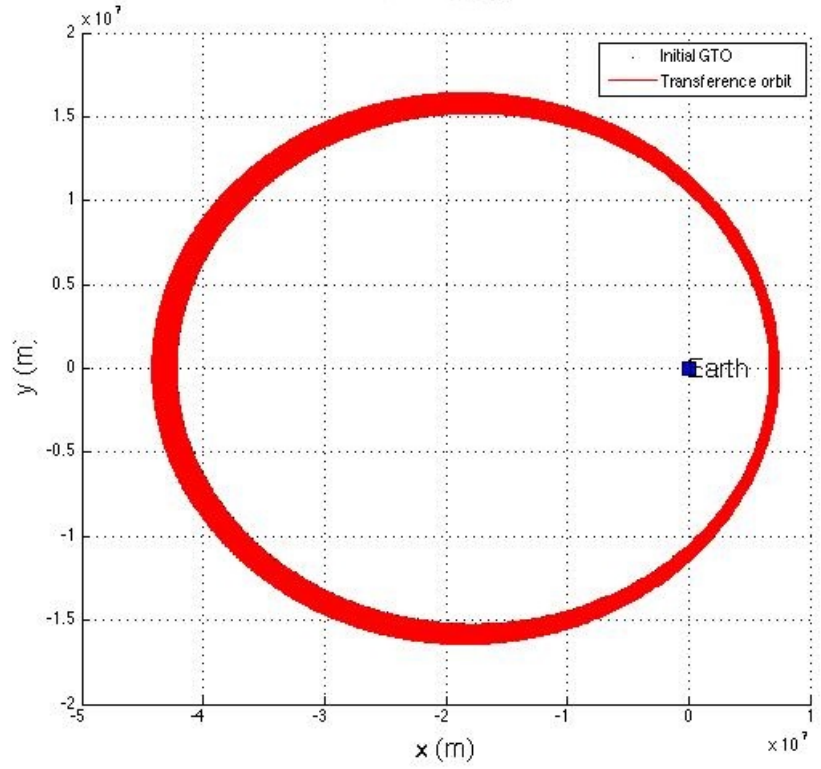

Figure 4.7: Orbit raising throughout the enough time to study the step.

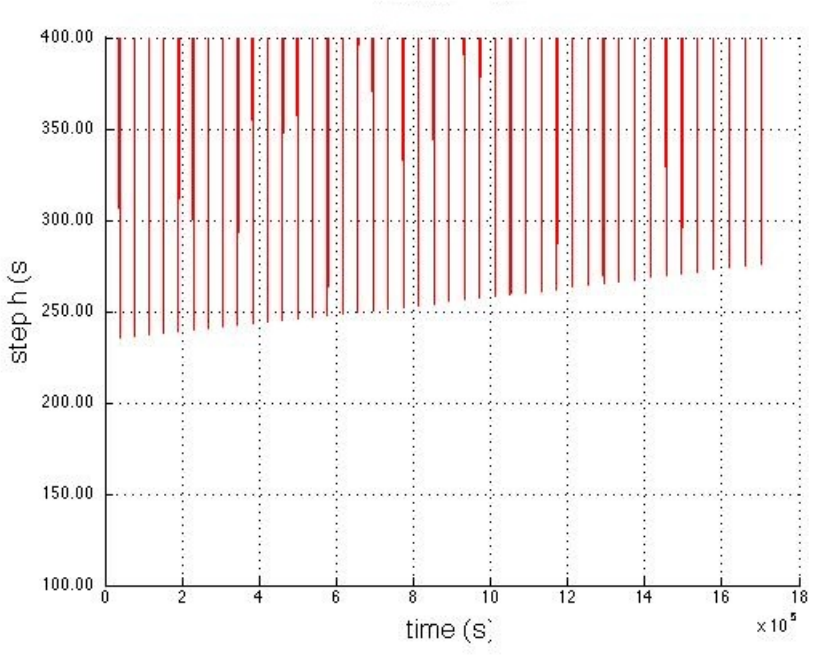

Figure 4.8: Variation of the step as a function of the time.

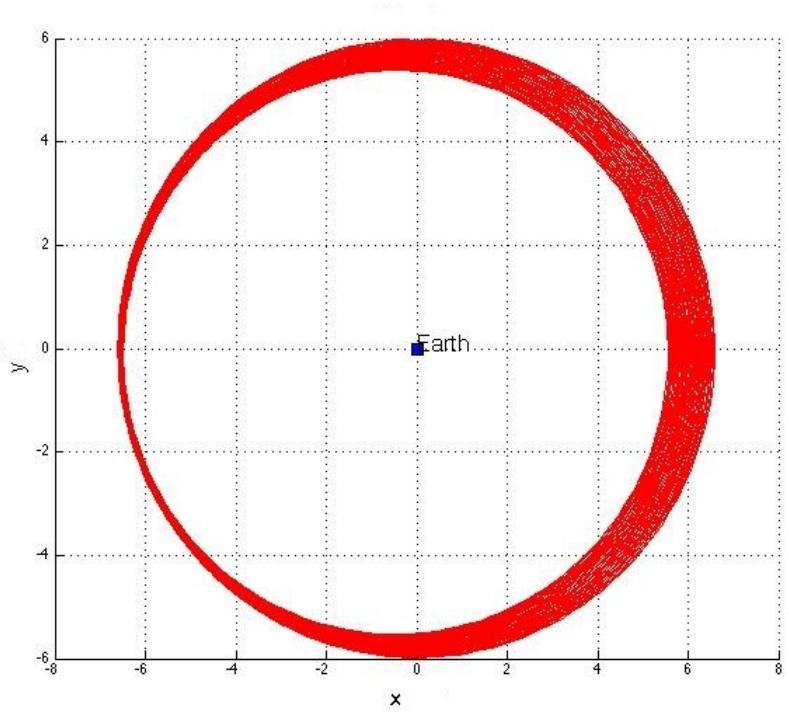

Figure 4.9: Resulting orbit of the first test.

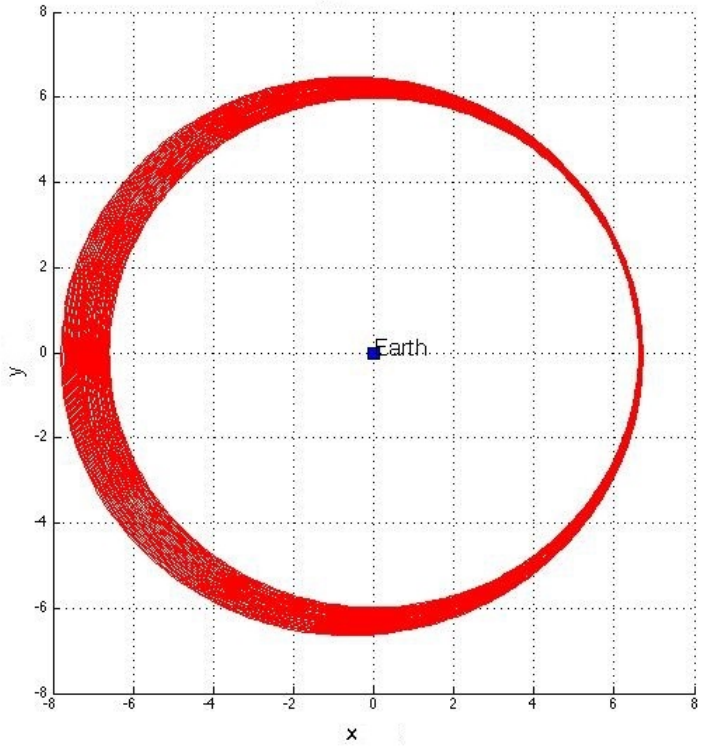

Figure 4.10: Resulting orbit of the second test.

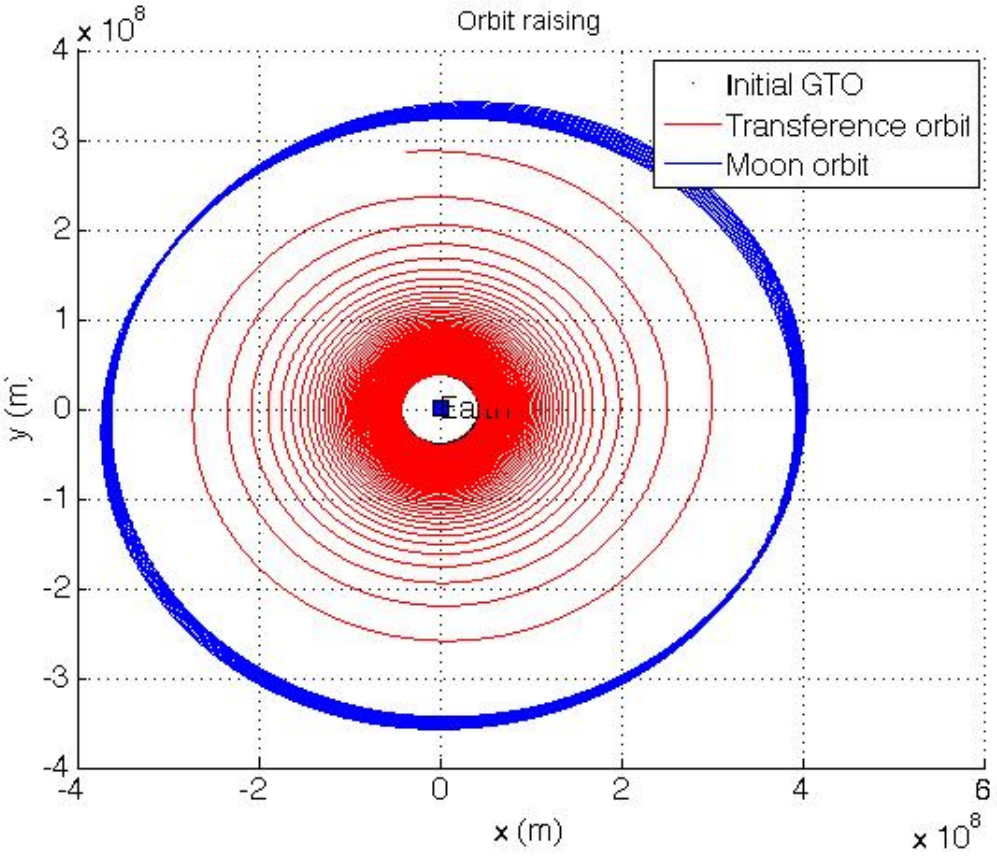

Figure 4.11: Resulting propagation from GEO to 318000 km with the thrust parallel to the velocity.

Chapter 5

Conclusions

The conclusions of this project are extensive, but firstly I would like to outline that its high level of difficulty together with its high level of maths and computation skills have helped me to learn how to deal with a real project, which might have a future impact into the development of solar sails and missions using optimal control.

With respect to the trajectory analysis, firstly the complete dynamical model explained in Chapter 2 has been completely coded in Fortran 95. The s/c has a total mass of 6 kg and its propulsion system consists in a solar sail of 50 m^2. In order to guarantee a good propagation of the orbit, several tests were carried out in order to compute the optimum parameters for the RKF 7(8) integrator. Once the orbit integrator worked efficiently, other tests have been carried out in order to see how the accelerations due to the Sun, the Moon and J2, vary as a function of the height. All these computations are performed taking into account an ideal reflecting solar sail and a thrust that is always tangent to the transference orbit. Inside this code, a study of the eclipses generated by the Earth and the Moon is also included. This eclipses are computed by means of a double-cone eclipse model.

As far as optimal control is concerned, the project has provided the reader a good insight into how to solve optimal control problems, showing that most of engineering problems that deal with optimitation can be solved with this method very efficiently. Regarding the way to solve optimal control problems, the difficulties and main drawbacks of nonlinear programming have also been presented. This project sticks to the idea that MINPACK-1 is a good Fortran library that solve nonlinear problems and can be used by anyone who understand about

nonlinear programming. Due to its flexibility and amount of different subroutines, most of nonlinear problems can be solved with this library.

The problem is simplificated in order to reach a solution more easily. When trying to find out the TPBVP of this simplificated problem, firstly we tried to differenciate H as a function of the pitch and yaw angles (μ and ψ), resulting in the following:

$$\begin{aligned}
\frac{\delta H}{\delta \mu} &= 0 = k_{sun}\left(\mathbf{d}_{Su}\cdot\mathbf{n}\right)^2\left(\lambda_{vx}\sin\psi\sin\mu - \lambda_{vy}\cos\psi\sin\mu + \lambda_{vz}\cos\mu\right) \\
&+ \left(-\lambda_{vx}\sin\psi\cos\mu + \lambda_{vy}\cos\psi\cos\mu + \lambda_{vz}\sin\mu\right)\times 2k_{sun}\left(\mathbf{d}_{Su}\cdot\mathbf{n}\right) \\
&\times \frac{(r_x - r_{sx})\sin\mu\sin\psi - (r_y - r_{sy})\sin\mu\cos\psi + (r_z - r_{sz})\cos\mu}{|\mathbf{r}-\mathbf{r}_s|}, \qquad (5.1) \\
\frac{\delta H}{\delta \psi} &= 0 = -k_{sun}\left(\mathbf{d}_{Su}\cdot\mathbf{n}\right)^2\cos\mu\left(\lambda_{vx}\cos\psi + \lambda_{vy}\sin\psi\right) \\
&+ \left(\lambda_{vx}\sin\psi\cos\mu - \lambda_{vy}\cos\psi\cos\mu - \lambda_{vz}\sin\mu\right)\times 2k_{sun}\left(\mathbf{d}_{Su}\cdot\mathbf{n}\right)\cos\mu \\
&\times \frac{(r_x - r_{sx})\cos\psi + (r_y - r_{sy})\sin\psi}{|\mathbf{r}-\mathbf{r}_s|}. \qquad (5.2)
\end{aligned}$$

Nevertheless, since we needed μ and ψ explicitly for not solving the previous equations by means of numerical methods, we had to proceed to differenciate H as a function of the radiation incidence angle, α. Finally, α becomes the control parameter in the TPBVP and therefore the normal vector, $\mathbf{n}$, is always pointed towards the optimal direction in order to give the maximum thrust to the s/c for every period of the transference orbit.

Once the dynamical equations and the conjugate equations from the TPBVP are obtained, some tests are carried out in order to see if the code works. In this tests, the reader can perceive that depending on the values of the initial λ_{r0} and λ_{v0}, the resulting orbit is different.

Finally, it has been studied how to solve this problem by means of MINPACK-1. 500 iterations of HYBRD1 are required in order to find which are the best λ_{r0} and λ_{v0} and which is the minimum final time of the propagation. What is more, as it was fairly explained in Chapter 3, MINPACK-1 needs to iterate an undefined number of times the orbit propagation in order to reach the optimum solution. This in conjunction with the huge amount of days (360-600 days) that means every propagation until the L1 point concludes that the time that the code needs to be working in order to reach the final result is very huge, maybe days.

In addition, this project entails difficulties of high magnitudes when trying to understand nonlinear programming and how to solve optimal control problems. Hence, these are the main reasons why the optimal Earth-to-Moon trajectory is out of scope of this project.

Nevertheless, our team will definitely continue working until the optimal Earth-to-Moon trajectory is found out.

Appendix A

Runge-Kutta-Fehlberg 7(8) coefficients

The four coefficients that are used in the integrator RKF 7(8) are presented hereunder:

$$\alpha_m = \begin{bmatrix} 0 & 2/27 & 1/9 & 1/6 & 5/12 & 1/2 & 5/6 & 1/6 & 2/3 & 1/3 & 1 & 0 & 1 \end{bmatrix}, \quad \text{(A.1)}$$

$$\beta_{mn} = \begin{bmatrix} 0 & 0 & 0 & 0 & 0 & 0 & 0 & 0 & 0 & 0 & 0 & 0 \\ 2/27 & 0 & 0 & 0 & 0 & 0 & 0 & 0 & 0 & 0 & 0 & 0 \\ 1/36 & 1/12 & 0 & 0 & 0 & 0 & 0 & 0 & 0 & 0 & 0 & 0 \\ 1/24 & 0 & 1/8 & 0 & 0 & 0 & 0 & 0 & 0 & 0 & 0 & 0 \\ 5/12 & 0 & -25/16 & 25/16 & 0 & 0 & 0 & 0 & 0 & 0 & 0 & 0 \\ 0.05 & 0 & 0 & 0.25 & 0.2 & 0 & 0 & 0 & 0 & 0 & 0 & 0 \\ -25/108 & 0 & 0 & 128/108 & -65/27 & 125/54 & 0 & 0 & 0 & 0 & 0 & 0 \\ 31/300 & 0 & 0 & 0 & 61/225 & -2/9 & 13/900 & 0 & 0 & 0 & 0 & 0 \\ 2 & 0 & 0 & -53/6 & 704/45 & -107/9 & 67/90 & 3 & 0 & 0 & 0 & 0 \\ -91/108 & 0 & 0 & 23/108 & -976/135 & 311/54 & -19/60 & 17/6 & -1/12 & 0 & 0 & 0 \\ 2383/4100 & 0 & 0 & -341/164 & 4496/1025 & -301/82 & 2133/4100 & 45/82 & 45/164 & 18/41 & 0 & 0 \\ 3/205 & 0 & 0 & 0 & 0 & -6/41 & -3/205 & -3/41 & 3/41 & 6/41 & 0 & 0 \\ -1777/4100 & 0 & 0 & -341/164 & 4496/1025 & -289/82 & 2193/4100 & 51/82 & 33/164 & 12/41 & 0 & 1 \end{bmatrix}, \quad \text{(A.2)}$$

$$c_7 = \begin{bmatrix} 41/840 & 0 & 0 & 0 & 0 & 34/105 & 9/35 & 9/35 & 9/280 & 9/280 & 41/840 & 0 & 0 \end{bmatrix}, \quad \text{(A.3)}$$

$$c_8 = \begin{bmatrix} 0 & 0 & 0 & 0 & 0 & 34/105 & 9/35 & 9/35 & 9/280 & 9/280 & 0 & 41/840 & 41/840 \end{bmatrix}. \quad \text{(A.4)}$$

Appendix B

Budget

In this section we present the budget of the *Study of Earth-Moon trajectories with solar sail propulsion* project. Firstly, one should take into account that this budget is stated as if the engineer started from zero, that is to say, buying the computers, licenses, etc. Hence, the software and hardware used is taken into account. Tab. B.1 shows a detailed budget, but an outline is presented next.

Nine months were spent on the project, most of them on part-time basis. This amounts a total of 615 hours of man hours. Taking into account that the price per hour is 15 e , the total cost of the engineering work is 9225 e. Power consumption is also included in this budget due to the extensive processing time: approximately 600 hours, hence the electic power consumed is 66 e. The software and hardware employed sum up a total cost of 4123 e. As a result, the total cost is close to 13414 e.

$Concept$	$Quantity(h)$	€$/h$	$Cost$(€)
Mission analysis			
Research of missions	35	15	525
Optimal control bibliography	40	15	600
Nonlinear programming bibliography	25	15	375
Subtotal of the mission analysis	100	15	1500
Code implementation			
Formulation development	100	15	1500
Implementation of the formulation into fortran	125	15	1875
MINPACK-1 application	100	15	1500
Matlab representations	40	15	600
Subtotal of code implementation	365	15	5475
Writing of the report	150	15	2250
Subtotal of worked hours	615	15	9225
Simulations			
Trajectory simulations	500	0.11	55
Other tests and results	100	0.11	11
Subtotal of simulations	600	0.11	66
Hardware			
PC (Intel Core 2 Quad CPU Q8400 3Gb-RAM@ 2.67GHz)			1000
MacBook Pro (2 GHz Intel core i7 8Gb-RAM)			2000
Subtotal of hardware			3000
Software			
Microsoft Windows 8 (Student)			0
Matlab 8.3 R2014a (Win64)			500
Microsoft Visual Studio 2012 (Student)			0
Intel Fortran Composer XE 2013			622.57
STK 10 (Student)			0
TeXlive 2013 + Texmaker 4.1.1			0
Subtotal of software			1122.57
Total	615		13414

Table B.1: Budget of the *Study of Earth-Moon trajectories with solar sail propulsion* project.

Bibliography

[1] Josep Masdemont Elena Fantino, Gerard Gómez and Yuan Ren. Low-energy transfers to the moon.

[2] J. Pulido J. Schoenmaekers and R. Jehn. Smart-1 mission analysis: Moon option. *Tech.Rep. S1-ESC-RP-5001, European Space Agency, directorate of Technical and Operational Support, Ground Systems engineering Department.*, Sept. 1998.

[3] Bion L. Pierson and Craig A. Kluever. Optimal earth-moon trajectories using nuclear electric propulsion. *Journal of Guidance, Control and Dynamics*, 20, No.2, April 1997.

[4] B. Dachwald A. Ohndorf and E. Gill. Optimization of low-thrust earth-moon transfers using evolutionary neurocontrol. *IEEE Congress on Evolutionary Computation*, 2009.

[5] Gyeong Eon Jeon Tae Soo No, Ji Marn Lee and Daero Lee. A study on earth-moon transfer orbit design. *International Journal of Aeronautical and Space Sciences*, March 6, 2012.

[6] Craig A. Kluever and Bion L. Pierson. Optimal low-thrust three-dimensional earth-.moon trajectories. *Journal of Guidance, Control and Dynamics*, 18, No. 4, August 1995.

[7] F. TOPPUTO G. MINGOTTI and F. BERNELLI-ZAZZERA. A method to design sun-perturbed earth-to-moon low-thrust transfers with ballistic capture. *XIX Congresso Nazionale AIDAA*, 21 Settembre 2007.

[8] R. B. Powers and V. Coverstone. Optimal solar sail orbit transfers to synchronous orbits. *The Journal of the Astronautical Sciences*, Vol. 49, No. 2, pp. 269-281., 2001,.

[9] G. W. Hughes and C. R. McInnes. Solar sail hybrid trajectory optimization for non-keplerian orbit transfers. *Journal of Guidance Control & Dynamics*, Vol. 25, No. 3, pp. 602-604., 2002.

[10] Orzuri Rique. Design of a plug and play solar sail module as the propulsion system for nanosatellites. *64th International Astronautical Congress, Beijing, China*, 09/2013.

[11] R. Gamkrelidze L. Pontryagin, V. Boltyanskii and E. Mischenko. The mathematical theory of optimal processes. *Wiley-New York*, 1962.

[12] M. Athans and P. Falb. *Optimal Control*. 1966.

[13] Jr. Arthur E. Bryson and Yu-Chi Ho. *Applied Optimal Control (Optimization, Estimation, and Control)*. Taylor & Francis Group, LLC, 1975.

[14] C.A. Kluever and B.L. Pierson. *Optimal Low-Thrust Three-Dimensional Earth-Moon trajectories*, volume 18. Journal of Guidance, Control, and Dynamics, 1995.

[15] R. Mattheij U.M. Ascher and R. Russell. Numerical solution of boundary value problems for ordinary differential equations. *SIAM, Philadelphia, second edition*, 1995.

[16] L. C. Young. Optimal control theory. *Cambridge University Press*, 2nd edition, 1980.

[17] S. S. Sastry. Lecture notes 8. optimal control and dynamic games. REVISED March 29th.

[18] Ed Bueler. Two-point boundary value problems: Numerical approaches. *Dept of Mathematics and Statistics*, Spring 2010.

[19] J.M. Juan Zornoza J. Sanz Subirana and M. Hernández-Pajares. Reference systems and frames. *Technical University of Catalonia, Spain*, 2011.

[20] Aalborg University Thomas Bak, Institute of Electronic Systems. Modelling of spacecraft dynamics.

[21] Bernd Dachwald and the Solar Sail Degradation Model Working Group. Potential solar sail degradation effects on trajectory and attitude control. *AAS/AIAA Astrodynamics Specialists Conference*, August 2005.

[22] W.A. Heiskanen and H. Moritz. Physical geodesy. *W.H. Freeman and Co., San Francisco*, 1967.

[23] J.K. Factor R.G. Trimmer N.K. Pavlis D.S. Chinn C.M. Cox S.M. Klosko S.B. Luthcke M.H. Torrence Y.M. Wang R.G. Williamson E.C. Pavlis R.H. Rapp F.G. Lemoine, S.C. Kenyon and T. R. Olson. The development of the joint nasa gsfc and the national imagery and mapping agency (nima) geopotential model egm96. *National Aeronautics and Space Administration*, page Section 10, July 1998.

[24] Steve C. Kenyon Nikolaos K. Pavlis, Simon A. Holmes and John K. Factor. The development and evaluation of the earth gravitational model 2008 (egm2008). *National Geospatial-Intelligence Agency, 7500 GEOINT Drive, S73-IBG, Springfield, Virginia 22150, USA*, 2008.

[25] S. Bettadpur D. Chambers M. Cheng F. Condi B. Gunter Z. Kang P. Nagel R. Pastor T. Pekker S. Poole B. Tapley, J. Ries and F. Wang. Ggm02: An improved earth gravity field model from grace. *Journal of Geodesy*, 2005.

[26] David A. Vallado. Fundamentals of astrodynamics and applications. *Microcosm Press, El Segundo, CA. p. 157.*, 2001.

[27] E.M. Standish. Approximate mean ecliptic elements of the lunar orbit. *JPL IOM 312.F-01-004*, 2001.

[28] E M Standish. Keplerian elements for approximate positions of the major planets. *Solar System Dynamics Group. JPL / Caltech*.

[29] Sagur Srihari. The hessian matrix. *Machine learning*.

[30] Stanford University David G. Luenberger, Stanford University; Yinyu Ye. *Linear and Nonlinear Programming*. Springer, 2008.

[31] John W. Chinneck. Practical optimization: a gentle introduction. 2012.

[32] Knut–Andreas Lie. Introduction to finite differences. *SINTEF ICT, Dept. Applied Mathematics*.

[33] Andreas Griewank. Broyden updating, the good and the bad! *Documenta Math*, 2010.

[34] Burton S. Garvow Jorge J. Moré and Kenneth E. Hillstrom. User guide for minpack-1. *CERN Libraries, Geneva*, 1974.

[35] Hannah Rae Kerner. The lagrangian points: An application of linear algebra. Spring 2013.

[36] Bion L. Pierson and Craig A. Kluever. Three-stage approach to optimal low-thrust earth-moon trajectories. *Journal of Guidance, Control and Dynamics*, 17, No. 6, December 1994.

[37] Yang Gao. Advances in low-thrust trajectory optimization and flight mechanics. *University of Missouri-Columbia*, December 2003 (Revised 2009).

[38] Bruce A. conway. *Spacecraft Trajectory Optimization*^{o}. Cambridge University Press, 2010.

[39] J D Faires & R L Burden. Initial-value problems for odes: Error control & runge-kutta-fehlberg method. In *Numerical Methods (4th Edition)*, 2012.

[40] Howard D. Curtis. *Orbital Mechanics for Engineering Students*. Butterworth-Heinemann (Elsevier), (Burlington, MA, US) ISBN: 978-0- 12-374778-5., 2010.

[41] Taketomo Mitsui. Runge-kutta type integration formulas including the evaluation of the second derivative: Part i. *Publ. RIMS, Kyoto Univ. 18 (1982), 325-364*.

[42] R.J. Serfling. Approximation theorems of mathematical statistics. *John Wiley, New York*, 1980.